Zhu, Bin; Fan, Liangdong; Mushtaq, Naveed; Raza, Rizwan; Sajid, Muhammad; Wu, Yan; Lin, Wenfeng; Kim, Jung Sik; Lund, Peter D.; Yun, Sining

## Semiconductor Electrochemistry for Clean Energy Conversion and Storage

REVIEW ARTICLE

# Semiconductor Electrochemistry for Clean Energy Conversion and Storage

Bin Zhu[1] · Liangdong Fan[2] · Naveed Mushtaq[1] · Rizwan Raza[3] · Muhammad Sajid[3] · Yan Wu[4] · Wenfeng Lin[5] · Jung-Sik Kim[6] · Peter D. Lund[7] · Sining Yun[8]

## Abstract

Semiconductors and the associated methodologies applied to electrochemistry have recently grown as an emerging field in energy materials and technologies. For example, semiconductor membranes and heterostructure fuel cells are new technological trend, which differ from the traditional fuel cell electrochemistry principle employing three basic functional components: anode, electrolyte, and cathode. The electrolyte is key to the device performance by providing an ionic charge flow pathway between the anode and cathode while preventing electron passage. In contrast, semiconductors and derived heterostructures with electron (hole) conducting materials have demonstrated to be much better ionic conductors than the conventional ionic electrolytes. The energy band structure and alignment, band bending and built-in electric field are all important elements in this context to realize the necessary fuel cell functionalities. This review further extends to semiconductor-based electrochemical energy conversion and storage, describing their fundamentals and working principles, with the intention of advancing the understanding of the roles of semiconductors and energy bands in electrochemical devices for energy conversion and storage, as well as applications to meet emerging demands widely involved in energy applications, such as photocatalysis/water splitting devices, batteries and solar cells. This review provides new ideas and new solutions to problems beyond the conventional electrochemistry and presents new interdisciplinary approaches to develop clean energy conversion and storage technologies.

**Keywords** Semiconductor electrochemistry · Fuel cells · Lithium-ion batteries · Solar cells · Built-in electric field · Energy system integration

## 1 Introduction

Electrochemical devices, including fuel cells, batteries and electrolyzers have shown great potential for large-scale clean energy conversion and storage applications. In clean energy conversion, fuel cells directly convert the chemical energy from fuels into electricity with high efficiency and low emissions, while in clean energy storage, a battery is a typical storage device with high energy density and good reversibility and durability. We selected these two systems for the present study, because they represent the current and near-future energy conversion and storage technologies with a high potential to be combined with renewable and sustainable energy sources. We use them as examples to give a comprehensive review of current research frontiers with emphases on semiconductor and band theory applications in both materials and devices/technologies as well as fundamental sciences, followed by extensions to related fields, e.g., photoelectrolysis or photocatalysts, solar cells, metal-air batteries, and electrolyzers.

The knowledge and operating principles of fuel cells have largely remained the same over the last century [1, 2]. The yttrium-stabilized zirconia (YSZ) electrolyte, a

Bin Zhu, Liangdong Fan, Rizwan Raza, Naveed Mushtaq contributed equally to this work.

✉ Bin Zhu
zhu-bin@seu.edu.cn; binzhu@kth.se

✉ Liangdong Fan
fanld@szu.edu.cn

✉ Rizwan Raza
rizwanraza@cuilahore.edu.pk

✉ Sining Yun
yunsining@xauat.edu.cn

Extended author information available on the last page of the article

typical oxide material, has been the main focus of research and development for solid oxide fuel cells (SOFCs). However, the full and successful commercialization of SOFCs is hampered by the requirement for high temperature materials associated with high costs despite the inherent benefits of the technology. The high operating temperature, which is directly related to the ionic conductivity of solid oxide electrolytes, requires special attention from the aspects of the material durability and manufacturing. It also adversely affects the costs, impeding wide application of SOFC technology. For instance, many works have focused on developing ultrathin film electrolyte layers of YSZ and alternative doped ceria (e.g., $Sm_{0.2}Ce_{0.8}O_{2-\delta}$ (SDC)) to minimize device ohmic loss and maintain desirable power output at reduced temperatures.

The oxygen transport properties in the electrode and electrolyte materials are not only of technological interest, as noted above, but also of fundamental importance. The energetics of oxygen transport in these oxides are affected by the material structure, composition, oxygen stoichiometry, doping and elastic strain, which comprise a wide range of parameters in optimizing the transport properties. In addition, lowering the temperature can cause slower electrode and electrolyte dynamic processes. To speed up the development of SOFCs, new solutions to these key challenges for the electrolytes and electrodes need to be found, i.e., to achieve sufficient ionic conductivity electrolytes and highly electrocatalytically active electrodes at lower operating temperatures. In addition, more radical approaches alternative to the traditional approach of using the three-layer anode-electrolyte-cathode electrochemical device structure and material systems are greatly sought after. In 2013, Singh et al. [3] noted that the anode, cathode and electrolyte in SOFCs, in terms of semiconductor principles, can be associated with an n-type regime, a p-type regime and an ion conducting electrolyte, respectively, as shown in Fig. 1a. In 2018, Asghar et al. [4] further proposed that wide bandgap semiconductors can be used for replicating the electrolyte functionality. This means that an SOFC could be conceptually handled as a semiconductor fuel cell system. If the middle electrolyte layer of the SOFC is removed or replaced with a wide bandgap semiconductor, then the fuel cell effectively resembles a p–n junction device (as Fig. 1b); i.e., a p–n junction is formed in situ under a fuel cell atmosphere by the same material that can block electrons, thus preventing short circuiting of the fuel cell in much the same way as in solar cells. Based on this principle, two types of novel fuel cell devices may be constructed based on either $O^{2-}$ or $H^+$ conduction/transfer, as illustrated in Fig. 1c, d. We designate these devices as electrolyte-layer-free fuel cells (EFFCs) to distinguish them from the traditional SOFC structure. Naturally, the EFFC has the same functionalities

as the traditional SOFC, but these can be realized through a different methodology employing a vastly simplified configuration. This difference delivers several advantages over a conventional three-layer fuel cell such as the following: (1) the two anode/electrolyte and cathode/electrolyte interfaces that cause major power loss due to the ionic/electronic interfacial polarizations are eliminated [1, 5]; (2) redox reactions, such as the hydrogen oxidation reaction (HOR) and the oxygen reduction reaction (ORR), can be readily performed to generate electricity on the spot, and ionic transport occurs in a more efficient way to complete the fuel cell reactions (Fig. 1a); and (3) a built-in electric field is formed at the anode (n) and cathode (p) junction, which can increase the $H^+$ (Fig. 1c) and $O^{2-}$ (Fig. 1d) transfer mechanics to enhance the overall efficiency of the cell. EFFCs with simpler configurations and harmonious cell components have led to significant progress in the SOFC field.

The transition from the conventional ionic electrochemistry to advanced semiconductor electrochemistry is widely evidenced as reported for many other energy conversion and storage devices [6, 7], which makes the application of semiconductors and associated methodologies to the electrochemistry in energy materials and relevant electrochemical devices an emerging field. For instance, the successful development of photoelectrolysis from photoelectrochemical devices using semiconductors has made photocatalysts and water splitting hot topics [8–10]. Lithium-ion batteries (LIBs) have also experienced new progress based on the semiconductor properties of materials used in devices, e.g., energy band/heterojunction/built-in electric field [11, 12]. Semiconductors and their methodologies complement the conventional electrochemistry, introducing the new topic "semiconductor electrochemistry" and a new frontier in ion conducting semiconductors and novel fuel cell devices [1, 13, 14]. The name of this topic refers to the similarities found between the development of photocatalysts and LIBs and that of fuel cells.

Fuel cells and photoelectrochemical electrolysis have much the same origin as electrolyte-based electrochemical devices with anodes and cathodes, i.e., photoelectrochemical cells (PECs). Today, PECs are well known to be transferrable to photo-water splitting based on semiconductors and band structures [15]. A similar situation occurs for batteries, where semiconductors and energy bands, as well as built-in-field effects, play a significant role in designing material functions and the device performance. Solar cells have taken a reverse route from typical physics to electrochemistry, where ions play an important role in state-of-the-art perovskite solar cells (PSCs). The electrochemistry of the semiconductor–electrolyte interface or semiconductor–semiconductor interface provides great promise to handle these challenges through a deeper understanding.
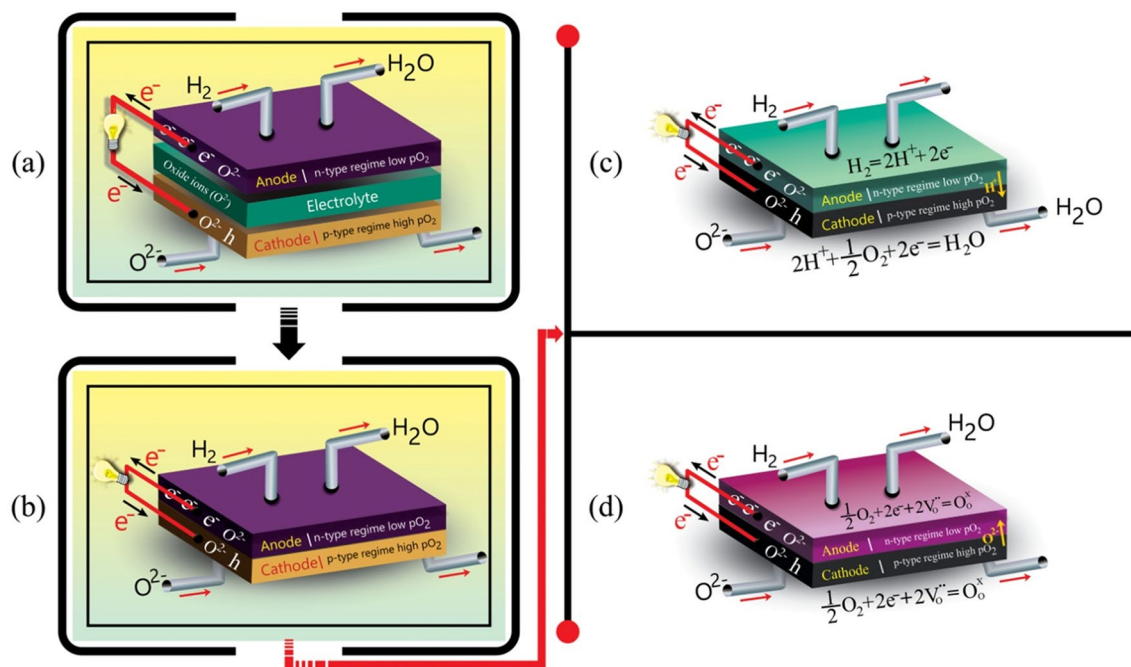
**Fig. 1** Transition of the fuel cell from an ionic electrolyte device (**a**) to an electrolyte-layer-free device, e.g., an n–p junction assembly (**b**), along with the further $H^+$ conducting fuel cell (**c**) and the $O^{2-}$ conducting fuel (**d**), in which a built-in electric field is formed between the anode (n) and cathode (p) junction to promote $H^+$ and $O^{2-}$ transfer to complete the redox reactions and electricity generation on-site without the interfacial polarization and losses caused by the ionic electrolyte separator in conventional fuel cells (**a**) [3]. Partially redrawn with permission from Ref. [3]. Copyright 2013 RSC

A logical deduction can be made that by employing semiconductor electrochemistry, because a semiconductor provides two energy levels (the conduction band (CB) and the valence band (VB)), the charge transfer occurring at these two energy levels can be easily controlled. Therefore, our idea about the variation in the electron density that is helpful for ionic transport at these two energy levels and the interfaces for clean energy conversion and storage devices need to be recapitulated. This work provides a new view of these novel aspects of state-of-the-art research and development in the energy sector, where the two typical fields of fuel cells and batteries are focused on realizing a comprehensive understanding of the roles of semiconductors and bands in energy conversion and storage, with extension to other energy applications in a broader view.

## 2 Electrochemistry of the Semiconductor–Electrolyte Interface and Fuel Cells

Electrochemistry is the core of developing multilayer devices and is most commonly used in assembling two-electrode cells and for referring the voltage to a reference electrode (RE). The science of electrochemistry is central to the manufacturing, performance, and reliability of multilayer devices. Semiconductor electrochemistry is a particularly relevant and fundamental area for fuel cell devices, including ion transport in fuel cells [14]. Semiconductor heterostructure-based fuel cells are convenient to scale using the energy levels relative to the vacuum level (VL) compared to those with an intrinsic ionic conductor. This allows us to track the local variations in energy, electrostatic potential, and Fermi energy ($E_F$) inside the solids by a standard representation. Control of the flowing charge carriers across the junction is the most important point for SOFCs in that electrons must be prevented from crossing over the electrolyte membrane. Before we discuss the properties of the semiconductor-electrolyte interface, examining some of the general aspects of electron and ion transfer reactions at the semiconductor-electrolyte interface from the perspective of the energy band positions is beneficial.

An electrochemical cell (e.g., an SOFC) contains two electrodes (anode and cathode) separated by an electrolyte for completion of the redox reactions. However, to realize the redox reactions and prevent electrons from crossing over the electrolyte membrane, many different methods can be employed, e.g., (1) creating a metal–electrolyte interface (the Schottky-type junction, see Fig. 2a, or the Mott transition from a metal conductor to an electronic insulator (Fig. 2b) related to the band description of the Mott transition induced by $H_2$ or $H^+$ incorporation) where electrons are localized while ions conduct (a typical example is the

strongly correlated perovskite SmNiO$_3$, Fig. 2c); (2) constructing a semiconductor (n-type)-semiconductor (p-type) heterostructure to suppress electron conduction (Fig. 2d); (3) using electronically insulating and ionically conductive electrolytes in conventional fuel cells with the anode/electrolyte/cathode configuration (Fig. 2e); and (4) replacing this configuration by the "three-in-one" single-layer device in which macro-redox reactions occur at the anode and cathode separated by the electrolyte while nano-redox reactions can occur at nano-redox units, where each anode, electrolyte and cathode component can be compacted into n-type, ionic and p-type particles, respectively, as shown in Fig. 2f. Since a metal can provide or accept electrons easily at the surface when it is used as either an anode or a cathode, control of the semiconductor-electrolyte interface (SEI) structure and properties to allow stable ionic conductivity is a critical and highly challenging task. That is why the semiconductor–semiconductor interface (Fig. 2f, fuel cell reaction at the nanoscale) can provide more advantages than metals or SEIs because they have distinct energy levels, the CB and the VB. A spontaneous charge transfer reaction can occur depending on the nature of the doping and charge carrier density. In the case of the SEI, a spontaneous charge transfer reaction can occur depending on the nature of the energy levels or their

overlap with those of the redox electrolytes. There are three distinct possibilities for such an overlap: (1) overlap with the CB, (2) overlap with the VB, and (3) overlap with both bands. These processes lead to energy band alignment or energy band reorientation.

The electrode/electrolyte interfaces in SOFCs are of significant importance, which, on the one hand, provide the active sites for electrode electrochemical reactions and, on the other hand, contribute to a major loss of the power output due to the different ionic and electronic natures [3, 4]. Gleaning an understanding from the fundamental aspects is therefore necessary to develop sustainable SOFCs in the future. Normally, electron–hole (e$^-$/h$^+$) pairs are separated on the anode and cathode sides by the band structure, i.e., CB and VB, and built-in electric field (BIEF) depending on the nature of materials, so the energy band provides an important pathway for the electrochemical reactions to occur.

At the interface of two distinct materials, the free electrons and holes in the CB ($E_c$) and the VB ($E_v$) of the anode and cathode exchange their charges with the electrolyte by diffusion-based processes, and charge neutrality accumulates at the interface. The Fermi levels ($E_F$) attempt to reach an equilibrium position due to charge diffusion processes, and
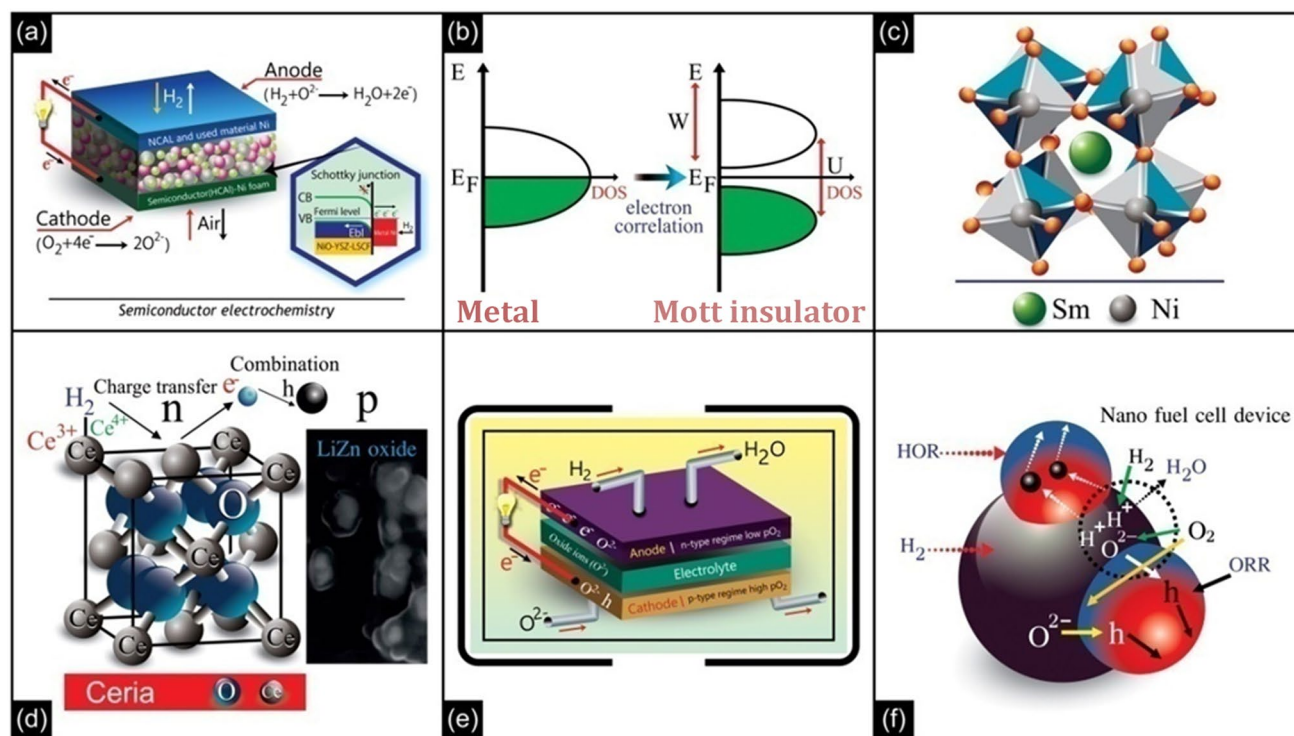


**Fig. 2** Various methods to block electron transfer: **a** Creating a metal–electrolyte interface (the Schottky-type junction). **b** Using the Mott transition to block electrons transferring to the electrolyte; **c** the strongly correlated perovskite SmNiO$_3$ is an example of such a fuel cell. Reproduced with permission from Ref. [16]. Copyright 2016

Springer Nature. **d** Using a p–n heterostructure material to tune the semiconductor into an ionic conductor with no net electron conduction. Reproduced with permission from Ref. [17]. Copyright 2014 RSC. **e** Realizing the fuel cell redox reactions at the electrolyte-separated macroscale and **f** nonelectrolyte or EFFC nanoscale

the resultant $E_F$ can be associated with the difference in the positions of their respective $E_F$(s). These processes force the energy band structures to be rearranged and hence induce band bending. In semiconductors, the position of $E_F$ normally depends on the dopants (n-type or p-type) and their contents; in addition, there are no other reference energy states to assess the energy levels. Therefore, the position of $E_F$ is assessable only when the distance between $E_F$ and $E_c$ or $E_v$ is known. The position of $E_F$ is composed of two parts, the chemical potential ($\mu_e$) and electrostatic potential ($e_x$), and can be expressed as the following Eq. (1), providing that there is no additional charge:

$$E_F = (\mu_e - e_x) = -e\varphi \qquad (1)$$

where $\mu_e$ is the chemical potential of the bulk, while $e_x$ arises from the surface dipole; in the case of heterostructure semiconductors, dipoles are formed by the surface structure due to a particular ionic charge distribution. These effects depend on the crystal plane and the reconstruction of the surface atoms. This dipole also influences the electron affinity. In agreement with the band of a semiconductor with an electrolyte, the electrolyte can be visualized as possessing two distinct energy levels: an empty level as the oxidized level (represented by the most probable energy level $E_{ox}^O$) and a filled level as the reduced level (represented by the most probable energy level $E_{re}^O$).

Generally, band bending due to charge transfer at the interface can be of two types: (1) upward band bending and (2) downward band bending, depending on the type of material. In the case of an n-type semiconductor (the anode), the Fermi level is usually at higher energy (less negative) than the Fermi level of the electrolyte, and electrons try to move from the semiconductor (the anode) to the electrolyte to equilibrate the Fermi level. In this case, the Fermi level of the semiconductor decreases in energy until both Fermi levels overlap; hence, $E_F$ shifts to lower energy, which results in upward band bending, as shown in Fig. 3a, and creates a depletion layer close to the surface of the anode/electrolyte interface. In the case of p-type (normally on the cathode side) semiconductors, the Fermi level normally exists at lower energy (near the VB and more negative) than that of the electrolyte, and its $E_F$ shifts to higher energy (downward band bending) at the interface. A positive space charge region ($h^+$) is therefore created near the surface of the anode interface due to electronic transformation in the electrolyte to achieve electronic equilibrium. A positive space charge means that fewer electrons are in this region. Hence, a charge accumulation/depletion region is formed at the cathode/electrolyte interface. Additionally, on the electrolyte side, when it is fully charged, the electrolyte interface will be left with non-absorbed ions with opposite charges, and they will form a Helmholtz double layer (Fig. 3a).
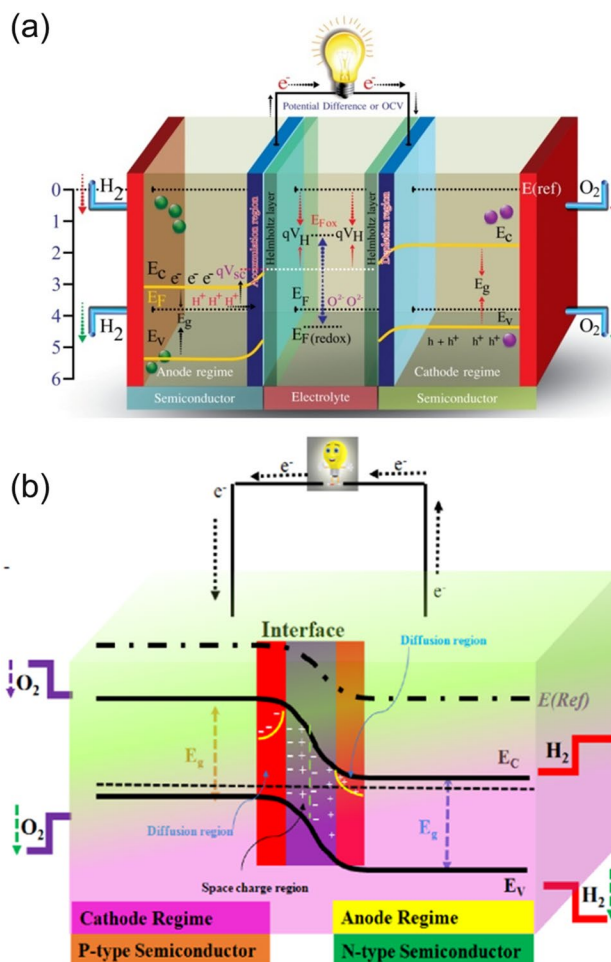


**Fig. 3** **a** Schematic of the working principle and energy diagram at the SOFC electrode (semiconductor) interface with the electrolyte in which Fermi levels are in equilibrium positions, and **b** schematic of the working principle and energy diagram for an SOFC without an electrolyte

A space charge region (created due to a change in $E_F$ position) can be expected on the semiconductor side due to the difference in electrostatic potential in the process, and its charge will be transferred to the electrolyte, leading to energy loss and band structure rearrangement (see Fig. 3a). The concentration of the charges in the space charge region depends on the potential difference between the semiconductor and the electrolyte. The potential drop in the space charge region is much more than that in the Helmholtz layer because the former spreads over a large area and exists due to ionization of the acceptor solid, while the latter is built up at the single-atom level away from the electrolyte surface. The inhomogeneous distribution of charges in the interfacial region establishes a BIEF that crosses over the electrode–electrolyte interface (EEI), which can also aid in ion or charge carrier crossing of the interface barrier. In other words, the created electric field produces a "built-in

potential difference". Another significant aspect of such a built-in potential at the interface is to oppose the flow of electrons and holes across the junction, so it is denoted as the potential barrier to establish the device voltage. In practical devices, instead of using two interfaces (anode/electrolyte and cathode/electrolyte), a one-interface device (as shown in Fig. 3b), such as by joining an n-type semiconductor and a p-type semiconductor, can work efficiently (low space charge region) by creating a BIEF to block electron penetration while enabling high ionic transport. This advanced configuration should be employed to construct a device with one electrode by ohmic contact to reduce the polarization loss.

# 3 Semiconductor Electrochemistry in Fuel Cells

Based on the fundamentals of semiconductor electrochemistry briefly discussed in the above section, we further discuss both conventional ion-based electrolytes and semiconductor-based membranes for fuel cells, with an emphasis on how semiconductor-ionic conductors replace conventional ionic electrolytes, resulting in different scientific principles.

Generally, SOFC reactions can be expressed in Kröger-Vink notation as follows: in an $O^{2-}$ conducting electrolyte, the cathode reaction is $0.5O_2 + 2e^- + \rightarrow O_O^x$, and the anode reaction is $H_2 + O_O^x \rightarrow H_2O + 2e^- + V_O^{\cdot\cdot}$, where $V_O^{\cdot\cdot}$ is the oxygen ion vacancy and $O_O^x$ is the lattice oxygen ion in the electrolyte.

In $H^+$ conducting fuel cells, the reaction at the fuel side (anode) is $H_2 \rightarrow 2H^+ + 2e^-$, and that at the air side (cathode) is $2H^+ + \frac{1}{2}O_2 + 2e^- \rightarrow H_2O$. In both cases, the overall cell reaction is $H_2 + \frac{1}{2}O_2 \rightarrow H_2O$. Both anode and cathode materials can now easily be conceptualized as semiconductors in a strongly reducing or oxidizing atmosphere. More importantly, electronic exchange with chemicals or electron/hole transport is crucial to realize electrochemical reactions and current collection. However, semiconducting properties were not explicitly noted until they were addressed by K. Singh in 2013 (see also Fig. 1a) [3]. The electrical conduction behavior of the electrode material of SOFCs changes at different oxygen partial pressures, leading to electron or hole conduction in reducing or oxidizing atmospheres, respectively. A particular example is the perovskite oxide series that has been extensively developed and investigated as electrode materials for SOFCs [18–25]. They have been used as electrode materials to yield reduced material and cell fabrication costs and higher resistance to carbon deposition and sulfur poisoning due to amphiprotic electron and hole conduction under different oxygen partial pressures [26, 27].

## 3.1 Electrolyte-based SOFCs

Regarding the electrolyte materials in SOFCs, significant effort has been put in developing materials with higher ionic conductivity but limited electronic conduction in a fuel cell atmosphere. Indeed, a large number of new oxide ionic conductor materials have been developed and reported in the literature, such as doped ceria [28], $La_{0.9}Sr_{0.1}Ga_{0.8}Mg_{0.2}O_3$ [29], $BaZr_{0.1}Ce_{0.7}Y_{0.2-x}Yb_xO_{3-\delta}$ [30], $Ln_{10}(SiO_4)_6O_3$ [31], calcium-doped $LaNbO_4$ [32], $Na_{0.5}Bi_{0.5}TiO_3$ [33], and $Sr_{1-x}Na_xSiO_{3-0.5x}$ [34]. Most of them show higher ionic conductivity than that of the state-of-the-art electrolyte YSZ, particularly for low-temperature operation. In addition, proton conductors for low-temperature (LT) SOFCs have recently stimulated worldwide interest and research input [23, 25, 35–38]. However, none of these materials can replace YSZ for industrial deployment yet due to the intrinsic issues with these materials, such as the high reactive activity with cell components and instability under fuel cell conditions. In addition, neither YSZ nor the newer generation of $O^{2-}$ or $H^+$ conducting materials can meet the high ionic conductivity demand of 0.1 S cm$^{-1}$ below 600 °C, the so-called LT range. The electrolyte material and resultant system challenges remain in SOFCs.

In parallel, another stream of LT SOFC research involves developing two-phase composite electrolytes that have better ionic conductivity than single-phase electrolytes, as discussed above for single $O^{2-}$ or $H^+$ ion conducting electrolytes, which highly rely on the oxygen vacancy concentration of the oxide matrix. These composite electrolytes originate from ceria-salt composites [39], with a focus on ceria-carbonate composite systems [5, 40–48]. In addition, ceria-carbonate electrolytes have a unique characteristic of hybrid or dual $H^+$ and $O^{2-}$ conduction [5, 48–60], which was even stable over 6000 h [61]. Figure 4 illustrates these three types of ion conducting electrolyte-based SOFC devices. In all these electrolyte-based electrode devices, semiconductors, commonly perovskite oxides, for example, (La,Sr)(Co,Fe)O₃, (La,Sr)MnO₃, (La,Sr)CoO₃, and (Ba,Sr)(Co,Fe)O₃ [62–64, 64, 66], and transition metal oxides, e.g., $LiNiO_2$ and $LiNiCoAlO_2$ [67, 68], are used as electrode materials, and they can be described in the semiconductor electrochemical way as discussed in Sect. 2. Another interesting report given by Kim et al. [69] presented the development of a hybrid solid oxide cell-based mixed $H^+$ and $O^{2-}$ conductive $BaZr_{0.1}Ce_{0.7}Y_{0.1}Yb_{0.1}O_{3-\delta}$ electrolyte for the simultaneous electrolysis of water at the anode and cathode; significantly improved the electrolysis cell performance and stable operation during 60 h of nonstop testing were achieved.

Different from classic heteroelement structural doping, the oxygen ionic conduction in doped ceria occurs through bulk diffusion via oxygen vacancies, while Zhu et al. [68, 70] recently reported that nondoped $CeO_2$ itself acts as a

super proton conductor under fuel cell conditions. The precipitated $CeO_{2-x}$ materials treated at different temperatures (as-synthesized, 600 and 1000 °C) all showed defective particle surfaces with many oxygen defects on the surface according to careful high-angle annular dark-field scanning transmission electron microscopy and electron energy loss spectroscopy analyses. The lower the treatment temperature, the higher the oxygen vacancy concentration is. In addition, a charge depletion layer is formed between the interface of core ceria (intrinsic-type semiconductor, $Ce^{4+}$) and surface ceria (n-type semiconductor, $Ce^{3+}$), which favors superionic conduction. Moreover, the ionic transport through ceria was determined to be a proton conduction contribution instead of an oxygen ion contribution by intentionally adding a pure proton conductor layer between the electrolyte and cathode. An isotopic effect study also supported the claims. Consequently, the constrained surface region of $CeO_{2-\delta}$ is believed to build long-term proton shuttles, suggesting a new methodology for and understanding of the proton transport in general oxides and a promising electrolyte material for new-generation proton ceramic fuel cells.

## 3.2 Semiconductor Membrane Fuel Cells

According to traditional knowledge, electrolytes with partial electronic conductivity will significantly reduce the cell voltage and system energy efficiency [71]. In 1992, Riess proposed the use of mixed ionic and electronic conductors (MIECs) to replace solid-state electrolytes to run SOFCs when the FC is operated close to its maximum power output [72]. More recently, a new research emphasis has been put on using semiconductor oxides, more specifically electronic insulating oxides under an applied fuel cell atmosphere, to substitute conventional ion conducting electrolytes for SOFCs. This research was initiated by the revolutionary inventions called a single-layer fuel cell (SLFC) and an EFFC. In these cases, one-layer semiconductor-ionic conductor composite components can replace the conventional three-layer components of the anode, electrolyte and cathode while providing functions that can make the fuel

cell operate in the same way [73–77]. Such a single-layer material is made of a semiconductor-ionic mixed or heterostructure composite, which leads to the same fuel cell functionality and holds the potential for lower temperature and higher performance applications. Later, a series of semiconductor materials were shown as SLFCs in the same way, e.g., $La_{0.9}Sr_{0.1}InO_{3-\delta}$ [78, 79], $Li_xAl_{0.5}Co_{0.5}O_2$ [80], $SmNiO_3$ [16], $La_{0.2}Sr_{0.25}Ca_{0.45}TiO_3$ [81], $TiO_2$ [82], $LiZnO$ [83], and $Na_{0.5}Bi_{0.5}TiO_3$ [33]. From a classic SOFC perspective, electronic conduction through the electrolyte/membrane will cause significant losses in both cell voltage (open-circuit voltage, OCV) and energy efficiency, while for the semiconductor fuel cell, the fuel cell behavior is not influenced. Generally, the electrical conduction behavior of semiconducting materials is well recognized to be a function of the applied oxygen partial pressure, as seen from the aforementioned symmetric perovskite oxide electrode materials in SOFCs. Moreover, some materials show interesting electronic, pure ionic and hole conduction under low, intermediate and high oxygen partial pressure conditions at a certain temperature [78]. For example, the electrical conductivity of $La_{0.9}Sr_{0.1}InO_{3-\delta}$ changes only slightly with oxygen partial pressures from $10^{-5}$ to $10^{-20}$ between 600 and 800 °C, a typical ionic conduction behavior, while it exhibits typical p-type and n-type semiconducting behavior under higher and lower oxygen partial pressure conditions [78, 79]. The constructed SOFCs based on only the $La_{0.9}Sr_{0.1}InO_{3-\delta}$ material, called SLFCs, gave an OCV of higher than 1.0 V and a maximum power output of 3 mW ● $cm^{-2}$ at 800 °C. However, in such a single layer fuel cell, a functional layer of $La_{0.9}Sr_{0.1}InO_{3-\delta}$ performing as an electrolyte layer remains, which is similar to that in the classic SOFC, its p- and n-type conduction behavior is utilized for electrode functionality.

Therefore, in semiconductor-based fuel cell devices, the working principles built on semiconductor and heterostructure membranes should differ from those of ion electrolyte membrane-based fuel cells. A technical illustration of the difference between classic and newly developed semiconductor-based SOFCs is shown in Fig. 5, which shows the SOFC based on the $O^{2-}$ conducting electrolyte without
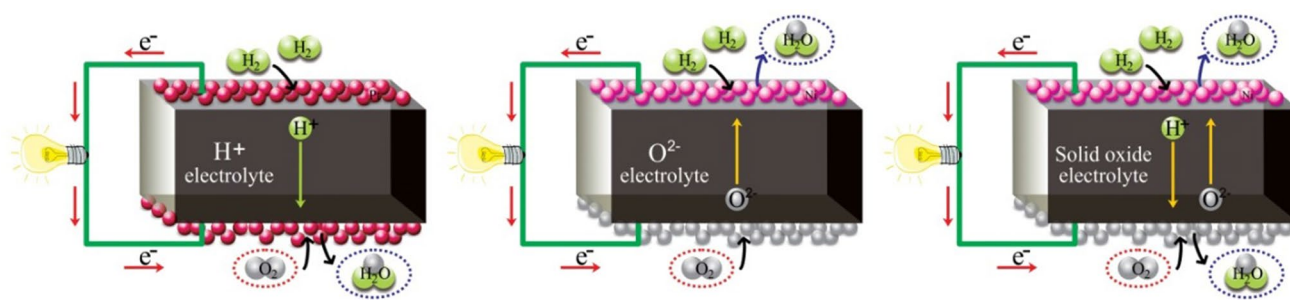


**Fig. 4** Electrolyte-based SOFCs with $O^{2-}$, $H^+$ or hybrid $H^+/O^{2-}$ conducting membranes

electron passage. However, in Fig. 5b, the coexistence of both ions (e.g., the $O^{2-}$ case) and electrons, which is commonly the case in semiconductors and their heterostructures, takes over the electrolyte. Surprisingly, the latter (Fig. 5b) can display even better performance than the electrolyte-based SOFC. This is truly a new phenomenon, and therefore, the semiconductor electrochemistry of fuel cells shows high potential for further deployment. It is naturally introduced in term of semiconductors and physical principles in the following.

Different from the above case, recently, mixed ionic and electronic conducting single-phase oxides have also been transformed into ionic conductors with ionic transfer number close to unity under fuel cell conditions, more accurately by proton incorporation, according to the reports by Lan [80] and Zhou et al. [16]. As a typical LIB electrode, the layered structure $Li_xAl_{0.5}Co_{0.5}O_2$ (LCAO) can accommodate protons in the layer between two transition metal oxide layers or by replacing lithium ions (Fig. 6a). Therefore, the obtained proton-intercalated $Li_xH_yCoO_2$ at the cathode leads to a change in the oxidation states of transition metal ions, which consequently relieves the electronic conduction of traditional semiconducting $LiCoO_2$; the substitution of Co with Al also leads to suppressed electronic conduction in the materials, changing the semiconductor to a pure ionic conductor with an almost unity ionic transfer number.

Similarly, a distinguished work by Zhou et al. [16] reported that the highly electronically conducting perovskite oxide $SmNiO_3$ (SNO) was transformed into a unity-transference ionic conductor under fuel cell conditions ($H_2$, Pt/SNO/Pt, air, Fig. 6b). An in-depth investigation showed that when SNO is exposed to a hydrogen anode, hydrogen dissociates into protons and electrons accompanied by the reduction of $Ni^{3+}$ cations in SNO to $Ni^{2+}$. The proton incorporation into the SNO lattice forms H-SNO because the concentration and potential gradient lead to
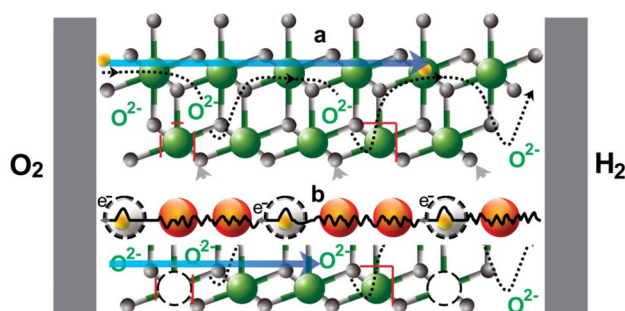
filling-controlled Mott transitions such that electrons are no longer able to transport through the $E_g^2$ manifold because of the large electronic bandgap. Such a transition enables hydrogenated SNO to provide the electrolyte functionality for SOFCs. Moreover, according to experimental measurements, the proton conductivity in H-SNO is higher than that in well-known high proton conductivity $Ba(Ce,Zr)O_3$-based perovskite oxides at reduced temperatures. A micro-SOFC with optimal electrolyte thickness and an active Pt metal electrode gave a maximum power density of 225 mW$\bullet$ cm$^{-2}$ at 525 °C, which is comparable to the best value in the applied temperature range. Therefore, both LCAO and SNO materials eventually transform from high electron (hole) conductors to common proton conducting electrolyte-based fuel cells, i.e., the proton ceramic fuel cell (PCFC) process, even though the SOFC devices are initially constructed as a semiconductor device. Hydrogenation of oxides leads to wide electronic bandgap materials, which is an interesting approach to design and obtain new-generation electrolytes for SOFCs working at low temperatures [4].

Another work by Dong et al. [82] reported that thin film $TiO_2$, a typical semiconductor, could be used as an electrolyte for LT SOFCs. SOFCs based on a $TiO_2$ thin film were fabricated by a spin coating method on an electrode supporter, giving an OCV of 1.1 V and a maximum power output of 364 mW$\bullet$ cm$^{-2}$ at 550 °C. This certificates that typical semiconductors can be used as electrolytes for SOFCs. In this work, Dong proposed the use of the universal energy band principle instead of electronic conduction theory to evaluate the possible application of novel materials for fuel cell and photocatalysis applications. They proposed that the electronic conduction in electrolyte materials should not be blamed if the energy band diagram can be well aligned in a real fuel cell. Under a fuel cell atmosphere, $TiO_2$ possesses a higher CB above the redox potential of $H_2/H^+$ and a lower VB than the redox potential of $O_2/O^{2-}$, which can help effectively block electron transport through the electrolyte. When $TiO_2$ is combined with the electrode material $LiNi_{0.8}Co_{0.15}Al_{0.05}O_2$, a LT high-activity symmetric electrode, the electrons produced at the anode cannot move to the CB of $TiO_2$; therefore, they can only follow the external circuit of the cell and transfer to the cathode, realizing the fuel cell function. The nearly Nernst theoretical voltage and excellent LT power output verified the feasibility and correctness of the adopted approach. More recently, SOFCs using the pure $SrTiO_3$ "electrolyte" delivered a peak power output of 620 mW $\bullet$ cm$^{-2}$ at 550 °C [81, 84, 85], while it is an intrinsic semiconductor and presents a high n-type electronic conductivity. Moreover, the ionic conductivity reached 0.24 S $\bullet$ cm$^{-1}$ at 550 °C, which is higher than that of most current



**Fig. 5** **a** Conventional $O^{2-}$ conduction based on oxygen vacancies in YSZ or ceria electrolyte, and **b** coexistence of electronic and ionic conduction in the semiconductor or its heterostructure material membranes
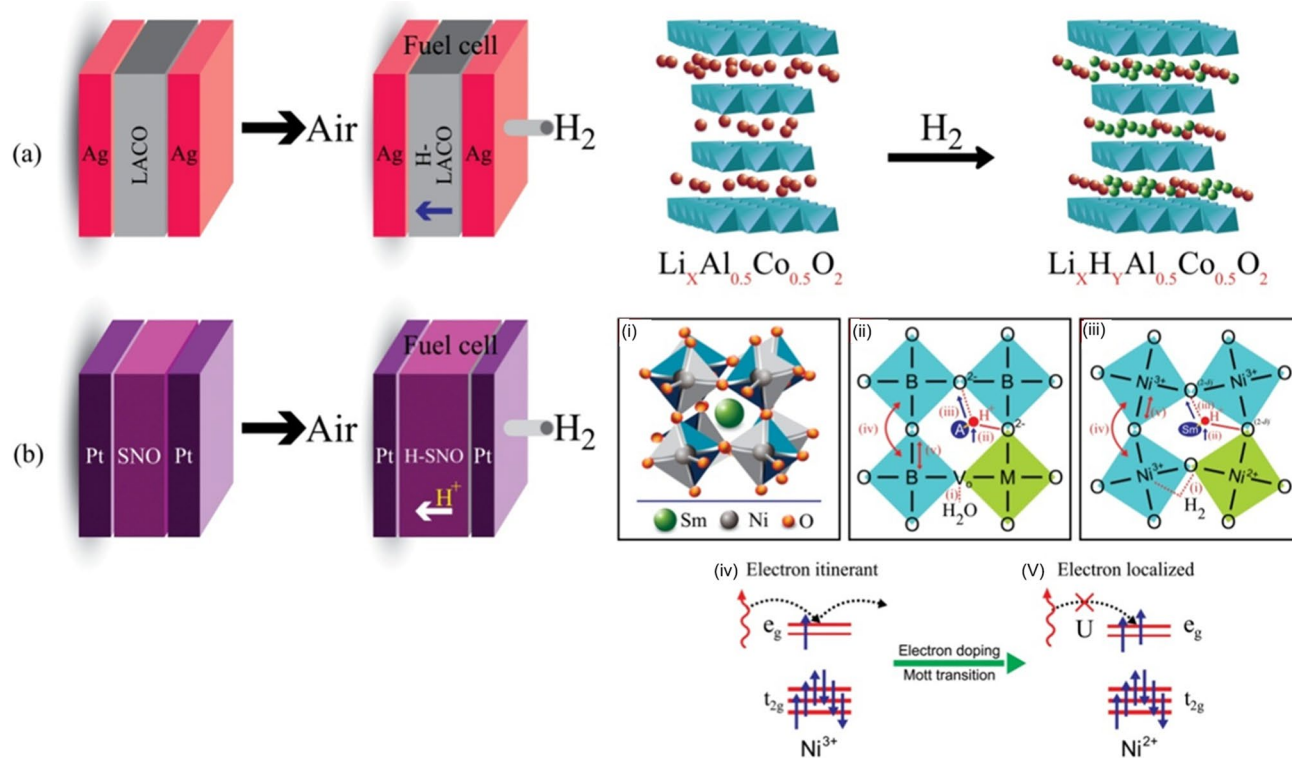
**Fig. 6** Working principle of SLFCs operated based on existing SOFC science, i.e., ionic (in the case of H$^+$ conduction) electrolyte devices formed during in situ fuel cell operation, regardless of the construction of the semiconductor layer configuration. **a** For the LCAO case.

Reproduced with permission from Ref. [80]. Copyright 2014 Wiley–VCH. **b** For the SNO case. Reproduced with permission from Ref. [16]. Copyright 2016 Springer Nature

single-phase pure solid-state ionic conductive electrolyte materials. A deep examination of the material texture and morphology confirmed that a superhigh ionic conductivity layer with an amorphous structure is formed on the surface of SrTiO$_3$ [85]. Regardless, the superior electrochemical activity suggests a new approach for LT SOFC applications.

### 3.3 Semiconductor Heterostructure Materials

Commonly, compared to the single-phase electrolyte drawback that it cannot meet all the strict requirements for reliable, robust and durable SOFCs, semiconductor heterostructures with one ionic material or another semiconductor phase incorporated can provide better performance, such as higher ionic conductivities, than conventional electrolytes and increase the triple-phase boundary for electrode reactions [1, 86]. For example, bulk p-n heterostructure materials have been proposed to tune semiconductors to superionic conduction because the p and n materials can balance free electrons/holes, thus suppressing electron leakage and resulting in no net electrons [17, 67, 87–95]. Compositing p-type LiZnO with the ionic conductor doped ceria (n-type under fuel electrode conditions) for LT SOFCs has been

reported. Interestingly, this bulk hybrid electrolyte exhibits superionic conductivity (> 0.1 S • cm$^{-1}$ over 300 °C) and excellent electrolytic performance (400–630 mW • cm$^{-2}$) between 480 and 550 °C. Unexpectedly, the hybrid semiconductor shows net-electron-free transport in the electrolyte, as reflected by the sufficient OCV under H$_2$/air fuel cell conditions. Later, as demonstrated by Zhu et al. [77] and Wang et al. [89], fuel cells based on the planar/bulk n-type/p-type semiconducting heterostructure gave impressive fuel cell performance under H$_2$/air conditions. Wu et al. [96] synthesized a ZnO/SrTiO$_3$ semiconductor by a hydrothermal method and used it as a photocatalytic hydrogen production catalyst and a fuel cell "electrolyte layer". The photocatalytic cell based on this n/n-type semiconducting heterostructure gave a H$_2$ production rate of 1317.44 μmol • g$^{-1}$ within 5 h under solar-light irradiation and an OCV of 1.14 V, and SOFCs presented a maximum power density of 564 mW • cm$^{-2}$ at 550 °C. In the interesting work by Cai et al. [97], they composited all the materials in a typical SOFC, such as a Ni(O)-YSZ anode, a YSZ electrolyte and an LSM-YSZ cathode, to identify each component that could function as a semiconductor-ionic membrane for electrolyte functioning. They also made an 'all-components-in-one' fuel cell, and the complex hybrid heterostructure layer with the NCAL

electrode displayed a three times higher device performance than the conventional YSZ electrolyte-based fuel cell under the same operating conditions (temperature and fuel/oxidant partial pressure). The "all-in-one" heterostructures appear to have much better ionic transport properties than existing ionic materials by creating a motorway for ionic transport along the semiconductor and ionic interfaces, which normally contain a space charge layer and present band bending and an induced BIEF, facilitating ionic transport/transfer, which cannot be manipulated by single-phase materials.

Moreover, an EFFC can be superior to traditional electrochemical fuel cells due to the physical removal of the conventional ionic electrolyte layer and two physical interfaces between the electrolyte and the electrodes (the anode/the cathode). In particular, in semiconductors and heterostructures, coupling interactions between charge carriers, electrons (holes) and ions impact ionic transport and redox reactions from the conventional macro-redox in three-layer devices to the nano-redox in single-layer configuration devices (as shown in Fig. 2f) as new-generation energy devices. These results suggest that semiconductor electrochemistry could play an important role in improving the fuel cell performance and developing new science and technology to continuously increase fuel cell R&D [1, 2]. By integrating the band structure and alignment fundamentals into fuel cell design, many new energy devices/technologies jointly harnessing semiconductors and electrochemistry have been demonstrated with plentiful examples. In addition, band alignment can also make significant contributions to speed up the HOR and ORR by adjusting the reactant and intermediate phase absorption energies, thus lowering the required activation energy, which has been commonly demonstrated in the photochemical water splitting process and other related fields [15, 98]. From a reaction product aspect, facilitating fuel cell functions for a reversible process via photochemical water splitting to $H_2$ and $O_2$ is desirable to generate $H_2O$ and simultaneously produce electricity. These new emerging trends of semiconductors and the associated methodologies have changed the fuel cell electrochemistry and brought new scenarios for fuel cell R&D toward semiconductor-fuel cell science, which may pave the commercialization roadmap for SOFCs and impact other areas in chemistry, such as photocatalysis/electrolysis and batteries.

Without the ion conducting/electron insulating layer, a key question arises: how does such a device work? In fact, various semiconductors and heterostructures have been widely applied without by using the traditional anode/electrolyte/cathode structure based on multiple built-in junctions. These devices have been developed by introducing new functional semiconductor materials or a semiconductor with an ionic conductor to form heterostructures. Figure 7 presents an overview of these novel fuel cells based on three-layer, two-layer, and single-layer structures. A three-layer

fuel cell device (Fig. 7a) employs a semiconductor (S) or a semiconductor heterostructure ($S^+$) membrane instead of the sole ionically conductive electrolyte, but it can be tuned to an ion conducting electrolyte (function) via a semiconductor-ionic conductor transition in the fuel cell environment. This device has the three-layer configuration of the anode (n-semiconductor or metal)/S or $S^+$/cathode (p-semiconductor). The abovementioned LCAO and SNO fuel cells belong to this type. This configuration may also include an electrolyte layer because the ionic conductor or wide bandgap semiconductor can be treated/tuned as an electrolyte [2]. Fig. 7b illustrates the fuel cell device constructed by using only two layers, an anode and a cathode; refer to Fig. 7b for a planar p–n junction device. Conventional SOFC technology commonly uses a three-layer structure, two electrodes using a mixture of semiconductor oxides, e.g., NiO for the anode and perovskite oxide for the cathode, and an ionic electrolyte, e.g., doped ceria or zirconia, to enhance the ionic conductivity in the electrodes and effectively minimize the electrode polarization while enhancing the power output. The double-layer device was previously reported [77] and has been verified by other interesting research work. These devices were constructed by using typical SOFC components/layers in contact without an electrolyte between them. By removing the middle electrolyte layer, the fuel cell can still function due to the p–n junction principle.

In the new semiconductor approach, as illustrated in Fig. 7c, the configuration looks very similar to that of the SOFC electrode component of mixed electrolyte and electrode materials: all three layer materials of anode, electrolyte, and cathode (where the anode and the cathode could be the same material, leading to symmetrical fuel cells) can function within a single component, i.e., the "three-in-one" type device [99], outperforming the traditional three-layer fuel cell functions, thus stimulating significant industrial and fundamental research interest with remarkable and additional contributions to fuel cell science and technology. From a technical aspect, the bulk heterojunction (BHJ) requires delicate nanoengineering to tailor the n and p conducting properties at the nanolevel using heterostructure composite technology.

In later developments, metal–semiconductor-based Schottky junctions were discovered to have a significant impact on fuel cell performance [100]. The Schottky junction fuel cell device, as shown in Fig. 7d, is constructed using only one type of semiconductor, either n- or p-type (more commonly) or a semiconductor-ionic heterostructure composite, as reported [100, 101]. In this case, a Schottky barrier is formed between the anodic reduced metal/alloy surface and a single layer of the p-type (or n-type) semiconductor (Fig. 7d), thus preventing electrons from passing through the device internally. Moreover, by applying energy band design/alignment to design fuel cells as a new
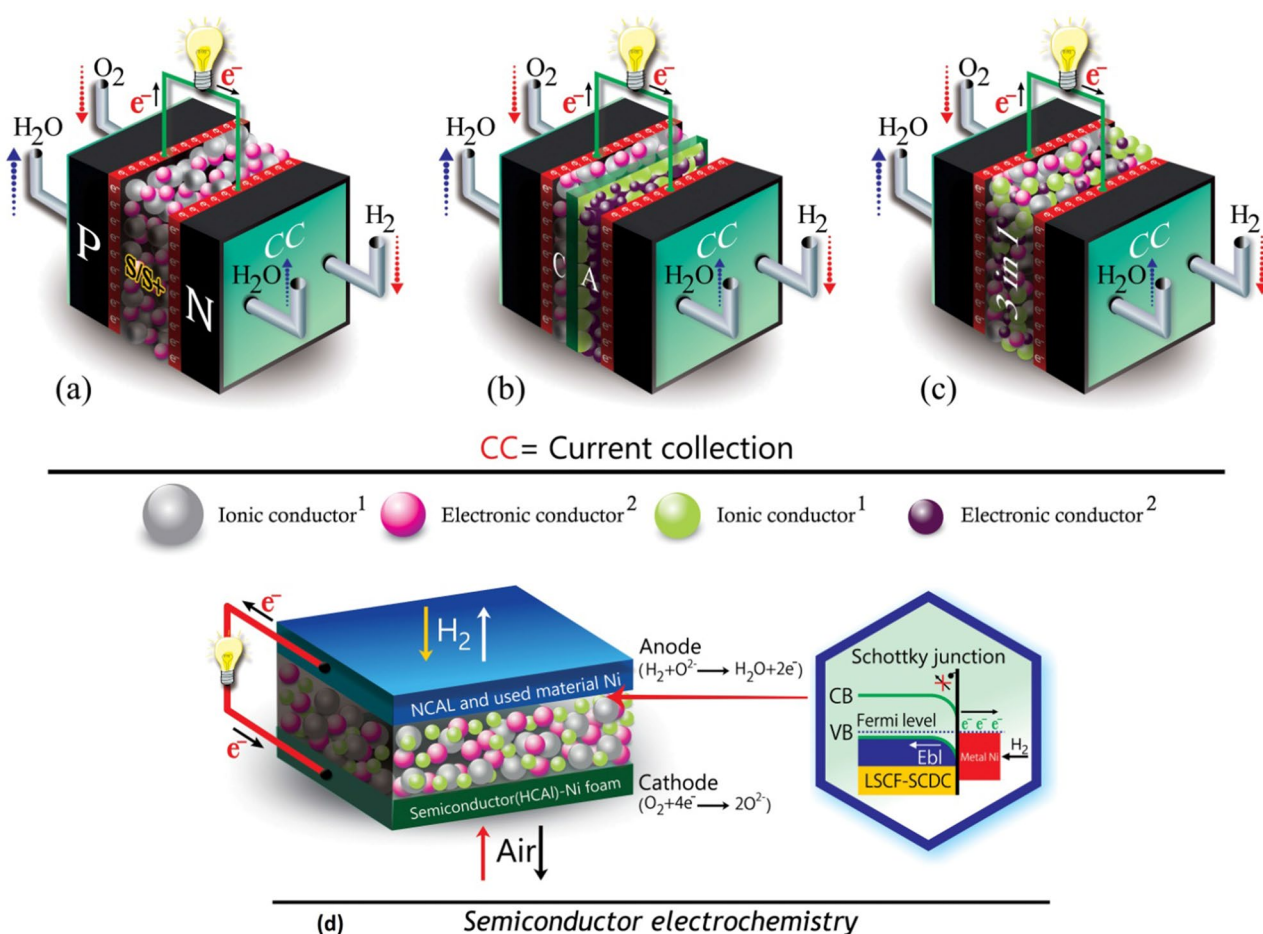
**Fig. 7** Schematic illustration of (**a**) a three-layer fuel cell device consisting of an n-semiconductor anode/semiconductor (S) or semiconductor heterostructure (S⁺) membrane/p-semiconductor cathode; (**b**) a two-layer fuel cell: A, anode; C, cathode; and (**c**) a 3-in-1 SLFC device. CC stands for current collection. All cases are considered with both $H^+$ and $O^{2-}$ conduction; in the case of only one type of ions, either $H^+$ or $O^{2-}$, the corresponding $H_2O$ formation is only on one side, the former in the cathode ($O_2$, which can be air) and the latter in the anode. Reproduced with permission from Ref. [77]. Copyright 2011 RSC. (**d**) Fuel cell constructed by a Schottky junction device, in which the Schottky junction barrier is caused by band bending at the metal/semiconductor (electrolyte) interface

fuel-to-electricity conversion technology, the performance can arguably surpass that of fuel cells [102]. The designed energy band and alignment based on PSC science can isolate the device (Fig. 8a, b), avoiding the electronic short-circuiting problem and simultaneously generating electricity with high power outputs > 1000 mW • cm⁻² at 550 °C. There is a unique charge separation mechanism, discovered by Zhu et al. [103], as shown in Fig. 8c.

This can be a general methodology for new conversion devices based on semiconductors and principles. In the latest research, Dong et al. [82] also used the same strategy to construct a fuel cell with $TiO_2$ as the electrolyte. They claimed that electronic conduction in electrolyte materials should not be blamed if the energy band diagram can be well aligned in a real fuel cell. In the fuel cell, the CB of the electrolyte, either a pure ionic conductor or a semiconductor, should be higher than the redox potential of $H_2/H^+$; therefore, the

electrons cannot jump to the CB of the electrolyte, or are blocked by the electrolyte layer. $TiO_2$ is a typical semiconductor with great application potential in photovoltaics and photoelectrochemistry [104–108]. At first glance, the use of $TiO_2$ will cause the short-circuiting issue in fuel cell conditions. This does not happen in this fuel cell case since $TiO_2$ possesses a higher CB above the redox potential of $H_2/H^+$ and a lower VB than the redox potential of $O_2/O^{2-}$ [98, 105, 109, 110], which can help effectively block electron transport through the electrolyte. When combined with the advanced NCAL symmetric electrode for demo-SOFCs, the reduced electrode materials in the anode have a lower CB than the redox potential of $H_2/H^+$ and a higher VB than the redox potential of $O_2/O^{2-}$. The electrons and holes can easily move to and be collected in the electrode. Such a fuel cell device has been successful demonstrated, delivering 1.10 V (OCV) and 364 mW cm⁻² at 550 °C under hydrogen/air

**Fig. 8 a** Nanoparticle contacts between the LSCF and Sm and Ca co-doped Ceria (SCDC), **b** energy diagram of the p–n BHJ for charge separation on the H$_2$ contact side at the particle level, and **c** energy band diagram at the device level. Reproduced with permission from Ref. [103]. Copyright 2017 Elsevier
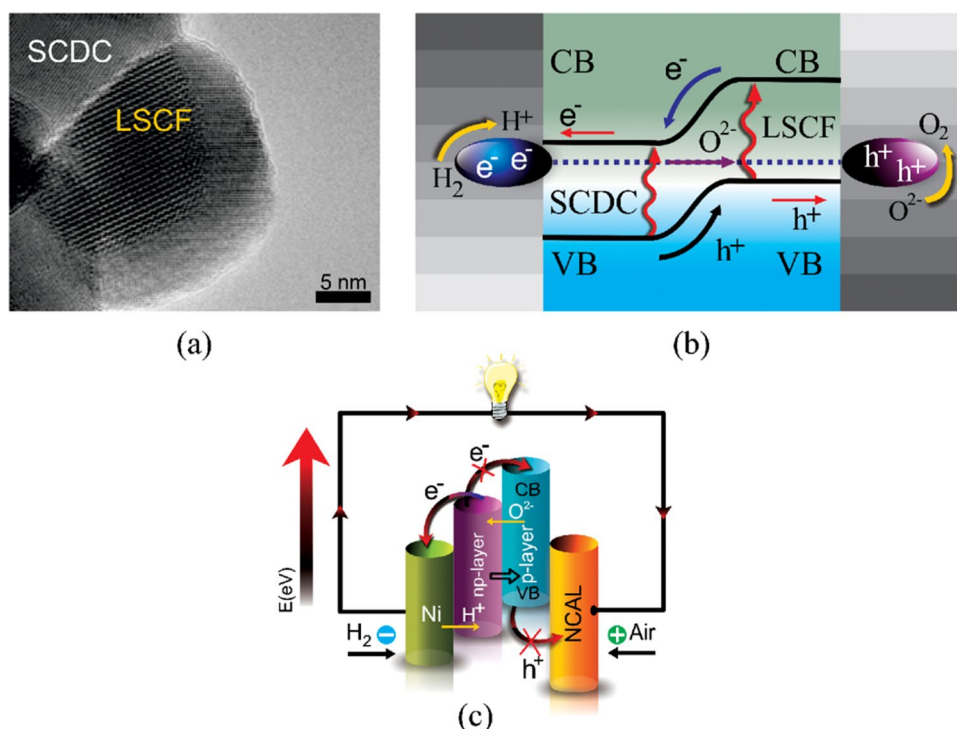
conditions. The nearly Nernst theoretical voltage and excellent power output have verified the proposed methodology. Electronic conduction in electrolytes could be well managed by properly choosing the electrode material based on the energy band diagram method [111, 112]. More details will be further discussed in Sect. 5.

To this end, a summary of the developed semiconductor and/or heterostructure material-based fuel cells and their corresponding electrical properties, including ionic conductivity and fuel cell electrochemical performance, is presented in Table 1. The ionic conductivities of semiconductor or heterostructure materials are much higher than those of single-phase oxide ion conducting electrolytes, which enables superior fuel cell electrochemical performance at low temperatures. Semiconductor-based fuel cells may suggest an alternative promising approach to develop next-generation SOFCs or PCFCs.

# 4 Semiconductors and Semiconductor Electrochemistry in Batteries

## 4.1 LIB as a Typical System

Extensive examples of employing semiconductor bands and physics in electrochemistry can be widely found. One of the featured fields is the rechargeable batteries or secondary batteries, such as LIBs, Na-ion batteries, and Zn- and Mg-ion batteries, which reversibly convert electrical and chemical energy via redox reactions, thus storing electrical energy as a chemical potential in their electrodes [122, 123]. Metal ions are reversibly transported between the anode and cathode and through the electrolyte, releasing or storing energy. Generally, the specific capacity of electrodes and the working voltage of the battery determine the energy density of these devices, i.e., the differential chemical potentials between the cathode and the anode. In these typical electrochemical devices, semiconductor properties and band theories provide a new comprehensive understanding of the scientific principles for improving the electrochemical reaction kinetics to increase the rate performance. Taking the LIB as a typical system, Fig. 9 shows an example of understanding the lithium battery electrochemistry and cathode (positive electrode) materials from the semiconductor band structure and physics (Fig. 9a). The LiCoO$_2$ positive electrode (cathode) energy as a function of the density of states, being relevant to the Fermi level of Co$^{4+/3+}$ redox couples, is presented in the device energy level diagram with respect to the highest occupied molecular orbital (HOMO) and the lowest unoccupied molecular orbital (LUMO) of the liquid electrolyte, as shown in Fig. 9b [124]. The battery voltage, i.e., the OCV $V_{OC}$ can be expressed as $V_{OC} = (\mu_c - \mu_a)/e$, where e is the magnitude of the electronic charge and the difference in chemical potential between the anode (a) and the cathode (c).

Normally, this working voltage is also determined by the electrochemical window of the electrolyte (see Fig. 9b), which is controlled by the energy gap between the HOMO

**Table 1** Electrical properties of the applied semiconductor-based fuel cells

| Number | Semiconductor materials | Fuel cell configuration | Ionic conductivity | Fuel cell electrochemical performance | References |
|---|---|---|---|---|---|
| 1 | $La_{0.9}Sr_{0.1}InO_{3-\delta}$ | $Pt/La_{0.9}Sr_{0.1}InO_{3-\delta}/Pt$ | $7.6 \times 10^{-3}$ S $\bullet$ cm$^{-1}$@900 °C | 3 mW $\bullet$ cm$^{-2}$ at 800 °C | [78, 79] |
| 2 | $Li_xAl_{0.5}Co_{0.5}O_2$ | $Ag/Li_xAl_{0.5}Co_{0.5}O_2$(0.79 mm)/ Ag | 0.1 S $\bullet$ cm$^{-1}$ at 500 °C | 173 mW $\bullet$ cm$^{-2}$ @525 °C | [80] |
| 3 | $SmNiO_3$ | $Pt/SmNiO_3/Pt$ | 2.17E-3 S $\bullet$ cm$^{-1}$@500 °C | 225 mW $\bullet$ cm$^{-2}$ at 500 °C | [16] |
| 4 | $La_{0.2}Sr_{0.25}Ca_{0.45}TiO_3$-SDC | Ni/LSCT-SDC/NCL | – | 175 mW $\bullet$ cm$^{-2}$ at 550 °C | [81] |
| 5 | $TiO_2$ | $NCAL/TiO_2/$ NCAL | – | 364 mW $\bullet$ cm$^{-2}$ at 550 °C | [82] |
| 6 | SDC-LiZnO | Ni/SDC-LiZnO/LiNiO | > 0.1 S $\bullet$ cm$^{-1}$ over 300 °C | 400–630 mW $\bullet$ cm$^{-2}$ at 480–550 °C | [17] |
| 6 | LiZnO | NCAL-pasted Ni/LiZnO/ NCAL-pasted Ni | 0.028–0.087 S $\bullet$ cm$^{-1}$ at 550 °C | 138–443 mW $\bullet$ cm$^{-2}$ at 425–550 °C | [83] |
| 7 | $Na_{0.5}Bi_{0.5}TiO_3$ | - | ~0.01 S $\bullet$ cm$^{-1}$ at 600 °C | – | [33] |
| 8 | Core–shell $CeO_2$-$CeO_{2-x}$ | $Ni-NCAL/CeO_2-CeO_{2-x}/NCAL-$ Ni | 0.16 S $\bullet$ cm$^{-1}$ @520 °C | 697 mW $\bullet$ cm$^{-2}$ @ 520 °C | [68] |
| 9 | BZCFY-ZnO | NCAL-Ni/BZFCY-ZnO/NCAL- Ni | 0.07 to 0.20 S $\bullet$ cm$^{-1}$ at 400–500 °C | 248–643 mW $\bullet$ cm$^{-2}$ at 400–500 °C | [67] |
| 10 | LSCF-SDC | Ag/NCAL/LSCF-SCDC/NCAL/ Ag | – | 1080 mW $\bullet$ cm$^{-2}$ at 550 °C | [102, 103] |
| 11 | 3C-SiC/ZnO | NCAL/3C-SiC-ZnO/NCAL | 0.12 S $\bullet$ cm$^{-1}$ | 270 mW $\bullet$ cm$^{-2}$ at 550 °C | [113] |
| 12 | $SrFe_{0.75}Ti_{0.25}O_{3-\delta}-$ $Sm_{0.25}Ce_{0.75}O_{2-\delta}$ | $NCAL/SrFe_{0.75}Ti_{0.25}O_{3-\delta}-$ $Sm_{0.25}Ce_{0.75}O_{2-\delta}/NCAL$ | 0.1 S $\bullet$ cm$^{-1}$ at 520 °C | 920 mW $\bullet$ cm$^{-2}$ at 520 °C | [114] |
| 13 | $La_{0.65}Sr_{0.3}Ce_{0.05}Cr_{0.5}Fe_{0.5}O_{3-\delta}$-SDC | NCAL/ $La_{0.65}Sr_{0.3}Ce_{0.05}Cr_{0.5}Fe_{0.5}O_{3-\delta}$-SDC/NCAL | – | 837 mW $\bullet$ cm$^{-2}$ at 550 °C | [115] |
| 14 | Nanocrystalline structure $Gd_{0.1}Ce_{0.9}O_2$ | NCAL/0.5 mm $Gd_{0.1}Ce_{0.9}O_2/$ NCAL | 0.37 S $\bullet$ cm$^{-1}$ at 520 °C | 591.8 cm$^{-2}$ at 550 °C | [116] |
| 15 | $SrTiO_3$ | $NCAL/SrTiO_3$(STO)/NCAL–Ni | 0.16–0.24 S $\bullet$ cm$^{-1}$ at 450–550 °C | 0.31–0.62 W $\bullet$ cm$^{-2}$ at 450–550 °C | [84, 85] |
| 16 | $Ce_{0.8}Sm_{0.2}O_{2-\delta}$ and $SrTiO_3$ | NCAL-Ni/SDC–STO/NCAL-Ni | 0.05–0.14 S $\bullet$ cm$^{-1}$ at 450–550 °C | 1.1 V 892 mW $\bullet$ cm$^{-2}$ | [93] |
| 17 | Natural hematite ore composited with ZnO | NCAL-Ni/composite/NCAL-Ni | – | 580 mW $\bullet$ cm$^{-2}$ at 550 °C | [117] |
| 18 | La/Pr codoped $CeO_2$-ZnO | NCAL-Ni/LCP-ZnO/NCAL-Ni | 0.08–0.29 S $\bullet$ cm$^{-1}$ at 475–550 °C | 1055 mW $\bullet$ cm$^{-2}$ at 550° | [118] |
| 20 | $La_{0.25}Sr_{0.75}TiO_3$ | $NCAL-Ni/La_{0.25}Sr_{0.75}TiO_3/$ NCAL-Ni | 0.221 S $\bullet$ cm$^{-1}$ at 550 °C | 908.2 mW $\bullet$ cm$^{-2}$ at 550 °C | [84] |
| 21 | NiO-YSZ-LSCF | NCAL-Ni/NiO-YSZ-LSCF/ NCAL-Ni | – | 1055 mW $\bullet$ cm$^{-2}$ at 550 °C OCV: 1.04 V | [97] |
| 22 | Hematite/$LaCePrO_x$-$La_{0.6}Sr_{0.4}Co_{0.2}Fe_{0.8}O_{3-\delta}$ | NCAL-Ni/hematite/$LaCePrO_x$-$La_{0.6}Sr_{0.4}Co_{0.2}Fe_{0.8}O_{3-\delta}$/NCAL-Ni | 0.153 S $\bullet$ cm$^{-1}$ at 600 °C | 303–662 mW $\bullet$ cm$^{-2}$ at 500 – 600 °C | [119] |
| 23 | Hematite-$La_{0.6}Sr_{0.4}Co_{0.2}Fe_{0.8}O_{3-\delta}$ | NCAL-Ni/composite/NCAL-Ni | 0.026 to 0.084 S $\bullet$ cm$^{-1}$ at 400–600 °C | 467 mW $\bullet$ cm$^{-2}$ at 600 °C | [120] |
| 24 | $Ba_{0.5}Sr_{0.5}Co_{0.8}Fe_{0.2}O_{3-\delta}$-$Sm_{0.2}Ce_{0.8}O_{1.9}$ | NCAL-Ni/composite/NCAL-Ni | – | 655 mW $\bullet$ cm$^{-2}$ at 550 °C | [101] |
| 25 | 3(H-PSCFN)–7LNSDC | Ag/3(H-PSCFN)-7LNSDC/Ag | – | 161.80 mW $\bullet$ cm$^{-2}$ at 600 °C | [90] |
| 26 | LiNiCuZn(Fe)-oxide-NKSDC mixture/BSCF–SDC | Ag/LiNiCuZn(Fe)-oxide-NKSDC mixture/BSCF–SDC/ Ag | – | 600 mW $\bullet$ cm$^{-2}$ at 550 °C | [77] |
| 27 | $LiNi_{0.8}Co_{0.15}Al_{0.05}O_2$/terbium-doped ceria | $Ag/LiNi_{0.8}Co_{0.15}Al_{0.05}O_2/$ terbium-doped ceria/Ag | – | 230 mW $\bullet$ cm$^{-2}$ at 500 °C | [89] |

**Table 1** (continued)

| Number | Semiconductor materials | Fuel cell configuration | Ionic conductivity | Fuel cell electrochemical performance | References |
|---|---|---|---|---|---|
| 28 | $La_{0.6}Sr_{0.4}Co_{0.2}Fe_{0.8}O_{3-\delta}$-$Ca_{0.04}Ce_{0.80}Sm_{0.16}O_{2-\delta}$ $Ca_{0.04}Ce_{0.80}Sm_{0.16}O_{2-\delta}$ | NCAL-Ni/composite/NCAL-Ni | 0.188 S $\bullet$ cm$^{-1}$ at 600 °C 0.039 S cm$^{-1}$ at 600 °C | 814 mW $\bullet$ cm$^{-2}$ | [121] |

*NCAL: $Ni_{0.8}Co_{0.15}Al_{0.05}LiO_2$; SDC: $Sm_{0.2}Ce_{0.8}O_2$



**Fig. 9** **a** Schematic energy level diagram for a lithium cell; **b** with LiCoO$_2$ as the cathode and lithium as the anode, illustrating the origin of Voc and relative energy positions with respect to the HOMO and the LUMO of the liquid electrolyte. The Fermi level of the lithium anode is drawn above the LUMO of the electrolyte, indicating that reduction of the electrolyte is usually observed. Note that the Fermi level of the cathode shifts downward during deintercalation. **c** Electronic band structure of LiCoO$_2$ (Li = 1, left), Li$_{0.5}$CoO$_2$ (Li = 0.5, middle) and CoO$_2$ (Li = 0, right), as deduced from DFT calculations and experimental measurements. Reproduced with permission from Ref. [126]
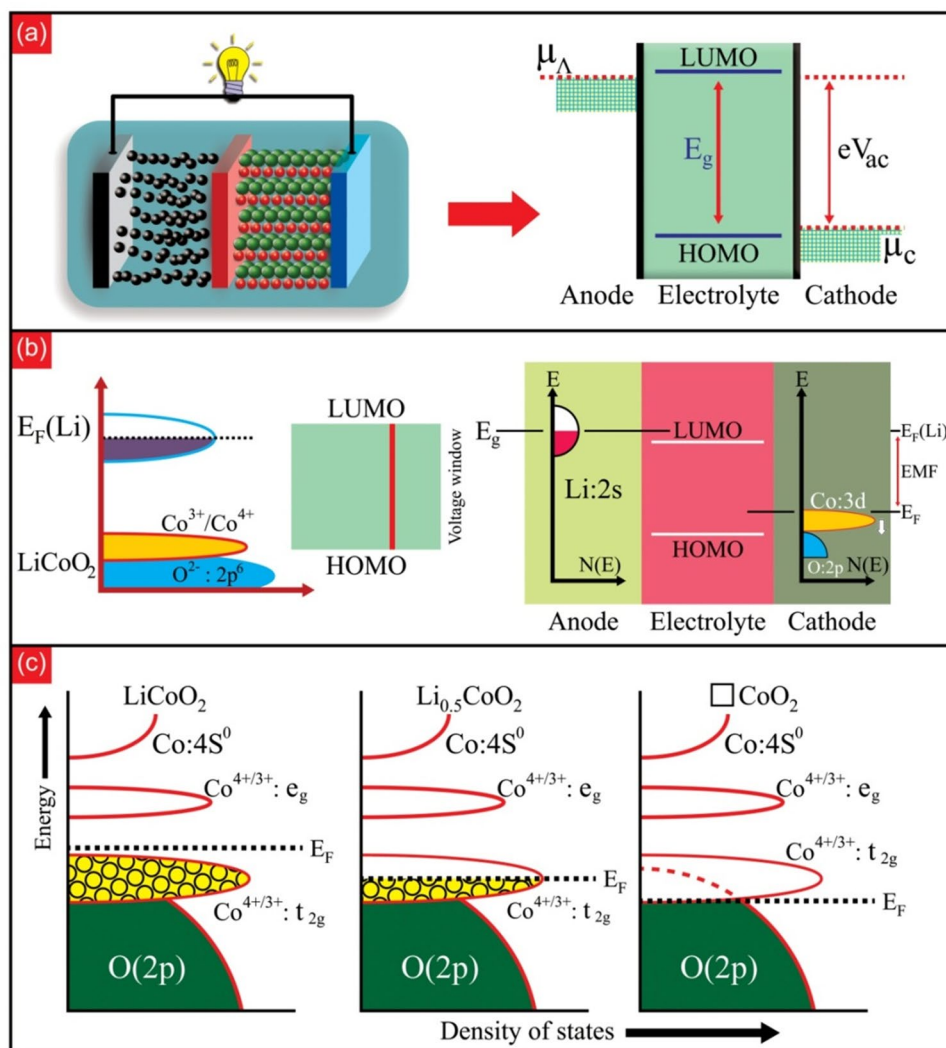
and the LUMO. To work properly, the anode and cathode materials must follow the rule that $\mu_a$ is below the LUMO and $\mu_c$ is above the HOMO; otherwise, the electrolyte will be reduced on the anode surface or oxidized in the cathode zone, forming a passivating solid electrolyte interphase (SEI) film [125]. From a physical point of view, one may relate the cell voltage to the difference in the (electro)chemical potential of the electrons between the cathode and anode, as given by the position of their Fermi levels (see Fig. 9a). However, we should keep in mind that the Fermi level

(electron chemical potential) of (single) electrode materials in the discussion of electrode potentials is not exact but quite often provides reasonable accuracy and results.

In Ensling's work, the authors highlighted the significance of the (partially) covalent character of the device capacity and stability as well as electrode kinetics after investigating the electronic structure of the LiCoO$_2$ cathode materials. Figure 9c presents three typical structures of LiCoO$_2$ (Li = 1, left), Li$_{0.5}$CoO$_2$ (Li = 0.5, middle) and CoO$_2$ (Li = 0, right) after Li$^+$ removal from the LiCoO$_2$ structure
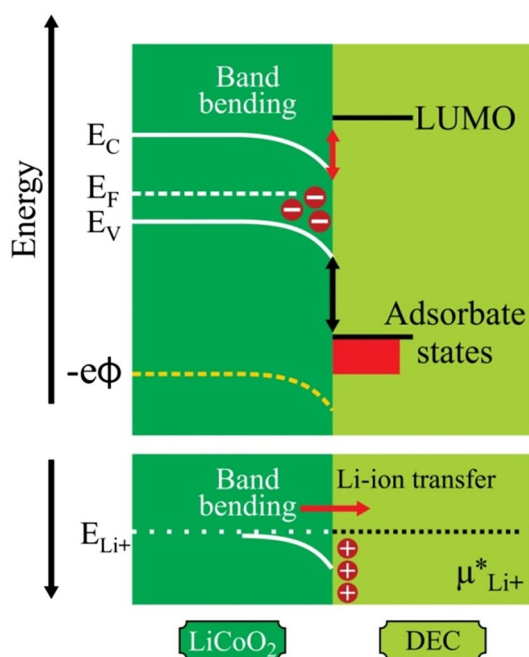
**Fig. 10** Electron and ion energy level diagram of the LiCoO₂/DEC interface established from LT adsorption of DEC (alkyl carbonate solvent) electrolyte. DEC: diethyl carbonate. Note that the Li-ion levels are deduced from theoretical considerations. Reprinted with permission from Ref. [130]. Copyright 2014 ACS

with different electronic bands, along with the differences in the chemical instability with respect to oxygen loss due to the overlapping of the $Co^{4+/3+}$:$t_{2g}$ band with the O 2p orbitals. The changes within the structure and occupation of the density of states (DOS) of $Li_xCoO_2$ during deintercalation are schematically summarized. The Fermi level (EF) reaches a critical value when the Co 3d states ($Co^{4+/3+}$ couple) cross the top of the O 2p bands, which is accompanied by hole transfer to the O 2p states. A significant number of electrons can be removed from the O 2p band, leading to oxidation of Co ions and/or formation of oxygen vacancies, which is not favored for cathodic durability. Therefore, the proximity in energy of the $t_{2g}$ and O 2p bands determines the intrinsic voltage limit for the LiCoO₂ cathode material [126]. The loss of oxygen from the lattice in the $Li_{1-x}CoO_2$ system may explain the limited capacity (140 mAh • g⁻¹), which is significantly lower than the theoretical value. Therefore, investigating the metastable character of partially deintercalated semiconductors of $Li_xCoO_2$ is very important for the device process kinetics and durability, where the band structure plays an important role.

In the LIB field, further improvements in electrodes and cells are generally limited by an incomplete understanding of the interfaces, involved charge transfer, charge compensation, and chemical reaction processes. Much attention has been paid in the past to the electric potential gradient at the

interface, although double (dipole) layers can have a significant impact on the energy level (mis)alignment [127]. Additionally, for ionic phases with low charge carrier concentrations, diffuse charge layers (space charge layers) are encountered at interfaces [128], which induce band bending and related charge carrier concentration changes that have a significant impact on the charge transfer rate and interface stability. Figure 10 shows an energy level diagram for the LiCoO₂/diethyl carbonate (DEC) (alkyl carbonate solvent) electrolyte interface with a focus on the formation of the electrochemical double layer. Li ions are generally aligned with the ionic electrochemical potential of Li⁺ in the two phases (the chemical potential of Li ions is initially very low in the DEC adsorbate phase). According to theoretical considerations, the Li-ion energy level is bent in the opposite direction to the electron energy levels due to the opposite charge of the ion. With such an energy level diagram, the interface and its kinetic properties can be understood, as it contains energy level offsets as well as any charge carrier concentration changes, as evidenced by band bending [129].

### 4.1.1 Band Theory for Tuning from Semiconducting to Ion Conducting Electrolytes

Currently, efforts are mainly devoted to the development of new solid-state electrolytes, such as oxide and sulfide, to increase the energy density and safety of lithium batteries. However, the ionic conductivity in solid-state ionic electrolytes is much lower than that in liquid electrolytes. The traditional design of ionic conductors is primarily based on substitutional doping of dissimilar valence cations into the unit lattice of the structure, resulting in inherent limits on the dopant concentration and thereby ionic conductivity. Recently, a very interesting example of applying semiconductors and electronic states to batteries is the strongly correlated perovskite SmNiO₃ (SNO), which shows applicable lithium ion conductivity at room temperature. SNO has a metal conduction nature and can be electrochemically transformed by Li⁺ injection from an electronic conductor to an electronic insulator and a superior Li⁺ conductor as the electrolyte for a LIB [131]. Based on extensive experimental and theoretical calculations [131], Li⁺ ion shuttling and simultaneous suppression of electronic transport via the Mott transition are induced in such a system, which provides an alternative approach to develop novel LIBs or other energy devices.

Figure 11a–c shows that a large amount of mobile Li⁺ can be found in an electrochemically lithiated SmNiO₃ (Li-SNO) system, which is located in interstitial sites of the perovskite, approaching one dopant ion per unit cell, accompanied by significant lattice expansion. Such interstitially inserted Li⁺ ions can facilitate fast Li⁺ conduction associated with a lower activation energy in comparison with the structural

case. Figure 11b presents a design principle for solid-state Li$^+$ conductors based on SNO. Pristine SNO is a narrow gap semiconductor after lithiation, i.e., the lithium-doped/inserted thin film SNO (Li-SNO), then transforms into an insulator, with a gap of approximately 3 eV (Fig. 11c). First-principles density functional theory (DFT) calculations showed that the pristine SNO exhibits a monoclinic cell without distortion, while with lithium entering SNO, Ni$^{3+}$ is converted to Ni$^{2+}$, resulting in a much different total DOS (Fig. 11d).

The Li$^+$-inserted Li-SNO has an expanded structure that allows for a 3D interconnected Li$^+$ diffusion channel, and the interstitial Li$^+$ is weakly bonded with oxygen ions, therefore exhibiting fast Li$^+$ conduction behavior. Accompanying this transition, the pristine SNO shows insulation due to suppression of electron transport in SNO. The Li$^+$ conductivity was determined to be $3.1 \times 10^{-3}$ S·cm$^{-1}$ at room temperature with an activation barrier of ~0.24 eV. The corresponding Li-SNO battery demonstrated LIB capacity and good lithiation and delithiation cycle life with average coulombic efficiency of 96.8%. This work provides evidence for ion shuttling in

the lattice and atomistic pathways [132–134]. Moreover, this strategy can be extended to other ions, such as Na$^+$, demonstrating the generality of the approach.

A theoretical design of the Li$^+$ conductor could be based on wide bandgap semiconductors. Wide bandgap semiconductors, especially dielectric materials, can potentially be used as electrolytes because of their large bandgap, which precludes the possibility of electrons being excited from the VB to the CB by thermal means. In addition, under electric field conditions, the electric dipole component in the dielectric materials can be adjusted, which may further affect the ionic transport properties [135–138]. Li$^+$ and Na$^+$ ions are large enough to form bent O-A-O symmetric bonds in some condensates of larger anion clusters with electric dipole moments, as illustrated in Fig. 12 for Na glass. The high-frequency dielectric constant is important because it represents the intrinsic property of the material and is directly related to the DC conductivity. Accompanying this electric dipole component, the electric dipole component of the electrolyte interface charge is increased by dipole coalescence. Using dielectric materials in the electrolyte may produce a very



**Fig. 11** Strongly correlated nickelate as the ionic conductor in a LIB. **a** Electronic configuration of pristine SmNiO$_3$ (SNO), a narrow gap semiconductor, at room temperature. **b** Self-designed electrochemical cell for lithiation of SNO. **c** Electronic configuration of lithiated SNO (Li-SNO). Electron filling leads to a large on-site Coulomb interaction, suppressing the electronic conduction pathway. Li$^+$ occupies multiple interstitial sites of the unit cell. Electron localization-induced perovskite lattice expansion facilitates Li$^+$ interstitial transport, which enables Li-SNO to be a potential lithium-ion conductor. **d** First-principles simulation of the total DOS for Li-SNO with 0–1 intercalated Li/SNO (gray). The projected DOS (PDOS) of the unoccupied Ni $E_g$ states are shown in color. The lighter hues indicate $E_g$ states of Ni$^{3+}$, and the darker hues indicate those of Ni$^{2+}$ including the newly occupied $E_g$ states due to the localization of the added electron from the intercalated lithium below the Fermi energy. Reproduced with permission from Ref. [131] Copyright 2018 National Academy of Sciences
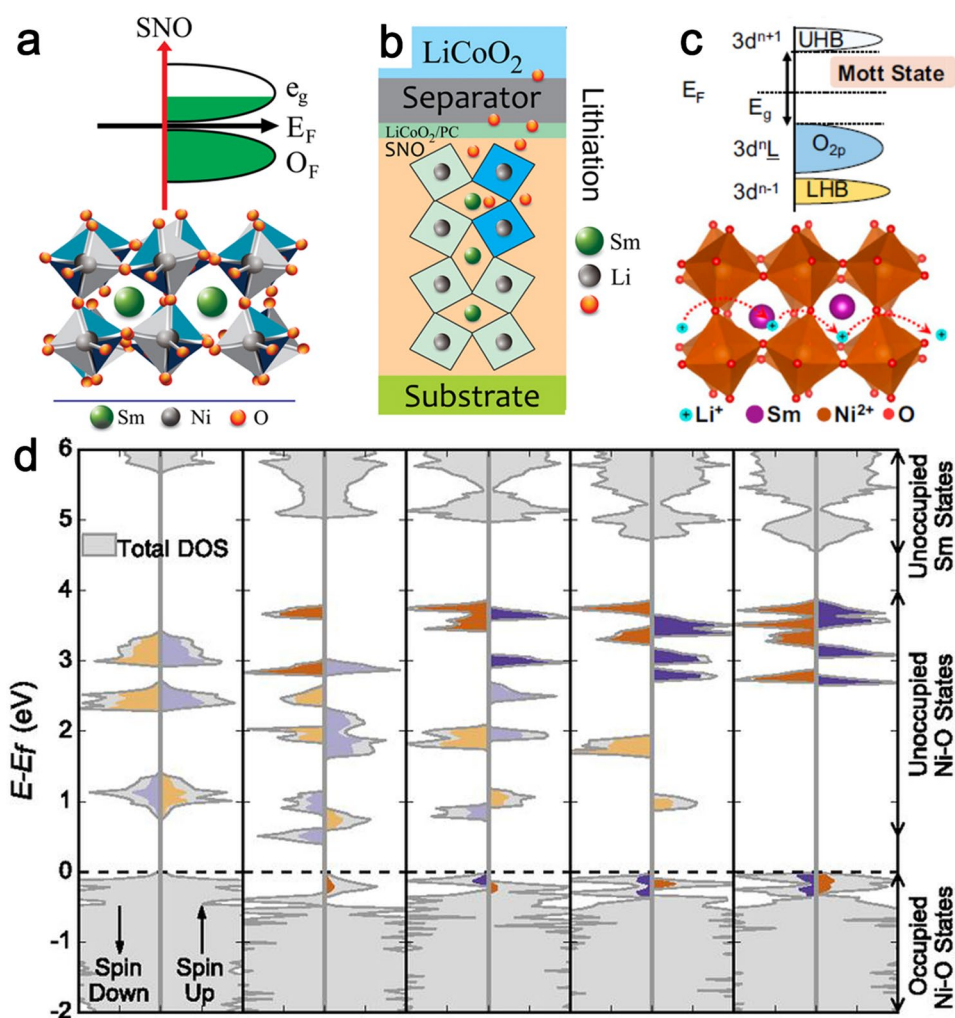
large energy gap window that makes it stable upon contact with both an alkali-metal anode and a high-voltage cathode without the formation of an SEI. The glass also contains electric dipoles that have a large dielectric constant. The Goodenough group applied dielectric materials as electrolytes for $Li^+$ and $Na^+$ batteries. For example, the $Li^+$ and $Na^+$ glass electrolytes $A_{2.99}Ba_{0.005}O_{1+x}Cl_{1-2x}$ with $A = Li$ or Na were reported [128–131]. Bragg and Goodenough et al. [128] reported that the dipoles are oriented under an applied electric field and aligned parallel to the field axis, which enables solid glass electrolytes $A_{2.99}Ba_{0.005}O_{1+x}Cl_{1-2x}$ with $A = Li$ or Na to yield an ionic conductivity $\sigma_i > 10^{-2}$ S • $cm^{-1}$ and a very large dielectric constant, which is extremely important to develop safe rechargeable batteries of high energy density and long cycle life.

### 4.1.2 Role of the BIEF in Batteries

One of the most exciting characteristics of semiconductor and energy band theories in the battery field is that the band alignment of different battery components or compositions

that induces a BIEF or alters the local electric field (LEF) can significantly improve the electrochemical performance of the device, including promotion of ion transport, increase of the cycle life and high-speed discharge–charge cycle, and enlargement of the battery capacity.

To speed up electrode Li intercalation at high charge–discharge rates and promote the $Li^+$ ion diffusion process, a BIEF at the semiconductor particle (material) level has been reported. A typical example is reported by Xia et al. [11] for a $TiO_2$-based electrode, as shown in Fig. 13. In comparison to bulk $TiO_2$ (Fig. 13a) and nanocrystal $TiO_2$ (Fig. 13b), Fig. 13c shows a structure consisting of a nanocrystalline stoichiometric core of an intrinsic-type $TiO_2$ semiconductor and an amorphized nonstoichiometric outer layer $TiO_{2-d}$ n-type shell. Such a structure creates an i-n heterostructure [11] with the BIEF direction from the outer layer to the core, which is expected to promote $Li^+$ diffusion during the lithium discharge process, i.e., help $Li^+$ insertion (Fig. 13d). Once $Li^+$ has been fully inserted or discharged into the $TiO_2$ nanocrystal, the core will become $Li_yTiO_2$, turning into an intrinsic semiconductor. In contrast, the disordered layer

**Fig. 12** Ab initio molecular dynamics calculations showing electric dipoles with a ratio of elementary dipoles to several unaligned clusters of 7:1 at 100 °C. **a** Box containing 81 $Na^+$, 7 $Cl^-$ and 37 $O^{2-}$ ions. **b** Elementary dipoles and clusters. **c** Chain segments calculated before and proposed after alignment. Reproduced with permission from Ref. [139]. Copyright 2016 ECS
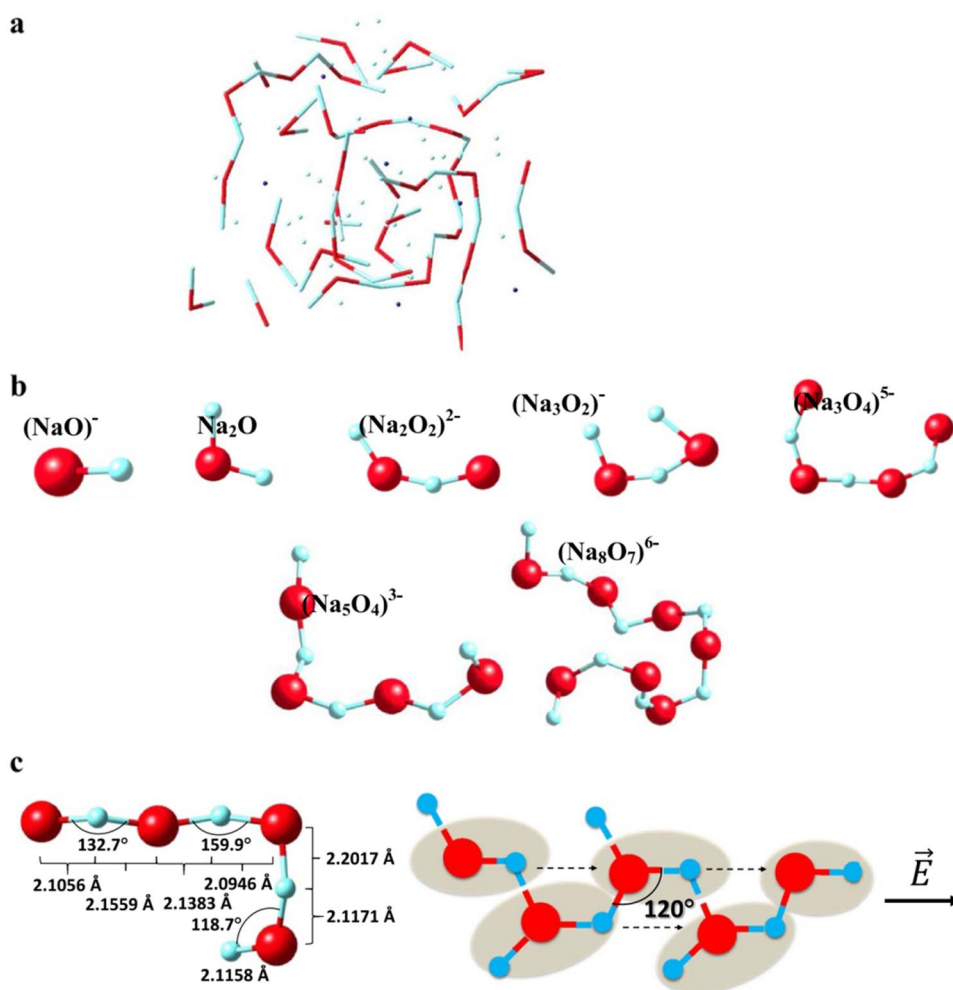
takes up much less Li$^+$ due to the existence of oxygen vacancies and becomes Li$_{y-2x-r}$TiO$_{2-d}$, corresponding to a relative p-type semiconductor compared with Li$_y$TiO$_2$. Therefore, a new i-p heterostructure and a BIEF will be formed at the core/shell interface; thus, the new BIEF directed from the disordered layer to the crystalline core facilitates Li$^+$ transport from the core to the shell, i.e., helps Li$^+$ extraction in the charging process (Fig. 13e). In the end, with the assistance of the in situ formed i-n and i-p heterostructure and BIEFs, a higher ionic diffusion capability is obtained during the Li$^+$ ion insertion/extraction process, increasing the rate performance.

Another interesting case is reported by Yan et al. [140] based on carbon-doped Co$_3$O$_4$ nanocrystals for superior Li-ion storage. The imbalanced charge distribution emerging from the carbon-dopant can induce an LEF to greatly facilitate charge transfer within unique sub-10 nm nanocrystal-assembled Co$_3$O$_4$ hollow nanotubes (HNTs). The resulting

carbon-doped Co$_3$O$_4$ HNT-based electrodes demonstrated an excellent reversible capacity of 950 mAh • g$^{-1}$ at 0.5 A • g$^{-1}$ after 300 cycles and superior rate performance of the full battery with 853 mAh • g$^{-1}$ at 10 A • g$^{-1}$. Zheng et al. [12] also reported that the LEF effect can be built at atomic interfaces on ultrathin Bi$_2$MoO$_6$ (BMO) nanosheets (Fig. 14a–c). The unbalanced charge distribution between the [Bi$_2$O$_2$]$^{2+}$ and [MoO$_4$]$^{2-}$ layers induces an interfacial electric field at the interfaces, while the lopsided charge distribution around oxygen vacancies results in a local in-plane electric field, thus promoting ion diffusion/electron transport. Additionally, the 2D ultrathin construction can provide interconnected charge migration paths formed on the open surfaces, which could facilitate the charge transfer process in the BMO sheets. Therefore, both the in-plane and interfacial electric fields, as illustrated in Fig. 14d, induced by atomic-level engineering (Fig. 14e) can cause an unbalanced charge distribution within the crystal and induce a
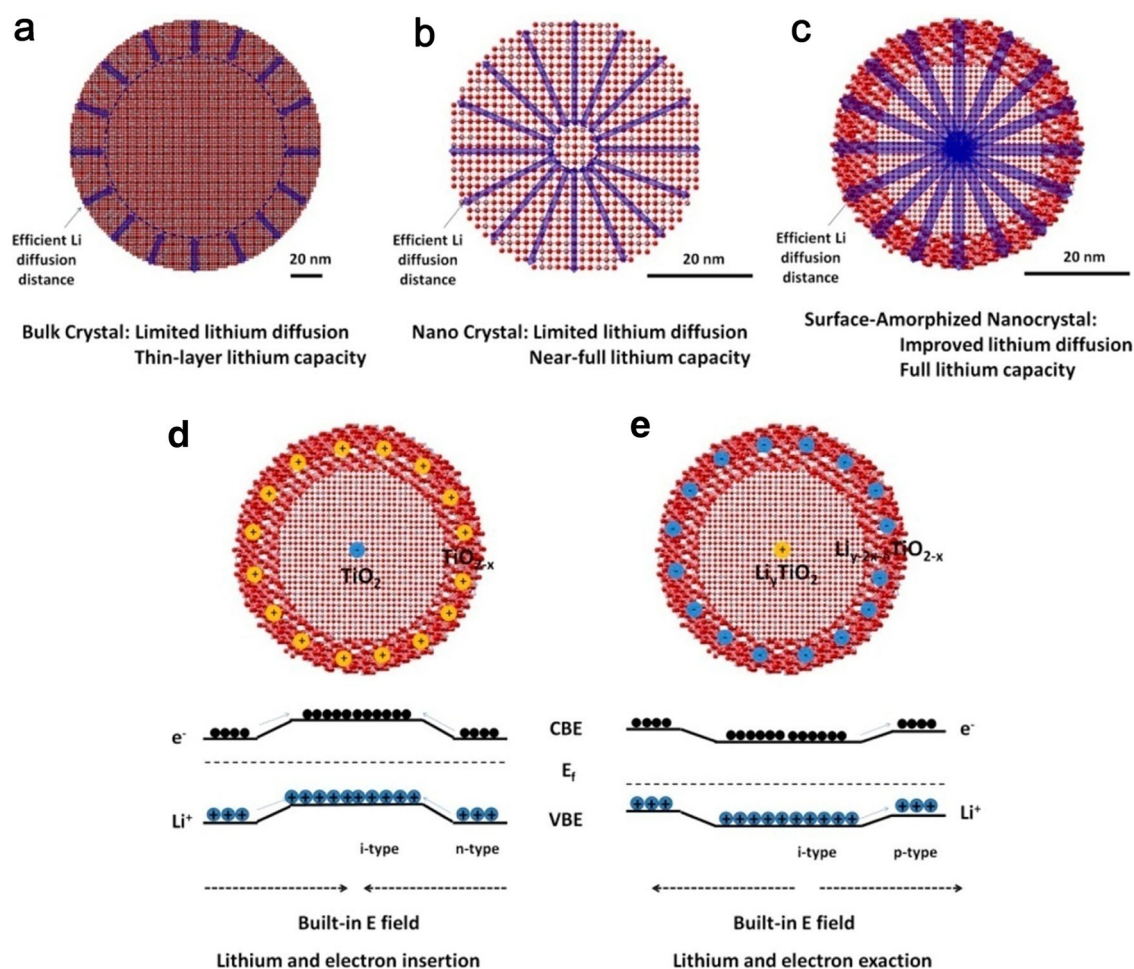


Fig. 13 Comparison of charge diffusion in electrode materials made of **a** bulk crystals, **b** nanocrystals, and **c** surface-amorphized nanocrystals, and illustration of the facilitation of charge transport under a BIEF during discharge (**d**) and charge (**e**) processes. The

length and width of the arrows illustrate the relative penetration depth and the charge transfer/transport coefficients of the lithium ion in the material, respectively. Reproduced with permission from Ref. [11]. Copyright 2013 ACS
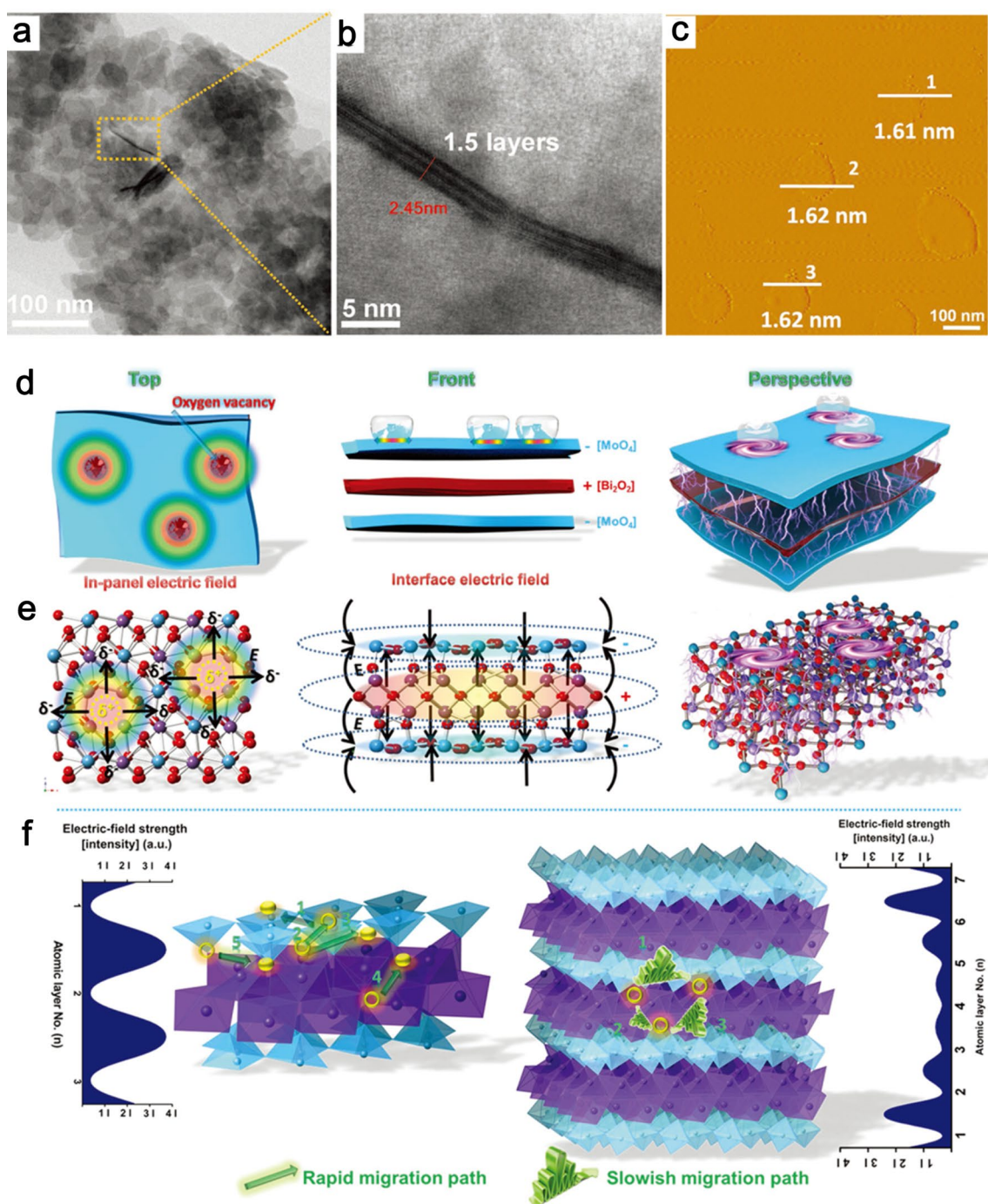
**Fig. 14** Morphology of obtained BMO sheets. **a** TEM image, **b** enlarged high-resolution TEM image, and **c** atomic force microscopy (AFM) image with corresponding height. **d** Schematic diagram of the induced in-panel electric field and the interface electric field within the BMO sheets viewed in different directions. **e** Electric field distribution and corresponding crystal structure of the BMO sheets in (**d**). **f** Relationship between the electric field, migration paths, and Li transfer kinetics in BMO sheets and bulk BMO. **d–f** Summary of the enhanced high rate capacity mechanism of the BMO sheets for Li-ion storage. Reproduced with permission from Ref. [12]. Copyright 2017 Wiley–VCH

BIEF, which can significantly boost the lithium-ion transfer dynamics. Impressively, the lithium battery using the BMO nanosheet electrode shows a long-term cycling performance at 2000 mA $\bullet$ g$^{-1}$. A possible mechanism for the improvement in lithium storage in atomically thin BMO nanosheets is proposed as shown in Fig. 14f.

In addition to LIBs, the construction of a BIEF/LEF has also been demonstrated to be very effective in developing
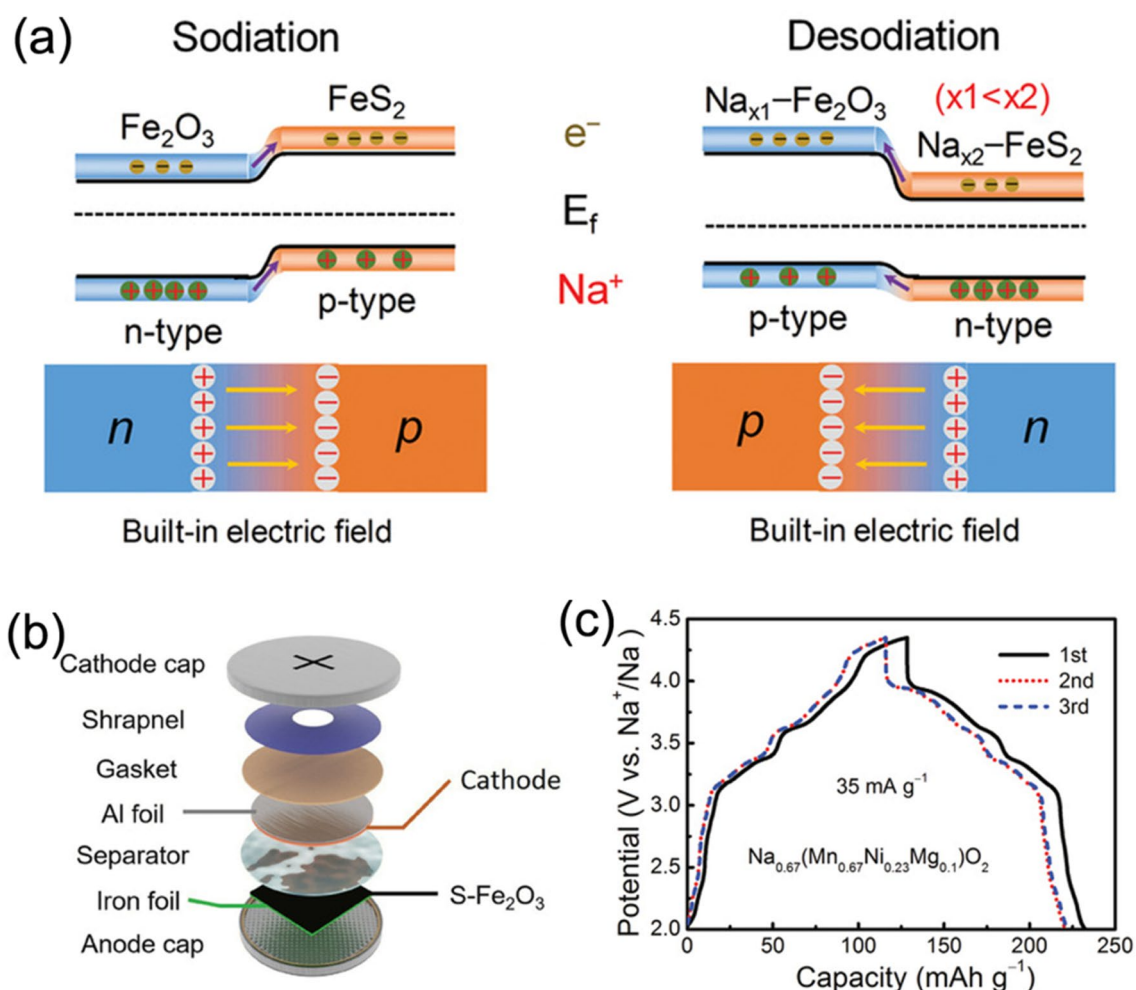
**Fig. 15** **a** Schematic of the formation of a BIEF and Na$^+$ storage mechanism upon discharge and recharge, and electrochemical performance of the full cell of Fe$_2$O$_3$//Na$_{0.67}$(Mn$_{0.67}$Ni$_{0.23}$Mg$_{0.1}$)O$_2$. **b** Schematic of the coin-type full cell. **c** Initial galvanostatic profiles of the S-Fe$_2$O$_3$//Na$_{0.67}$(Mn$_{0.67}$Ni$_{0.23}$Mg$_{0.1}$)O$_2$ full cell at a rate of 0.2 A g$^{-1}$ (based on the anode mass). Reproduced with permission from ref. [141]. Copyright 2019 Wiley–VCH

high-performance sodium-ion batteries [141, 142]. Ni et al. [141] found that a BIEF can reduce the activation energy and accelerate charge transport significantly based on the synergy of the ordered architecture of iron oxide-based nanotube arrays and a BIEF. Figure 15a schematically illustrates such a material system and the BIEF-related mechanism. A BIEF spontaneously develops at the heterogeneous interface of n-Fe$_2$O$_3$ and p-FeS$_2$, as verified by Kelvin probe force microscopy measurements across the heterointerface. Upon discharge (sodiation), the BIEF that has an n-to-p direction will push Na$^+$ ions from Fe$_2$O$_3$ to neighboring FeS$_2$, leading to enhanced transport kinetics. Then, for recharging, desodiation grows relatively Na$^+$-rich FeS$_2$ domains and Na$^+$-deficient Fe$_2$O$_3$ domains, yielding a new BIEF with an electric field direction from FeS$_2$ to Fe$_2$O$_3$ due to the potential difference. Therefore, the Na$^+$ diffusion kinetics can be boosted in such an S-Fe$_2$O$_3$ system in both sodiation

and desodiation states. More specifically, S-Fe$_2$O$_3$ exhibits a high initial current efficiency of 83%. The assembled S-Fe$_2$O$_3$//Na$_{0.67}$(Mn$_{0.67}$Ni$_{0.23}$Mg$_{0.1}$)O$_2$ battery shown in Fig. 15b afforded a reversible capacity of approximately 500 mAh $\bullet$ g$^{-1}$ (based on anode mass) and an average voltage of 2.5 V (Fig. 15c), leading to a specific energy of 160 Wh $\bullet$ kg$^{-1}$ (based on both active materials) at a power density of 60 W $\bullet$ kg$^{-1}$. The energy remained at 142 Wh $\bullet$ kg$^{-1}$ under a specific power of 330 W $\bullet$ kg$^{-1}$, which is comparable to that of commercial LiFePO$_4$ batteries. Similar promotion effects were also observed in Bi$_2$S$_3$-Bi$_2$O$_3$ [142] for Na-ion batteries and in C@N–C@N P–C graded heterostructures for aluminum-ion batteries (AIBs) [143]. Such a design also serves as a perfect platform for exploring the underlying correlation of the BIEF and the electrochemical performance of secondary batteries.

## 4.2 Coupled Energy Conversion and Storage Technologies with Semiconductors

The application of semiconductors to new energy conversion and storage has been widely reported. Coupling devices through the joining principle is an emergent frontier. Here, two typical examples of designing fuel cells by combining the approaches of solar cell coupling and using photoelectrolysis principles to design semiconductor-ionic fuel cell (SIFC) devices are reviewed. Figure 16a–c illustrates the band design of a fuel cell based on the PSC principle with the band structure and alignment as a new fuel-to-electricity conversion approach [102]. Similar to the PSC, we used electron and hole transport layers (ETL and HTL) and a semiconductor-ionic LSCF-SCDC material layer sandwiched between the ETL and HTL (Fig. 16b, c). Such a novel system consists of an LSCF-SCDC functional layer (Fig. 16d). The electrochemical performance was compared for a conventional 3-layer fuel cell, the type-I cell with an ETL and an HTL similar to a solar cell, and a type-II symmetrical heterojunction device (Fig. 16e). The latter two cells showed much-improved fuel cell performance over the conventional 3-layer fuel cell. In particular, the type-II cell provided a peak power density of 1080 mW $\bullet$ cm$^{-2}$ at 550 °C with hydrogen fuel/air oxidant. The outstanding electrochemical performance, we believe, is ascribed to the much-improved ionic conductivity of the LSCF-SCDC layer,

i.e., 0.188 S $\bullet$ cm$^{-1}$ (4 times higher than that of the individual SCDC electrolyte at 600 °C) because of the enriched oxygen at the interface of LSCF and SCDC [121]. This work highlighted exploring wide bandgap semiconductors and energy band design for new-generation fuel-to-electricity conversion. Well-aligned energy bands can be designed and realized by unique semiconductor-ionic materials from anode n-type conducting to cathode p-type conducting materials with junction formation incorporated with ionic functions to maintain fuel cell electrochemical reactions, all were integrated into one device [113, 122, 123]. The key issue in such a semiconductor-ionic device is that there must be a charge separation mechanism to prevent the electrons and holes from passing through the device internally and forming an electron short-circuiting problem [103].

In another case, fuel cell devices based on energy band alignment were experimentally demonstrated to show no e$^-$/h$^+$ flow causing short circuiting based on a TiO$_2$ functional layer as the electrolyte (Fig. 17) [82], in which a TiO$_2$ thin film was deposited on the p-conducting semiconductor NCAL (LiNi$_{0.8}$Co$_{0.15}$Al$_{0.05}$O$_2$) ceramic substrate, with another NCAL thin electrode on top completing the fuel cell construction (Fig. 17a, b). As a wide bandgap semiconductor, TiO$_2$ is suggested to hold the capability to suppress electron and hole conduction through the bulk (Fig. 17c), as reflected by an OCV close to the theoretical value based on the Nernst equation (Fig. 17d), and the cell gave a peak
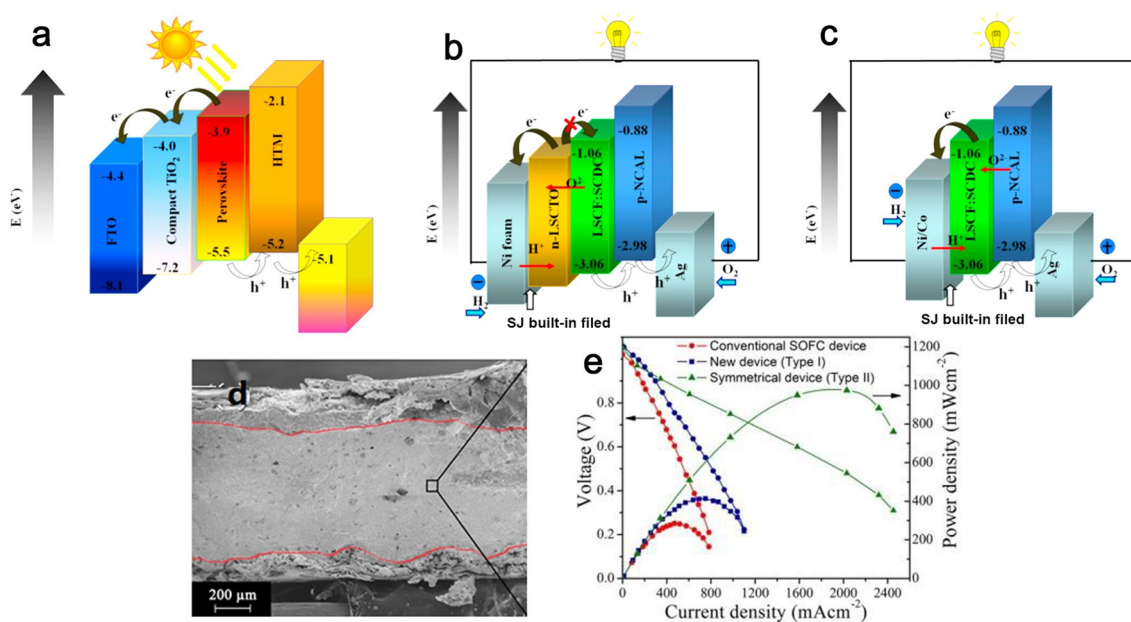


**Fig. 16** Energy level diagram of **a** a perovskite-type solar cell, **b** a fuel-to-electricity conversion device (fuel cell) inspired by the PSC structure (type I) and **c** a symmetrical fuel-to-electricity conversion device (type II) with an in situ formed Schottky junction. **d** Cross-sectional SEM image of the type-II device and close-up view of the

LSCF-SCDC functional layer. **e** Device electrochemical performance comparison of the conventional 3-layer fuel cell, the type-I fuel-to-electricity device with an ETL and an HTL, and the type-II symmetrical heterojunction fuel-to-electricity device. Reproduced with permission from ref. [102]. Copyright 2016 Elsevier
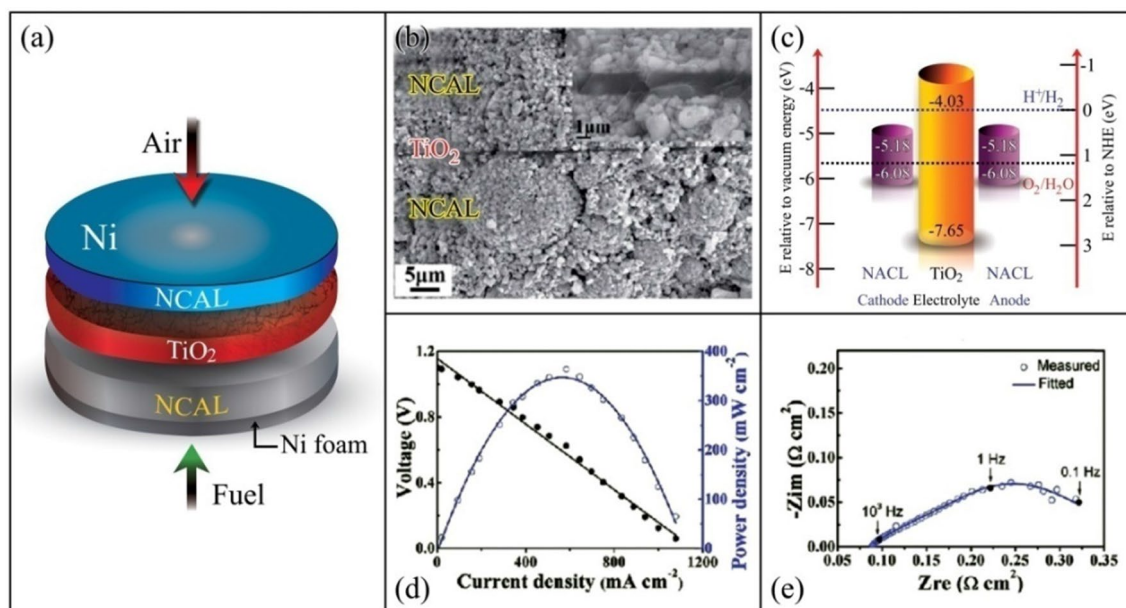
**Fig. 17** **a** Construction of the fuel cell device using a TiO$_2$ electrolyte functional layer; **b** SEM images of the cell configuration of the TiO$_2$ electrolyte-based fuel cell device, **c** energy band diagram of the resulting thin film TiO$_2$ electrolyte fuel cell with NCAL electrodes; **d**,

**e** electrochemical performance of a proof-of-concept of the fuel cell at 550 °C in H$_2$/air condition. Reproduced with permission from Ref. [82]. Copyright 2019 RSC

power output larger than 300 mW ● cm$^{-2}$ at 550 °C and an impressive electrochemical impedance value (Fig. 17e). This fundamental understanding and scientific design are important and naturally related to the photoelectrolysis and photocatalysis fields. The TiO$_2$ fuel cell provides for the first time, from the detailed band parameters relevant to the photo-water splitting process and the products, the view that the photo-water electrolysis process, H$_2$O = H$_2$ + O$_2$, is the reverse process to that in a fuel cell: H$_2$ + O$_2$ = H$_2$O. Compared to photocatalyst TiO$_2$ water splitting, there are some similarities in the TiO$_2$ electrolyte fuel cell band structure and alignment. Therefore, a new and universal design for TiO$_2$ electrolyte or other semiconductor-based fuel cells from the band structure and alignment in comparison with the TiO$_2$ photo-water splitting process is shown in Fig. 18, in which the electrolyte layer is extended from a typical electronic conductor to a wide bandgap semiconductor, providing the specific requirement mentioned in the following paragraph. According to energy band theory, to adjust the carrier transport behavior in a device, materials with different energy band structures should be carefully designed. For example, in a PEC water splitting device [15, 144], the Fermi level of the metal counter electrode must be higher than the redox potential of H$^+$/H$_2$, while the VB level of the semiconductor photoanode must be lower than the redox potential of H$_2$O/O$_2$ (Fig. 18a). The fuel cell reaction product can be regarded as a reverse product of water splitting. In a typical fuel cell, electrons are generated at the anode/

electrolyte interface and are then supposed to flow through the anode to the outer circuit when the circuit is connected. Meanwhile, no electrons are expected to flow through the electrolyte; otherwise, short circuiting occurs (Fig. 18b). Therefore, the electrons in the anode should be blocked by the electrolyte from the perspective of energy band theory. In a typical Ni-YSZ (Y-stabilized ZrO$_2$) fuel cell, the redox potential of H$_2$/H$^+$ is approximately 4.5 eV relative to the vacuum energy (RVE), and the work function for a typical anode material Ni is approximately 5.1 eV RVE, which is lower than the potential of H$_2$/H$^+$; hence, electrons stemming from the oxidation of H$_2$ can flow to the anode. Meanwhile, the CB of the YSZ electrolyte is higher than the redox potential of H$_2$/H$^+$; electrons cannot jump to the CB of the electrolyte; namely, the electrons are blocked by the electrolyte. However, if an electrolyte material has a lower CB level, then short-circuiting problems might occur (Fig. 18c). For example, the CB level of SDC, which is measured to be at approximately 5.65 eV, then the electron may flow to electrolyte, and the short-circuiting problem is often observed in SDC electrolyte fuel cells. When SDC is reduced by H$_2$ in fuel cell operation, its electronic conductivity rapidly increases, and electrons can flow through it [145]. This is why the short-circuiting problem was observed in an SDC electrolyte fuel cell after a period of operation. In short, the energy band structure of a good SOFC should obey the following rules: (1) the CB level of the electrolyte should be higher than the redox potential of H$_2$/H$^+$, (2) the Fermi
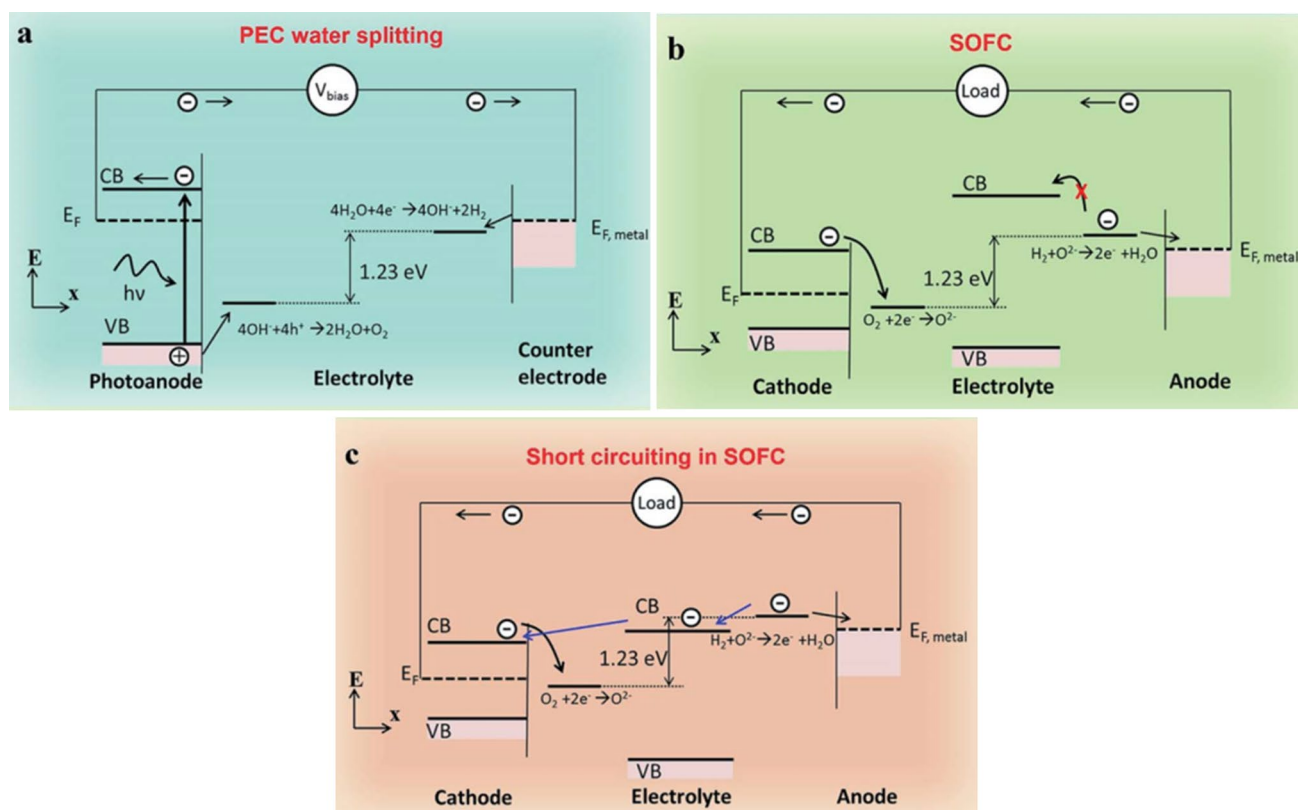
**Fig. 18** Energy band diagrams of **a** PEC water splitting (the Honda–Fujishima effect), **b** a fuel cell, and **c** the fuel cell with the occurrence of short circuiting. If the anode of the fuel cell is not a metal but a semiconductor, then the CB level of this semiconductor should be lower than the energy level of $H^+/H_2$, as the electrons generated by $H_2$ oxidation are expected to flow to the CB level of this semiconductor. Reproduced with permission from Ref. [82]. Copyright 2019 RSC

level of the metal anode (or the CB level of the semiconductor anode) should be lower than the redox potential of $H_2/H^+$, (3) the VB level of the electrolyte should be lower than the redox potential of $O_2/O^{2-}$, and (4) the CB level of the cathode should be higher than the redox potential of $O_2/O^{2-}$.

In addition to wide applications of semiconductors in fuel cells, coupling or integrating semiconductors/bands and fuel cell electrochemistry has recently emerged, involving metal-air batteries, photocatalytic fuel cells, photoenhanced fuel cells and many others [110, 146–152]. Rechargeable Li-$O_2$ batteries are frequently reported to be intensified by the photoassisted process. Generally, rechargeable Li-air batteries show high energy density above that of Li-ion batteries. However, their practical application is limited by the high voltage loss related to the cathode processes, oxygen reduction and evolution reactions, and coupling with the low conductivity lithium oxide that forms [153–155]. Reduction of the energy loss to accelerate the formation and decomposition of $Li_2O_2$ and $O_2$ evolution is the key. $C_3N_4$-carbon is the key to realizing such a coupling process of lithium-air batteries to realize high energy efficiency. Such a system consists of a Li anode, a nonaqueous electrolyte combined with an

$I^-$ ion redox mediator and g-$C_3N_4$ grown on carbon paper simultaneously as an oxygen electrode and a photoelectrode, as shown in Fig. 19a. Upon charging under illumination, the $I^-$ ions are oxidized to $I_3^-$ ions by photoexcited holes from the photocatalyst, and subsequently, $I_3^-$ ions diffuse to the oxygen electrode surface, oxidize $Li_2O_2$ to $O_2$ and are reduced back to complete a full redox cycle. Meanwhile, the photoexcited electrons transfer to the anode through the external circuit and reduce $Li^+$ to Li metal. Accordingly, the charging voltage of a Li–$O_2$ battery is compensated by the photovoltage generated on the photoelectrode. The photoassisted charging voltage equals the energy difference between the redox potential of the $Li^+/Li$ couple and the CB of the photocatalyst, as shown in Fig. 19b. A suitable photocatalyst for photoassisted rechargeable batteries must fulfill two essential conditions: the CB potential should be lower than the $O_2/Li_2O_2$ couple potential (that is, 2.96 V), and the VB potential should be higher than the $I^-/I_3^-$ couple potential to realize oxidization of $I^-$ ions to $I_3^-$ ions. The battery can deliver discharge and charge voltages of 2.76 and 3.56 V, respectively, proving that g-$C_3N_4$ can act as an ORR catalyst for Li-$O_2$ batteries. Solar cells and solid battery/fuel cells
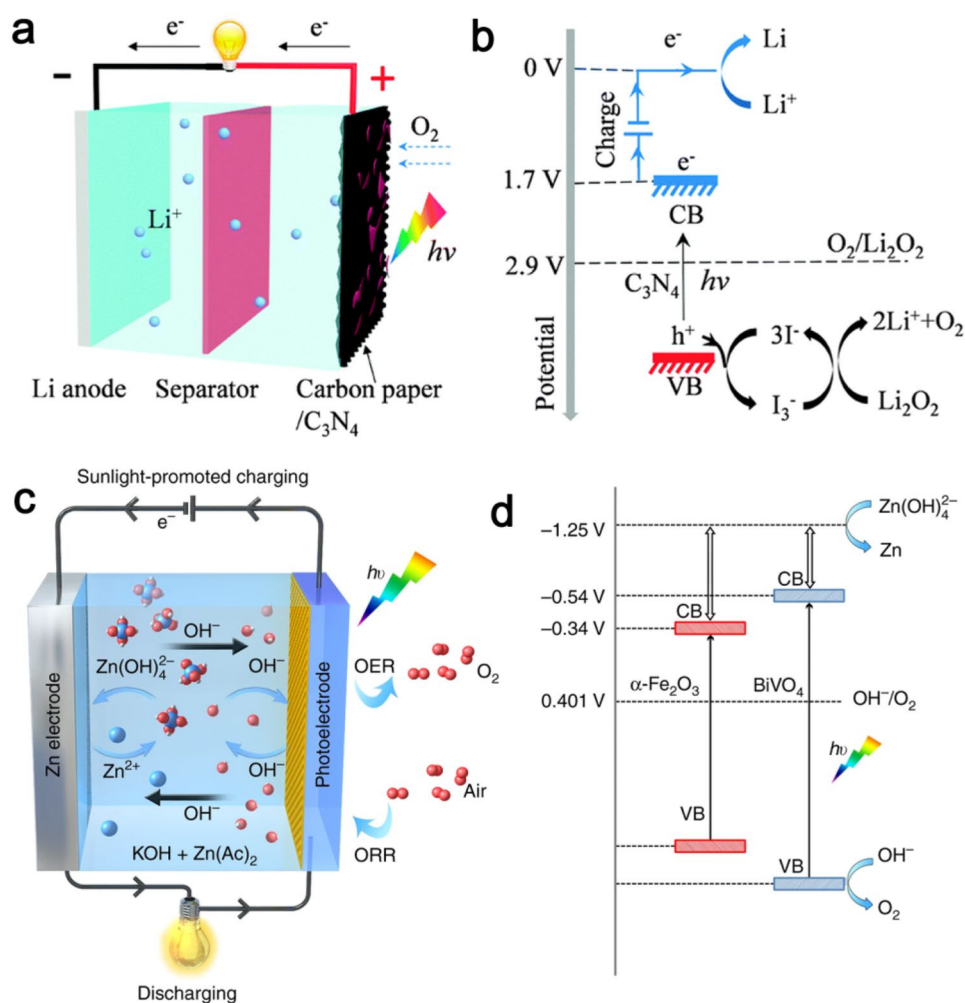
both convert energy of different forms into electricity. A combination of these two battery systems has demonstrated clean and energy-efficient functional integrity [7, 156–159]. Li-O$_2$ batteries have been the most focused on system to be successfully loaded with a photoresponsive electrode, where the in situ generated holes possessing positive charges directly or indirectly catalyze the oxygen evolution reaction (OER) [157, 160, 161]. Therefore, the notoriously large overpotential of the OER has been efficiently suppressed via this synergistic process, where solar energy is nominally stored in the rechargeable battery system and further consumed to compensate for the energy needed for battery charge. Additionally, recently, the utilization of solar energy to improve the OER kinetics has also been demonstrated in zinc-air batteries, which consist of a Zn electrode and a BiVO$_4$/α-Fe$_2$O$_3$ heterostructure semiconductor photoelectrode as an air electrode assembled in an alkaline electrolyte (Fig. 19c). The charging process is associated with the OER on the air electrode, which has intrinsically sluggish reaction kinetics, resulting in a large overpotential and low energy efficiency. As illustrated in the proposed sunlight-promoted

charging mechanism (Fig. 19d), a photovoltage is generated when the photoelectrode undergoes photoexcitation, which compensates for the high charge potential of the zinc-air battery; therefore, a higher electrical efficiency is achieved, as expected [157, 161]. These results can benefit from a more comprehensive understanding of fuel cell semiconductor electrochemistry and motivate new interesting frontier research and breakthroughs in scientific fundamentals, technologies, and applications.

Another interesting topic is the solar photocatalytic fuel cell (PFC), which can realize wastewater treatment and electricity generation simultaneously [163]. Figure 20a schematically shows the configuration of such a device, which consists of an effective photoanode and an ORR cathode. The photoanode is made of a CdS quantum dot-sensitized TiO$_2$ nanorod array deposited on FTO glass, and a gas diffusion electrode was employed to improve the ORR at the cathode. The ORR reaction utilizes protons produced from wastewater treatment to complete the fuel cell cathode reaction for power generation. Another interesting PFC constructed by using a photoanode made of heterostructured ZnFe$_2$O$_4$/
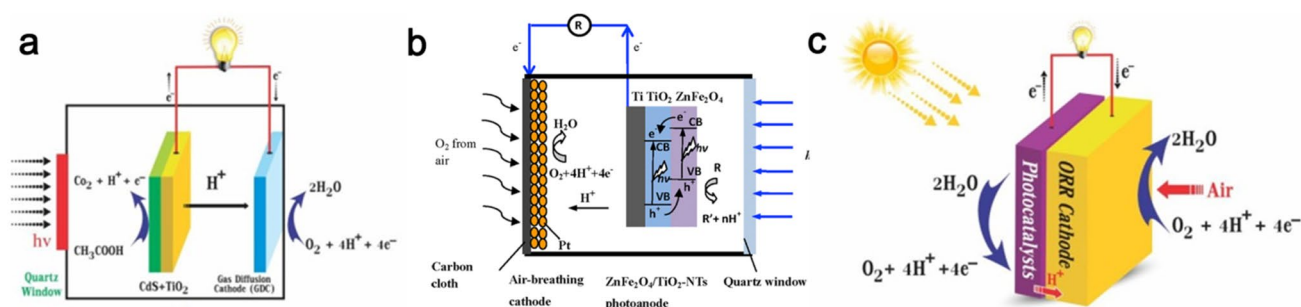
**Fig. 20** Schematic diagram of a photocatalytic fuel cell (PFC) **a** for treating wastewater and simultaneously converting chemically stored energy from wastewater into electricity [162]. **b** Schematic diagram of the PFC system with the $ZnFe_2O_4/TiO_2$-NT photoanode and air-breathing cathode for simultaneous pollutant removal and power production [163]. **c** Schematic diagram of the PFC system with a photo-water splitting anode and an air diffusion catalyst cathode for simultaneous water oxidation and power production. Reproduced with permission from Ref. [157]. Copyright 2019 Springer Nature

$TiO_2$-NTs and an air-breathing cathode was also proposed for simultaneous pollutant removal and power generation (Fig. 20b) [162]. Similar to the fuel cell electrochemical process, the electrolyte conductivity can effectively improve the PFC performance. The photoanode is based on band alignment to perform effective pollutant removal, and the cathode reaction can be realized again by taking protons produced from the photo-pollutant treatment process, thus simultaneously producing electricity. The same concept should be extended to future energy technology, i.e., an integrated highly efficient photo-water-splitting fuel cell, as illustrated in Fig. 20c, which not only treats wastewater but also acts as a standard water-powered electricity generator or self-generation device. In this device, $H^+$ can be produced by photo-water splitting and then used on-site in combination with the fuel cell air electrode to complete the ORR reaction for power generation. This may be an ideal solution to realize water as both "fuel" and "power", which is an advanced environmentally friendly and sustainable power generation system.

Furthermore, joint fuel cell and hydrogen production may be designed based on the same band design and alignment. For example, semiconductor $SrTiO_3/ZnO$ heterostructure materials have been assembled, as illustrated in Fig. 21. They showed a joint photocatalyst functionality for $H_2$ production (Fig. 21a, b) and fuel cell electricity generation (Fig. 21c, d) [96]. Wu et al. reported excellent results for both applications: a 1 317 μmol • $g^{-1}$ $H_2$ production rate was generated at room temperature (Fig. 21a, b), reaching an advanced level, and an excellent fuel cell power output of 564 mW • $cm^{-2}$ was achieved at 550 °C (Fig. 21c, d). This joint production of $H_2$ and electricity presents a good example of a comprehensive understanding of semiconductor-based fuel cell science. We expect that based on new understanding and guidance provided by semiconductor electrochemistry, many new advanced energy applications will be explored and developed for practical uses, which

should not be limited to the listed examples, e.g., photovoltachromic supercapacitors [7] and others.

In photoelectrolysis, semiconductor heterostructure materials are often employed, in which the energy band and semiconducting physics play important roles, as shown in Fig. 22. The basic mechanism and process of photocatalysis are focused on two strategies: (1) energy band modification to broaden the light absorption and (2) surface modification (surface sensitization, semiconductor combination, and noble metal deposition) to increase the lifetime of the carrier, as well as the reaction kinetics. Overall, a suitable band structure is key for visible-light harvesting and effective separation of the carriers of semiconductor photocatalysts. Following a similar working principle for novel semiconductor-based fuel cells, what is required is rather the same, that is, in terms of charge creation, separation, transport and reaction ('closing the circuit'), with $h^+/e^-$ being the key charges on electrodes and $H^+/O^{2-}$ being the charge carriers, to realize the charge transfer and redox reactions based on the band design.

Even in the photovoltaic field, typically, a perovskite-type solar cell is a very emerging concept [164], which greatly involves a deep fundamental understanding and technology scaling up and applications. Ion transport is responsible for unusual phenomena such as current–voltage hysteresis in photovoltaic devices, band structure changes, durability and anomalous above-bandgap photovoltages. Ion transport is governed in PSCs by intrinsic (ions, e.g., $MA^+$, $Pb^{2+}$, $I^-$, and $O^{2-}$; and point and extended defects) and extrinsic (light, heat, electrical fields, and chemical gradients) factors [165, 166]. These factors affect the photonic conductivity and offer valuable directions for both limiting ion transport, where required, and harnessing it to enable new functionalities, as shown in Fig. 23 [167, 168]. The transport of these ion defects exerts strong effects on the PSC performance, suggesting that electrons and ions are coupled and correlated in energy conversion

**Fig. 21** Schematic illustration of Energy band alignment for photocatalytic hydrogen evolution (**a**), with the corresponding $H_2$ production performance (**b**), and for fuel cell applications (**c**), with the full cell performance of the ZnO/SrTiO$_3$ heterostructure (**d**). The performances of control samples are also given in (**d**). Reproduced with permission from Ref. [96]. Copyright 2018 Elsevier
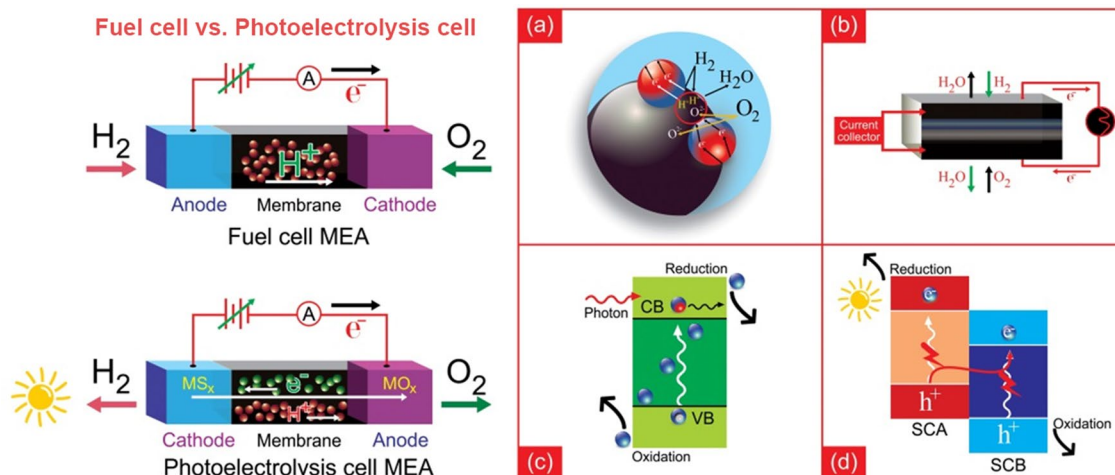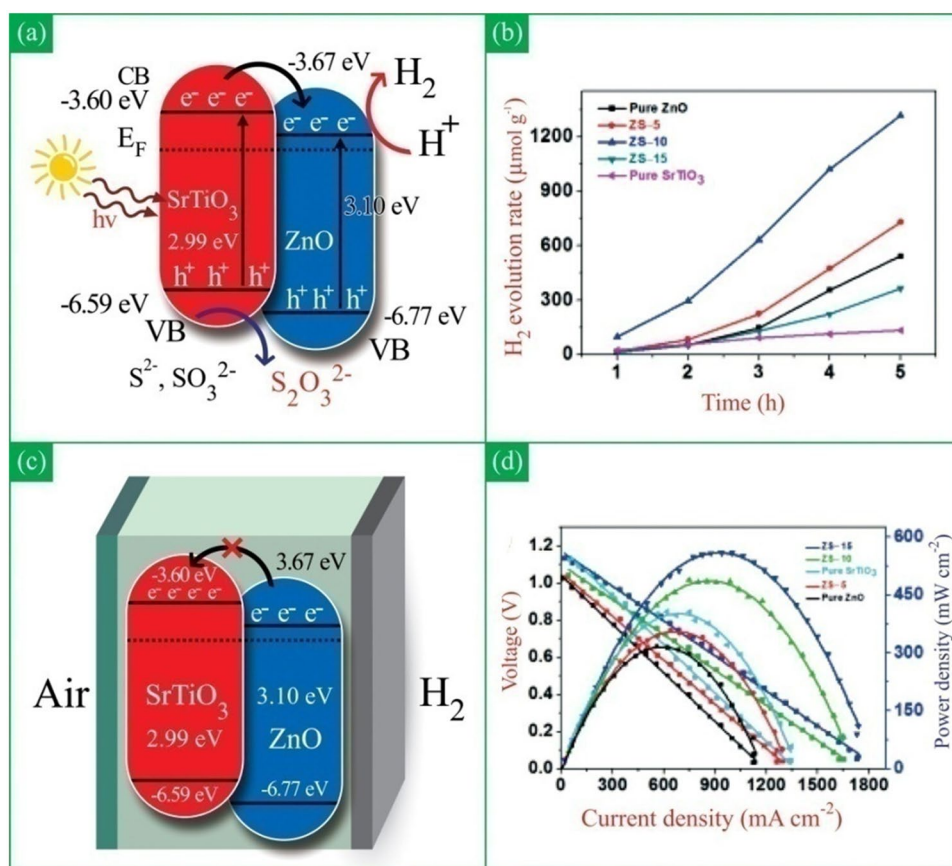


**Fig. 22** Schematic comparison of a fuel cell and a PEC. **a** Single-layer EFFC and **b** double-layer devices driven by the similar semiconductor p–n junction principle; **c, d** photoelectrolysis realized by semiconductor band structure design and alignment

and storage systems, although the focuses and applications are different because the device performances are dominated by either ions or electrons/holes. In our recent development, a semiconductor-ionic oxide was used as the PV functional layer, with successful demonstration of a PV cell with significant enhancement of both the device

voltage and photocurrent output (see Fig. 24) [169]. $Co_3O_4$ is a p-type semiconductor that is incorporated with lithium to form an ionic-type $Li_xCo_{3-x}O_4$ semiconductor oxide. The use of both $Co_3O_4$ and $Li_xCo_{3-x}O_4$ as the PV functional layer resulted in a very different device performance; an OCV enhanced by more than double and a
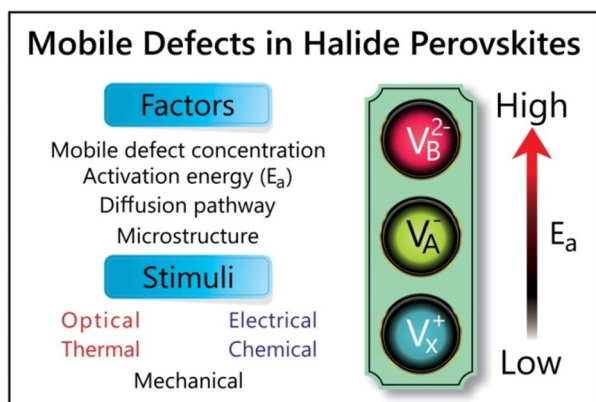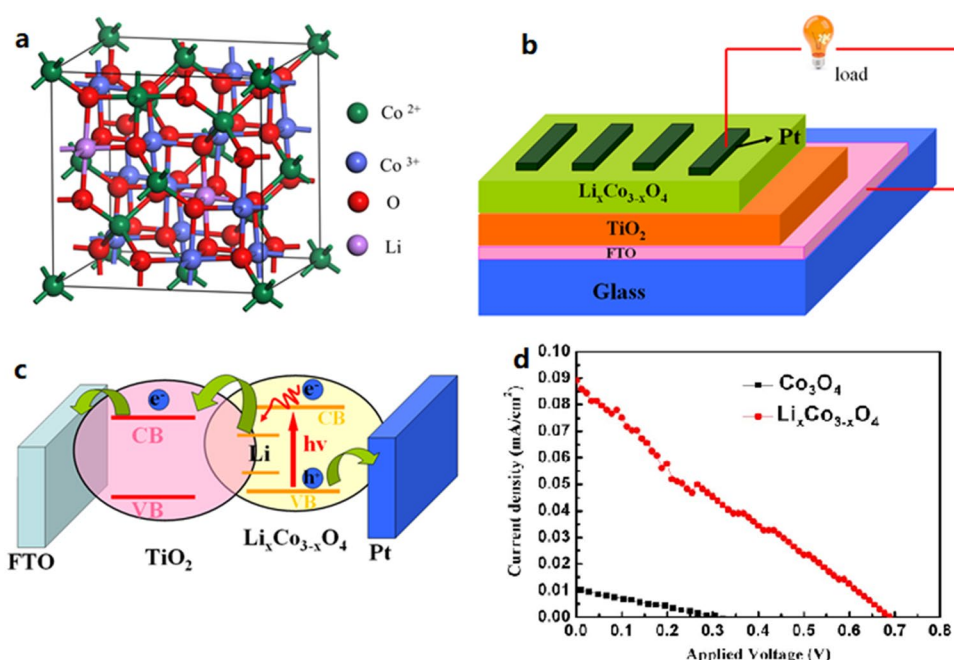
**Fig. 23** Effect of factors on mobile defects and the consequences for physical and chemical properties. Reproduced with permission from Ref. [168]. Copyright 2018 ACS

**Fig. 24** PV devices using $Co_3O_4$ and $Li_xCo_{3-x}O_4$ as the functional layer. **a** $Li_xCo_{3-x}O_4$ structure; **b** schematic diagram of $TiO_2/Li_xCo_{3-x}O_4$ heterojunction solar cells; **c** energy alignment diagram for $TiO_2/Li_xCo_{3-x}O_4$ heterojunction solar cells; **d** $J$–$V$ characteristics of the device under 100 mW cm$^{-2}$. Reproduced with permission from Ref. [169]. Copyright 2016 Elsevier



For example, the solar cell field is experiencing a highly interesting phase of development from physical p–n junction devices to electrochemical dye-sensitized and new perovskite-type solar cells. The latest developments show a trend of combining multiple types of energy devices (silicon solar cell (SSC), Cu(In,Ga)(Sn,Se)$_2$ (CIGS), organic solar cell (OSC), dye-sensitized solar cell (DSSC), perovskite solar cell (PSC), lithium-ion battery (LIB), nanogenerator (NG), supercapacitor (SC), photoelectrosynthetic cell (PESC), bio-fuel cell (BFC), photodetector (PD), and electrolysis cell (ELC), etc.,) into a single device, two of them, at most cases, can be integrated into one unit, such as DSSC/LIB, DSSC/SC, DSSC/NG, DSSC/LIB/NG, PSC/OSC, PSC/CIGS, PSC/PSC, PSC/SSC, SSC/SC, PSC/SC, OSC/SC, DSSC/PESC, PSC/PESC, PSC/ELC, LIB/SC, LIB/NG, BFC/NG, PD/BFC, SC/PD, and NG/SC/DSSC, for various applications [15, 123]. This field is strongly affected by interdisciplinary approaches. It is often complementary to traditional semiconductor p–n junction devices progressing towards new types of practical uses as well as new science. We also recognized early on the SLFC with a joint solar cell and fuel cell as the working principle [87]. Photoelectrolysis or water splitting by photons was well developed around the PEC in the past, but today, photocatalysis can be realized by using semiconductors and band structures [8–10, 170]. Notably, there is a very high degree of similarity historically between the fuel cell and the PEC.

The traditional electrolyte in the fuel cell has served as both an ionic conductor and as an electronic insulator
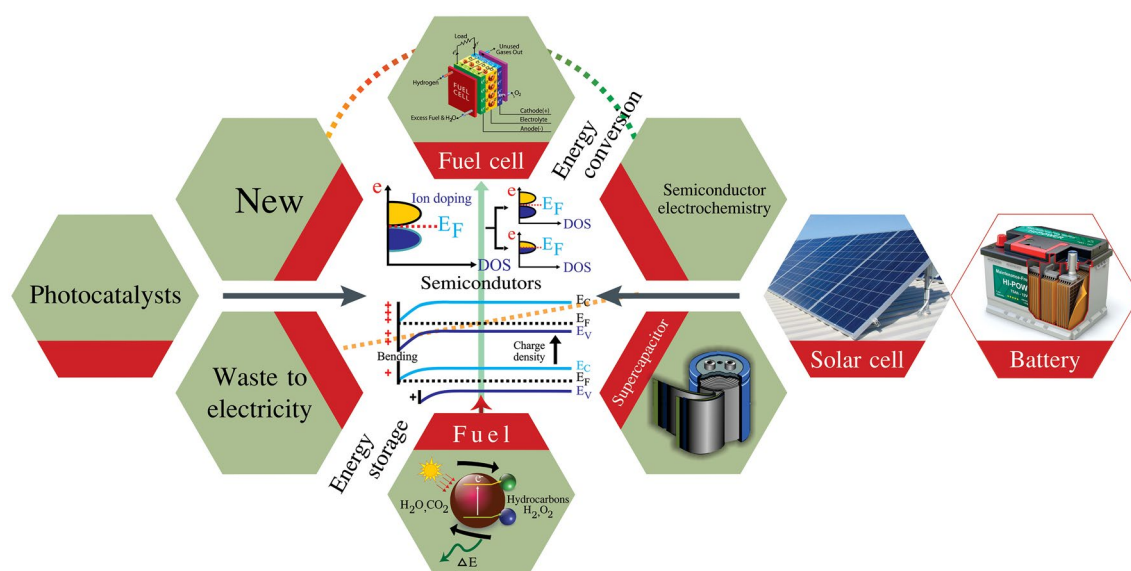
current output enhanced nine times were obtained, suggesting the feasibility of the project.

## 5 Summary and Remarks

This review intends to present new ideas and explore new solutions to clean electrochemical energy conversion and storage going beyond the existing knowledge raising a fundamental question: are there other ways to further develop fuel cells, e.g., by employing semiconductors and semiconductor electrochemistry? Other rapidly developing energy research could be taken as examples for further exploration.

**Fig. 25** Overview of semiconductors for a wide range of applications for energy conversion and storage, where the fuel cell area is just beginning

preventing short circuiting. In semiconductor and heterostructure membrane fuel cells, the short-circuiting problem can be solved through energy band alignment/junction formation and design, which have been successfully demonstrated in solar cells and photoelectrolysis, but now also adopted for fuel cells, e.g., SLFCs or semiconductor membrane fuel cells. Understanding of semiconductor bands and physics enabled conventional electrochemical photoelectrolysis and lithium battery to make use from the new aspects, which now may extend to fuel cell electrochemistry. A wide range of energy conversion and storage applications from the new scientific discoveries across the different disciplines of materials, technology, engineering, physics, and chemistry/electrochemistry could be envisioned as summarized in Fig. 25, where an overall understanding of semiconductors and semiconductor electrochemistry plays a vital role.

## Declarations

**Conflict of interest** All authors claim no conflicts of interest.

# References

1. Zhu, B., Yun, S.N., Lund, P.D.: Semiconductor-ionic materials could play an important role in advanced fuel-to-electricity conversion. Int. J. Energy Res. **42**, 3413–3415 (2018). https://doi.org/10.1002/er.4105

2. Lund, P.D., Zhu, B., Li, Y.D., et al.: Standardized procedures important for improving single-component ceramic fuel cell technology. ACS Energy Lett. **2**, 2752–2755 (2017). https://doi.org/10.1021/acsenergylett.7b00997

3. Singh, K., Nowotny, J., Thangadurai, V.: Amphoteric oxide semiconductors for energy conversion devices: a tutorial review. Chem. Soc. Rev. **42**, 1961–1972 (2013). https://doi.org/10.1039/c2cs35393

4. Asghar, M.I., Jouttijärvi, S., Jokiranta, R., et al.: Wide bandgap oxides for low-temperature single-layered nanocomposite fuel cell. Nano Energy **53**, 391–397 (2018). https://doi.org/10.1016/j.nanoen.2018.08.070

5. Fan, L.D., Zhu, B., Su, P.C., et al.: Nanomaterials and technologies for low temperature solid oxide fuel cells: recent advances, challenges and opportunities. Nano Energy **45**, 148–176 (2018). https://doi.org/10.1016/j.nanoen.2017.12.044

6. Garcia-Barriocanal, J., Rivera-Calzada, A., Varela, M., et al.: Colossal ionic conductivity at interfaces of epitaxial $ZrO_2$: $Y_2O_3$/$SrTiO_3$ heterostructures. Science **321**, 676–680 (2008). https://doi.org/10.1126/science.1156393

7. Zhou, F.C., Ren, Z.W., Zhao, Y.D., et al.: Perovskite photovoltachromic supercapacitor with all-transparent electrodes. ACS Nano **10**, 5900–5908 (2016). https://doi.org/10.1021/acsnano.6b01202

8. Feng, X.J., LaTempa, T.J., Basham, J.I., et al.: $Ta_3N_5$ nanotube arrays for visible light water photoelectrolysis. Nano Lett. **10**, 948–952 (2010). https://doi.org/10.1021/nl903886e

9. Osterloh, F.E.: Inorganic nanostructures for photoelectrochemical and photocatalytic water splitting. Chem. Soc. Rev. **42**, 2294–2320 (2013). https://doi.org/10.1039/c2cs35266d

10. Linsebigler, A.L., Lu, G.Q., Yates, J.T., Jr.: Photocatalysis on $TiO_2$ surfaces: principles, mechanisms, and selected results. Chem. Rev. **95**, 735–758 (1995). https://doi.org/10.1021/cr00035a013

11. Xia, T., Zhang, W., Murowchick, J., et al.: Built-in electric field-assisted surface-amorphized nanocrystals for high-rate lithium-ion battery. Nano Lett. **13**, 5289–5296 (2013). https://doi.org/10.1021/nl402810d

12. Zheng, Y., Zhou, T.F., Zhao, X.D., et al.: Atomic interface engineering and electric-field effect in ultrathin $Bi_2MoO_6$ nanosheets for superior lithium ion storage. Adv. Mater. **29**, 1700396 (2017). https://doi.org/10.1002/adma.201700396

13. Fong, D.D., Ramanathan, S.: Preface for special topic: ionotronics. APL Mater. **5**, 042201 (2017). https://doi.org/10.1063/1.4982238

14. Gerischer, H.: The impact of semiconductors on the concepts of electrochemistry. Electrochim. Acta **35**, 1677–1699 (1990). https://doi.org/10.1016/0013-4686(90)87067-C

15. Yun, S.N., Vlachopoulos, N., Qurashi, A., et al.: Dye sensitized photoelectrolysis cells. Chem. Soc. Rev. **48**, 3705–3722 (2019). https://doi.org/10.1039/c8cs00987b

16. Zhou, Y., Guan, X.F., Zhou, H., et al.: Strongly correlated perovskite fuel cells. Nature **534**, 231–234 (2016). https://doi.org/10.1038/nature17653

17. Fan, L.D., Ma, Y., Wang, X.D., et al.: Understanding the electrochemical mechanism of the core–shell ceria–LiZnO nanocomposite in a low temperature solid oxide fuel cell. J. Mater. Chem. A **2**, 5399 (2014). https://doi.org/10.1039/c3ta14098

18. Boukamp, B.A.: Fuel cells: The amazing perovskite anode. Nat Mater **2**, 294–296 (2003). https://doi.org/10.1038/nmat892

19. Shao, Z.P., Haile, S.M.: A high-performance cathode for the next generation of solid-oxide fuel cells. Nature **431**, 170–173 (2004). https://doi.org/10.1038/nature02863

20. Huang, Y.H., Dass, R.I., Xing, Z.L., et al.: Double perovskites as anode materials for solid-oxide fuel cells. Science **312**, 254–257 (2006). https://doi.org/10.1126/science.1125877

21. Tao, S.W., Irvine, J.T.S.: A redox-stable efficient anode for solid-oxide fuel cells. Nat. Mater. **2**, 320–323 (2003). https://doi.org/10.1038/nmat871

22. Neagu, D., Tsekouras, G., Miller, D.N., et al.: In situ growth of nanoparticles through control of non-stoichiometry. Nat. Chem. **5**, 916–923 (2013). https://doi.org/10.1038/nchem.1773

23. Duan, C.C., Tong, J.H., Shang, M., et al.: Readily processed protonic ceramic fuel cells with high performance at low temperatures. Science **349**, 1321–1326 (2015). https://doi.org/10.1126/science.aab3987

24. Sengodan, S., Choi, S., Jun, A., et al.: Layered oxygen-deficient double perovskite as an efficient and stable anode for direct hydrocarbon solid oxide fuel cells. Nat. Mater. **14**, 205–209 (2015). https://doi.org/10.1038/nmat4166

25. Vøllestad, E., Strandbakke, R., Tarach, M., et al.: Mixed proton and electron conducting double perovskite anodes for stable and efficient tubular proton ceramic electrolysers. Nat. Mater. **18**, 752–759 (2019). https://doi.org/10.1038/s41563-019-0388-2

26. Liu, Q., Dong, X.H., Xiao, G.L., et al.: A novel electrode material for symmetrical SOFCs. Adv. Mater. **22**, 5478–5482 (2010). https://doi.org/10.1002/adma.201001044

27. Su, C., Wang, W., Liu, M.L., et al.: Progress and prospects in symmetrical solid oxide fuel cells with two identical electrodes. Adv. Energy Mater. **5**, 1500188 (2015). https://doi.org/10.1002/aenm.201500188

28. Steele, B.C.H.: Appraisal of $Ce_{1-y}Gd_yO_{2-y/2}$ electrolytes for IT-SOFC operation at 500 °C. Solid State Ion. **129**, 95–110 (2000). https://doi.org/10.1016/S0167-2738(99)00319-7

29. Ishihara, T., Matsuda, H., Takita, Y.: Doped $LaGaO_3$ perovskite type oxide as a new oxide ionic conductor. J. Am. Chem. Soc. **116**, 3801–3803 (1994). https://doi.org/10.1021/ja00088a016

30. Yang, L., Wang, S.Z., Blinn, K., et al.: Enhanced sulfur and coking tolerance of a mixed ion conductor for SOFCs: $BaZr_{0.1}Ce_{0.7}Y_{0.2-x}Yb_xO_{3-\delta}$. Science **326**, 126–129 (2009). https://doi.org/10.1126/science.1174811

31. Nakayama, S., Aono, H., Sadaoka, Y.: Ionic conductivity of $Ln_{10}(SiO_4)_6O_3$ (Ln = La, Nd, Sm, Gd and Dy). Chem. Lett. **24**, 431–432 (1995). https://doi.org/10.1246/cl.1995.431

32. Haugsrud, R., Norby, T.: Proton conduction in rare-earth ortho-niobates and ortho-tantalates. Nat. Mater. **5**, 193–196 (2006). https://doi.org/10.1038/nmat1591

33. Li, M., Pietrowski, M.J., de Souza, R.A., et al.: A family of oxide ion conductors based on the ferroelectric perovskite $Na_{0.5}Bi_{0.5}TiO_3$. Nat. Mater. **13**, 31–35 (2014). https://doi.org/10.1038/nmat3782

34. Singh, P., Goodenough, J.B.: Monoclinic $Sr_{1-x}Na_xSiO_{3-0.5x}$: new superior oxide ion electrolytes. J. Am. Chem. Soc. **135**, 10149–10154 (2013). https://doi.org/10.1021/ja4042737

35. Norby, T.: The promise of protonics. Nature **410**, 877–878 (2001). https://doi.org/10.1038/35073718

36. Duan, C.C., Kee, R.J., Zhu, H.Y., et al.: Highly durable, coking and sulfur tolerant, fuel-flexible protonic ceramic fuel cells. Nature **557**, 217–222 (2018). https://doi.org/10.1038/s41586-018-0082-6

37. An, H., Lee, H.W., Kim, B.K., et al.: A 5 × 5 cm² protonic ceramic fuel cell with a power density of 1.3 W cm⁻² at 600 °C.

Nat. Energy **3**, 870–875 (2018). https://doi.org/10.1038/s41560-018-0230-0

38. Duan, C.C., Kee, R., Zhu, H.Y., et al.: Highly efficient reversible protonic ceramic electrochemical cells for power generation and fuel production. Nat. Energy **4**, 230–240 (2019). https://doi.org/10.1038/s41560-019-0333-2

39. Zhu, B.: Advantages of intermediate temperature solid oxide fuel cells for tractionary applications. J. Power Sources **93**, 82–86 (2001). https://doi.org/10.1016/S0378-7753(00)00564-4

40. Zhu, B.: Functional ceria-salt-composite materials for advanced ITSOFC applications. J. Power Sources **114**, 1–9 (2003). https://doi.org/10.1016/S0378-7753(02)00592-X

41. Zhu, B., Yang, X.T., Xu, J., et al.: Innovative low temperature SOFCs and advanced materials. J. Power Sources **118**, 47–53 (2003). https://doi.org/10.1016/S0378-7753(03)00060-0

42. Zhu, B.: Next generation fuel cell R&D. Int. J. Energy Res. **30**, 895–903 (2006). https://doi.org/10.1002/er.1195

43. Wang, X.D., Ma, Y., Raza, R., et al.: Novel core-shell SDC/amorphous $Na_2CO_3$ nanocomposite electrolyte for low-temperature SOFCs. Electrochem. Commun. **10**, 1617–1620 (2008). https://doi.org/10.1016/j.elecom.2008.08.023

44. Zhu, B., Li, S., Mellander, B.E.: Theoretical approach on ceria-based two-phase electrolytes for low temperature (300–600 °C) solid oxide fuel cells. Electrochem. Commun. **10**, 302–305 (2008). https://doi.org/10.1016/j.elecom.2007.11.037

45. Zhu, B.: Solid oxide fuel cell (SOFC) technical challenges and solutions from nano-aspects. Int. J. Energy Res. **33**, 1126–1137 (2009). https://doi.org/10.1002/er.1600

46. Ma, Y., Wang, X.D., Li, S.H., et al.: Samarium-doped ceria nanowires: novel synthesis and application in low-temperature solid oxide fuel cells. Adv. Mater. **22**, 1640–1644 (2010). https://doi.org/10.1002/adma.200903402

47. Raza, R., Wang, X.D., Ma, Y., et al.: Improved ceria-carbonate composite electrolytes. Int. J. Hydrog. Energy **35**, 2684–2688 (2010). https://doi.org/10.1016/j.ijhydene.2009.04.038

48. Fan, L.D., Wang, C.Y., Chen, M.M., et al.: Recent development of ceria-based (nano)composite materials for low temperature ceramic fuel cells and electrolyte-free fuel cells. J. Power Sources **234**, 154–174 (2013). https://doi.org/10.1016/j.jpowsour.2013.01.138

49. Fan, L.D., Zhang, G.Q., Chen, M.M., et al.: Proton and oxygen ionic conductivity of doped ceria-carbonate composite by modified Wagner polarization. Int. J. Electrochem. Sci. **7**, 8420–8435 (2012). https://doi.org/10.1002/cvde.201206981

50. Zhu, B., Mat, M.D.: Studies on dual phase ceria-based composites in electrochemistry. Int. J. Electrochem. Sci. **1**, 383–402 (2006).

51. Zhu, B., Albinsson, I., Andersson, C., et al.: Electrolysis studies based on ceria-based composites. Electrochem. Commun. **8**, 495–498 (2006). https://doi.org/10.1016/j.elecom.2006.01.011

52. Zhu, B., Liu, X.R., Schober, T.: Novel hybrid conductors based on doped ceria and BCY20 for ITSOFC applications. Electrochem. Commun. **6**, 378–383 (2004). https://doi.org/10.1016/j.elecom.2004.01.015

53. Huang, J.B., Mao, Z.Q., Liu, Z.X., et al.: Development of novel low-temperature SOFCs with co-ionic conducting SDC-carbonate composite electrolytes. Electrochem. Commun. **9**, 2601–2605 (2007). https://doi.org/10.1016/j.elecom.2007.07.036

54. Zhao, Y.C., Xia, C., Wang, Y.J., et al.: Quantifying multi-ionic conduction through doped ceria-carbonate composite electrolyte by a current-interruption technique and product analysis. Int. J. Hydrog. Energy **37**, 8556–8561 (2012). https://doi.org/10.1016/j.ijhydene.2012.02.053

55. Zhao, Y.C., Xia, C., Xu, Z.R., et al.: Validation of $H^+/O_2^-$ conduction in doped ceria-carbonate composite material using an electrochemical pumping method. Int. J. Hydrog. Energy **37**,

11378–11382 (2012). https://doi.org/10.1016/j.ijhydene.2012.05.015

56. Zhao, Y.C., Xu, Z.R., Xia, C., et al.: Oxide ion and proton conduction in doped ceria-carbonate composite materials. Int. J. Hydrog. Energy **38**, 1553–1559 (2013). https://doi.org/10.1016/j.ijhydene.2012.11.004

57. Xia, C., Li, Y., Tian, Y., et al.: Intermediate temperature fuel cell with a doped ceria-carbonate composite electrolyte. J. Power Sources **195**, 3149–3154 (2010). https://doi.org/10.1016/j.jpowsour.2009.11.104

58. Xia, C., Li, Y., Tian, Y., et al.: A high performance composite ionic conducting electrolyte for intermediate temperature fuel cell and evidence for ternary ionic conduction. J. Power Sources **188**, 156–162 (2009). https://doi.org/10.1016/j.jpowsour.2008.11.068

59. Zhang, G.H., Li, W.J., Huang, W., et al.: Strongly coupled $Sm_{0.2}Ce_{0.8}O_2$-$Na_2CO_3$ nanocomposite for low temperature solid oxide fuel cells: one-step synthesis and super interfacial proton conduction. J. Power Sources **386**, 56–65 (2018). https://doi.org/10.1016/j.jpowsour.2018.03.035

60. Wang, X.D., Ma, Y., Zhu, B.: State of the art ceria-carbonate composites (3C) electrolyte for advanced low temperature ceramic fuel cells (LTCFCs). Int. J. Hydrog. Energy **37**, 19417–19425 (2012). https://doi.org/10.1016/j.ijhydene.2011.09.096

61. Benamira, M., Ringuedé, A., Hildebrandt, L., et al.: Gadolinia-doped ceria mixed with alkali carbonates for SOFC applications: II—an electrochemical insight. Int. J. Hydrog. Energy **37**, 19371–19379 (2012). https://doi.org/10.1016/j.ijhydene.2011.10.062

62. Afzal, M., Raza, R., Du, S.F., et al.: Synthesis of $Ba_{0.3}Ca_{0.7}Co_{0.8}Fe_{0.2}O_{3-\delta}$ composite material as novel catalytic cathode for ceria-carbonate electrolyte fuel cells. Electrochimica Acta **178**, 385–391 (2015). https://doi.org/10.1016/j.electacta.2015.07.183

63. Sun, X.L., Li, S., Sun, J.C., et al.: Electrochemical performances of BSCF cathode materials for ceria-composite electrolyte low temperature solid oxide fuel cells. Int. J. Electrochem. Sci. **2**, 462–468 (2007)

64. Asghar, M.I., Heikkilä, M., Lund, P.D.: Advanced low-temperature ceramic nanocomposite fuel cells using ultra high ionic conductivity electrolytes synthesized through freeze-dried method and solid-route. Mater. Today Energy **5**, 338–346 (2017). https://doi.org/10.1016/j.mtener.2017.07.017

65. Rajesh, S., Pereira, J.R.S., Figueiredo, F.M.L., et al.: Performance of carbonate - $LaCoO_3$ and $La_{0.8}Sr_{0.2}Co_{0.2}Fe_{0.8}O_{3-\delta}$ composite cathodes under carbon dioxide. Electrochimica Acta **125**, 435–442 (2014). https://doi.org/10.1016/j.electacta.2014.01.157

66. Huang, J.B., Gao, R.F., Mao, Z.Q., et al.: Investigation of $La_2NiO_{4+\delta}$-based cathodes for SDC-carbonate composite electrolyte intermediate temperature fuel cells. Int. J. Hydrog. Energy **35**, 2657–2662 (2010). https://doi.org/10.1016/j.ijhydene.2009.04.022

67. Xia, C., Mi, Y.Q., Wang, B.Y., et al.: Shaping triple-conducting semiconductor $BaCo_{0.4}Fe_{0.4}Zr_{0.1}Y_{0.1}O_{3-\delta}$ into an electrolyte for low-temperature solid oxide fuel cells. Nat. Commun. **10**, 1707 (2019). https://doi.org/10.1038/s41467-019-09532-z

68. Xing, Y.M., Wu, Y., Li, L.Y., et al.: Proton shuttles in $CeO_2$/$CeO_{2-\delta}$ core–shell structure. ACS Energy Lett. **4**, 2601–2607 (2019). https://doi.org/10.1021/acsenergylett.9b01829

69. Kim, J., Jun, A., Gwon, O., et al.: Hybrid-solid oxide electrolysis cell: a new strategy for efficient hydrogen production. Nano Energy **44**, 121–126 (2018). https://doi.org/10.1016/j.nanoen.2017.11.074

70. Wang, B.Y., Zhu, B., Yun, S.N., et al.: Fast ionic conduction in semiconductor $CeO_{2-\delta}$ electrolyte fuel cells. NPG Asia Mater. **11**, 51 (2019). https://doi.org/10.1038/s41427-019-0152-8

71. Duncan, K.L., Lee, K.T., Wachsman, E.D.: Dependence of open-circuit potential and power density on electrolyte thickness in solid oxide fuel cells with mixed conducting electrolytes. J. Power Sources **196**, 2445–2451 (2011). https://doi.org/10.1016/j.jpowsour.2010.10.034

72. Riess, I.: The possible use of mixed ionic electronic conductors instead of electrolytes in fuel cells. Solid State Ion. **52**, 127–134 (1992). https://doi.org/10.1016/0167-2738(92)90098-A

73. Zhu, B., Ma, Y., Wang, X.D., et al.: A fuel cell with a single component functioning simultaneously as the electrodes and electrolyte. Electrochem. Commun. **13**, 225–227 (2011). https://doi.org/10.1016/j.elecom.2010.12.019

74. Zhu, B., Qin, H.Y., Raza, R., et al.: A single-component fuel cell reactor. Int. J. Hydrog. Energy **36**, 8536–8541 (2011). https://doi.org/10.1016/j.ijhydene.2011.04.082

75. Zhu, B., Raza, R., Abbas, G., et al.: An electrolyte-free fuel cell constructed from one homogenous layer with mixed conductivity. Adv. Funct. Mater. **21**, 2465–2469 (2011). https://doi.org/10.1002/adfm.201002471

76. Zhu, B., Raza, R., Qin, H.Y., et al.: Single-component and three-component fuel cells. J. Power Sources **196**, 6362–6365 (2011). https://doi.org/10.1016/j.jpowsour.2011.03.078

77. Zhu, B., Raza, R., Qin, H.Y., et al.: Fuel cells based on electrolyte and non-electrolyte separators. Energy Environ. Sci. **4**, 2986 (2011). https://doi.org/10.1039/c1ee01202a

78. He, H.P., Huang, X.J., Chen, L.Q.: A practice of single layer solid oxide fuel cell. Ionics **6**, 64–69 (2000). https://doi.org/10.1007/BF02375548

79. He, H.P., Huang, X.J., Chen, L.Q.: Sr-doped LaInO$_3$ and its possible application in a single layer SOFC. Solid State Ion. **130**, 183–193 (2000). https://doi.org/10.1016/S0167-2738(00)00666-4

80. Lan, R., Tao, S.W.: Novel proton conductors in the layered oxide material Li$_x$Al$_{0.5}$Co$_{0.5}$O$_2$. Adv. Energy Mater. **4**: 1301683. (2014). https://doi.org/10.1002/aenm.201401461

81. Dong, W.J., Yaqub, A., Janjua, N.K., et al.: All in one multifunctional perovskite material for next generation SOFC. Electrochim. Acta **193**, 225–230 (2016). https://doi.org/10.1016/j.electacta.2016.02.061

82. Dong, W.J., Tong, Y.Z., Zhu, B., et al.: Semiconductor TiO$_2$ thin film as an electrolyte for fuel cells. J. Mater. Chem. A **7**, 16728–16734 (2019). https://doi.org/10.1039/c9ta01941c

83. Xia, C., Qiao, Z., Shen, L.P., et al.: Semiconductor electrolyte for low-operating-temperature solid oxide fuel cell: Li-doped ZnO. Int. J. Hydrog. Energy **43**, 12825–12834 (2018). https://doi.org/10.1016/j.ijhydene.2018.04.121

84. Chen, G., Zhu, B., Deng, H., et al.: Advanced fuel cell based on perovskite La–SrTiO$_3$ semiconductor as the electrolyte with superoxide-ion conduction. ACS Appl. Mater. Interfaces **10**, 33179–33186 (2018). https://doi.org/10.1021/acsami.8b10087

85. Chen, G., Liu, H.L., He, Y., et al.: Electrochemical mechanisms of an advanced low-temperature fuel cell with a SrTiO$_3$ electrolyte. J. Mater. Chem. A **7**, 9638–9645 (2019). https://doi.org/10.1039/c9ta00499h

86. Shi, Y.N., Wang, L.Y., Wang, Z.Y., et al.: Defect engineering for tuning the photoresponse of ceria-based solid oxide photoelectrochemical cells. ACS Appl. Mater. Interfaces **13**, 541–551 (2021). https://doi.org/10.1021/acsami.0c17921

87. Zhu, B., Raza, R., Liu, Q.H., et al.: A new energy conversion technology joining electrochemical and physical principles. RSC Adv. **2**, 5066 (2012). https://doi.org/10.1039/c2ra01234k

88. Zhu, B., Lund, P., Raza, R., et al.: A new energy conversion technology based on nano-redox and nano-device processes. Nano Energy **2**, 1179–1185 (2013). https://doi.org/10.1016/j.nanoen.2013.05.001

89. Wang, G.J., Wu, X.Y., Cai, Y.X., et al.: Design, fabrication and characterization of a double layer solid oxide fuel cell (DLFC). J. Power Sources **332**, 8–15 (2016). https://doi.org/10.1016/j.jpowsour.2016.09.011

90. Shao, K., Li, F.J., Zhang, G.H., et al.: Approaching durable single-layer fuel cells: promotion of electroactivity and charge separation via nanoalloy redox exsolution. ACS Appl. Mater. Interfaces **11**, 27924–27933 (2019). https://doi.org/10.1021/acsami.9b08448

91. Fan, L.D., Wang, C.Y., Osamudiamen, O., et al.: Mixed ion and electron conductive composites for single component fuel cells: I. Effects of composition and pellet thickness. J. Power Sources **217**, 164–169 (2012). https://doi.org/10.1016/j.jpowsour.2012.05.045

92. Wu, J.S., Zhu, B., Mi, Y.Q., et al.: A novel core-shell nano-composite electrolyte for low temperature fuel cells. J. Power Sources **201**, 164–168 (2012). https://doi.org/10.1016/j.jpowsour.2011.10.084

93. Cai, Y.X., Chen, Y., Akbar, M., et al.: A bulk-heterostructure nanocomposite electrolyte of Ce$_{0.8}$Sm$_{0.2}$O$_{2-\delta}$-SrTiO$_3$ for low-temperature solid oxide fuel cells. Nano Micro Lett. **13**, 1–14 (2021). https://doi.org/10.1007/s40820-020-00574-3

94. Rauf, S., Zhu, B., Yousaf Shah, M.A.K., et al.: Application of a triple-conducting heterostructure electrolyte of Ba$_{0.5}$Sr$_{0.5}$Co$_{0.1}$Fe$_{0.7}$Zr$_{0.1}$Y$_{0.1}$O$_{3-\delta}$ and Ca$_{0.04}$Ce$_{0.80}$Sm$_{0.16}$O$_{2-\delta}$ in a high-performance low-temperature solid oxide fuel cell. ACS Appl. Mater. Interfaces **12**, 35071–35080 (2020). https://doi.org/10.1021/acsami.0c10061

95. Lu, Y.Z., Akbar, M., Xia, C., et al.: Catalytic membrane with high ion-electron conduction made of strongly correlated perovskite LaNiO$_3$ and Ce$_{0.8}$Sm$_{0.2}$O$_{2-\delta}$ for fuel cells. J. Catal. **386**, 117–125 (2020). https://doi.org/10.1016/j.jcat.2020.04.004

96. Wu, Y., Dong, B., Zhang, J., et al.: The synthesis of ZnO/SrTiO$_3$ composite for high-efficiency photocatalytic hydrogen and electricity conversion. Int. J. Hydrog. Energy **43**, 12627–12636 (2018). https://doi.org/10.1016/j.ijhydene.2018.03.206

97. Cai, Y.X., Wang, B.Y., Wang, Y., et al.: Validating the technological feasibility of yttria-stabilized zirconia-based semi-conducting-ionic composite in intermediate-temperature solid oxide fuel cells. J. Power Sources **384**, 318–327 (2018). https://doi.org/10.1016/j.jpowsour.2018.03.012

98. Han, F., Yun, S.N., Shi, J., et al.: Efficient dual-function catalysts for triiodide reduction reaction and hydrogen evolution reaction using unique 3D network aloe waste-derived carbon-supported molybdenum-based bimetallic oxide nanohybrids. Appl. Catal. B: Environ. **273**, 119004 (2020). https://doi.org/10.1016/j.apcatb.2020.119004

99. Fuel cells: Three in one. Nat. Nanotechnol. **6**, 330 (2011). https://doi.org/10.1038/nnano.2011.93.

100. Zhu, B., Lund, P.D., Raza, R., et al.: Schottky junction effect on high performance fuel cells based on nanocomposite materials. Adv. Energy Mater. **5**, 1401895 (2015). https://doi.org/10.1002/aenm.201401895

101. Afzal, M., Saleemi, M., Wang, B.Y., et al.: Fabrication of novel electrolyte-layer free fuel cell with semi-ionic conductor (Ba$_{0.5}$Sr$_{0.5}$Co$_{0.8}$Fe$_{0.2}$O$_{3-\delta}$- Sm$_{0.2}$Ce$_{0.8}$O$_{1.9}$) and Schottky barrier. J. Power Sources **328**, 136–142 (2016). https://doi.org/10.1016/j.jpowsour.2016.07.093

102. Zhu, B., Huang, Y.Z., Fan, L.D., et al.: Novel fuel cell with nanocomposite functional layer designed by perovskite solar cell principle. Nano Energy **19**, 156–164 (2016). https://doi.org/10.1016/j.nanoen.2015.11.015

103. Zhu, B., Wang, B.Y., Wang, Y., et al.: Charge separation and transport in La$_{0.6}$Sr$_{0.4}$Co$_{0.2}$Fe$_{0.8}$O$_{3-\delta}$ and ion-doping ceria heterostructure material for new generation fuel cell. Nano Energy

**37**, 195–202 (2017). https://doi.org/10.1016/j.nanoen.2017.05.003

104. Yun, S.N., Zhou, H.W., Wang, L., et al.: Economical hafnium oxygen nitride binary/ternary nanocomposite counter electrode catalysts for high-efficiency dye-sensitized solar cells. J. Mater. Chem. A **1**, 1341–1348 (2013). https://doi.org/10.1039/c2ta00680d

105. Yun, S.N., Zhang, H., Pu, H.H., et al.: Metal oxide/carbide/carbon nanocomposites: in situ synthesis, characterization, calculation, and their application as an efficient counter electrode catalyst for dye-sensitized solar cells. Adv. Energy Mater. **3**, 1407–1412 (2013). https://doi.org/10.1002/aenm.201300242

106. Yun, S.N., Wu, M.X., Wang, Y.D., et al.: Pt-like behavior of high-performance counter electrodes prepared from binary tantalum compounds showing high electrocatalytic activity for dye-sensitized solar cells. Chemsuschem **6**, 411–416 (2013). https://doi.org/10.1002/cssc.201200845

107. Yun, S.N., Wang, L., Zhao, C.Y., et al.: A new type of low-cost counter electrode catalyst based on platinum nanoparticles loaded onto silicon carbide (Pt/SiC) for dye-sensitized solar cells. Phys. Chem. Chem. Phys. **15**, 4286 (2013). https://doi.org/10.1039/c3cp44048f

108. Yun, S.N., Wang, L., Guo, W., et al.: Non-Pt counter electrode catalysts using tantalum oxide for low-cost dye-sensitized solar cells. Electrochem. Commun. **24**, 69–73 (2012). https://doi.org/10.1016/j.elecom.2012.08.008

109. Vedhanarayanan, B., Shi, J., Lin, J.Y., et al.: Enhanced activity and stability of $MoS_2$ through enriching 1T-phase by covalent functionalization for energy conversion applications. Chem. Eng. J. **403**, 126318 (2021). https://doi.org/10.1016/j.cej.2020.126318

110. Yun, S.N., Si, Y.M., Shi, J., et al.: Electronic structures and catalytic activities of niobium oxides as electrocatalysts in liquid-junction photovoltaic devices. Sol. RRL **4**, 1900430 (2020). https://doi.org/10.1002/solr.201900430

111. Filip, M.R., Hillman, S., Haghighirad, A.A., et al.: Band gaps of the lead-free halide double perovskites $Cs_2BiAgCl_6$ and $Cs_2BiAgBr_6$ from theory and experiment. J. Phys. Chem. Lett. **7**, 2579–2585 (2016). https://doi.org/10.1021/acs.jpclett.6b01041

112. Pessoa, R.S., Fraga, M.A., Santos, L.V., et al.: Nanostructured thin films based on $TiO_2$ and/or SiC for use in photoelectrochemical cells: a review of the material characteristics, synthesis and recent applications. Mater. Sci. Semicond. Process. **29**, 56–68 (2015). https://doi.org/10.1016/j.mssp.2014.05.053

113. Xing, Y.M., Hu, E.Y., Wang, F.Z., et al.: Cubic silicon carbide/zinc oxide heterostructure fuel cells. Appl. Phys. Lett. **117**, 162105 (2020). https://doi.org/10.1063/5.0021460

114. Mushtaq, N., Xia, C., Dong, W.J., et al.: Tuning the energy band structure at interfaces of the $SrFe_{0.75}Ti_{0.25}O_{3-\delta}$–$Sm_{0.25}Ce_{0.75}O_{2-\delta}$ heterostructure for fast ionic transport. ACS Appl. Mater. Interfaces **11**, 38737–38745 (2019). https://doi.org/10.1021/acsami.9b13044

115. Meng, Y.J., Wang, X.Y., Zhang, W., et al.: Novel high ionic conductivity electrolyte membrane based on semiconductor $La_{0.65}Sr_{0.3}Ce_{0.05}Cr_{0.5}Fe_{0.5}O_{3-\delta}$ for low-temperature solid oxide fuel cells. J. Power Sources **421**, 33–40 (2019). https://doi.org/10.1016/j.jpowsour.2019.02.100

116. Chen, G., Sun, W.K., Luo, Y.D., et al.: Advanced fuel cell based on new nanocrystalline structure $Gd_{0.1}Ce_{0.9}O_2$ electrolyte. ACS Appl. Mater. Interfaces **11**, 10642–10650 (2019). https://doi.org/10.1021/acsami.8b20454

117. Wu, Y., Liu, L., Yu, X.X., et al.: Natural hematite ore composited with ZnO nanoneedles for energy applications. Compos. B: Eng. **137**, 178–183 (2018). https://doi.org/10.1016/j.compositesb.2017.11.020

118. Qiao, Z., Xia, C., Cai, Y.X., et al.: Electrochemical and electrical properties of doped $CeO_2$-ZnO composite for low-temperature solid oxide fuel cell applications. J. Power Sources **392**, 33–40 (2018). https://doi.org/10.1016/j.jpowsour.2018.04.096

119. Xia, C., Cai, Y.X., Wang, B.Y., et al.: Strategy towards cost-effective low-temperature solid oxide fuel cells: a mixed-conductive membrane comprised of natural minerals and perovskite oxide. J. Power Sources **342**, 779–786 (2017). https://doi.org/10.1016/j.jpowsour.2016.12.120

120. Wu, Y., Xia, C., Zhang, W., et al.: Natural hematite for next-generation solid oxide fuel cells. Adv. Funct. Mater. **26**, 938–942 (2016). https://doi.org/10.1002/adfm.201503756

121. Wang, B.Y., Wang, Y., Fan, L.D., et al.: Preparation and characterization of Sm and Ca co-doped ceria–$La_{0.6}Sr_{0.4}Co_{0.2}Fe_{0.8}O_{3-\delta}$ semiconductor–ionic composites for electrolyte-layer-free fuel cells. J. Mater. Chem. A **4**, 15426–15436 (2016). https://doi.org/10.1039/c6ta05763b

122. Yun, S.N., Zhang, Y.W., Xu, Q., et al.: Recent advance in new-generation integrated devices for energy harvesting and storage. Nano Energy **60**, 600–619 (2019). https://doi.org/10.1016/j.nanoen.2019.03.074

123. Yun, S.N., Qin, Y., Uhl, A.R., et al.: New-generation integrated devices based on dye-sensitized and perovskite solar cells. Energy Environ. Sci. **11**, 476–526 (2018). https://doi.org/10.1039/c7ee03165c

124. Goodenough, J.B., Park, K.-S.: The Li-ion rechargeable battery: a perspective. J. Am. Chem. Soc. **135**(4), 1167–1176 (2013). https://doi.org/10.1021/ja3091438

125. Goodenough, J.B., Kim, Y.: Challenges for rechargeable Li batteries. Chem. Mater. **22**, 587–603 (2010). https://doi.org/10.1021/cm901452z

126. Ensling, D., Cherkashinin, G., Schmid, S., et al.: Nonrigid band behavior of the electronic structure of $LiCoO_2$ thin film during electrochemical Li deintercalation. Chem. Mater. **26**, 3948–3956 (2014). https://doi.org/10.1021/cm501480b

127. Jaegermann, W., Klein, A., Mayer, T.: Interface engineering of inorganic thin-film solar cells - materials-science challenges for advanced physical concepts. Adv. Mater. **21**, 4196–4206 (2009). https://doi.org/10.1002/adma.200802457

128. Maier, J.: Physical chemistry of ionic materials. Chichester, UK: John Wiley & Sons, Ltd, 2004. https://doi.org/10.1002/0470020229

129. Sato, N.: Mixed electrodes. Electrochemistry at Metal and Semiconductor Electrodes. Amsterdam: Elsevier, 1998: 373–389. https://doi.org/10.1016/b978-044482806-4/50011-8

130. Becker, D., Cherkashinin, G., Hausbrand, R., et al.: Adsorption of diethyl carbonate on $LiCoO_2$ thin films: formation of the electrochemical interface. J. Phys. Chem. C **118**, 962–967 (2014). https://doi.org/10.1021/jp405714x

131. Sun, Y.F., Kotiuga, M., Lim, D., et al.: Strongly correlated perovskite lithium ion shuttles. PNAS **115**, 9672–9677 (2018). https://doi.org/10.1073/pnas.1805029115

132. Wang, C., Yun, S.N., Fan, Q.Y., et al.: A hybrid niobium-based oxide with bio-based porous carbon as an efficient electrocatalyst in photovoltaics: a general strategy for understanding the catalytic mechanism. J. Mater. Chem. A **7**, 14864–14875 (2019). https://doi.org/10.1039/c9ta03540k

133. Yun, S.N., Zhou, X., Even, J., et al.: Theoretical treatment of $CH_3NH_3PbI_3$ perovskite solar cells. Angewandte Chemie Int. Ed. **56**, 15806–15817 (2017). https://doi.org/10.1002/anie.201702660

134. Yun, S.N., Hagfeldt, A., Ma, T.L.: Pt-free counter electrode for dye-sensitized solar cells with high efficiency. Adv. Mater. **26**, 6210–6237 (2014). https://doi.org/10.1002/adma.201402056

135. Yun, S.N., Wang, X.L., Li, J.F., et al.: Investigation of dielectric relaxation mechanism in bismuth doped barium calcium titanate

ceramics by dielectric and Raman spectroscopy. Mater. Chem. Phys. **116**, 339–343 (2009). https://doi.org/10.1016/j.matchemphys.2009.02.057

136. Yun, S.N., Wang, X.L., Li, J.F., et al.: Linear dielectric response and dielectric relaxation behavior of bismuth-doped $(Ba_{1-x}Ca_{x/2}Sr_{x/2})TiO_3$ ceramics. Phys. Stat. Sol. (a) **206**, 303–310 (2009). https://doi.org/10.1002/pssa.200824272

137. Yun, S.N., Wang, X.L.: Dielectric properties of $(Ba_{1-2x}Sr_xCa_x)$ $TiO_3$ ferroelectric ceramics. J. Electroceramics **21**, 585–588 (2008). https://doi.org/10.1007/s10832-007-9252-x

138. Yun, S.N., Wang, X.L.: Dielectric properties of bismuth doped $Ba_{1-x}Ca_xTiO_3$ ceramics. Mater. Lett. **60**, 2211–2213 (2006). https://doi.org/10.1016/j.matlet.2005.12.122

139. Braga, M.H., Ferreira, J.A., Murchison, A.J., et al.: Electric dipoles and ionic conductivity in a $Na^+$ glass electrolyte. J. Electrochem. Soc. **164**, A207–A213 (2016). https://doi.org/10.1149/2.0691702jes

140. Yan, C.S., Zhu, Y., Li, Y.T., et al.: Local built-in electric field enabled in carbon-doped $Co_3O_4$ nanocrystals for superior lithium-ion storage. Adv. Funct. Mater. **28**, 1705951 (2018). https://doi.org/10.1002/adfm.201705951

141. Ni, J.F., Sun, M.L., Li, L.: Highly efficient sodium storage in iron oxide nanotube arrays enabled by built-in electric field. Adv. Mater. **31**, 1902603 (2019). https://doi.org/10.1002/adma.201902603

142. Luo, W., Li, F., Li, Q., et al.: Heterostructured $Bi_2S_3$-$Bi_2O_3$ nanosheets with a built-in electric field for improved sodium storage. ACS Appl. Mater. Interfaces **10**, 7201–7207 (2018). https://doi.org/10.1021/acsami.8b01613

143. Li, C., Dong, S., Tang, R., et al.: Heteroatomic interface engineering in MOF-derived carbon heterostructures with built-in electricfield effects for high performance Al-ion batteries. Energy Environ. Sci. **11**, 3201–3211 (2018). https://doi.org/10.1039/c8ee01046c

144. Yun, S.N., Freitas, J.N., Nogueira, A.F., et al.: Dye-sensitized solar cells employing polymers. Prog. Polym. Sci. **59**, 1–40 (2016). https://doi.org/10.1016/j.progpolymsci.2015.10.004

145. Shen, S.L., Yang, Y.P., Guo, L.J., et al.: A polarization model for a solid oxide fuel cell with a mixed ionic and electronic conductor as electrolyte. J. Power Sources **256**, 43–51 (2014). https://doi.org/10.1016/j.jpowsour.2014.01.041

146. Zhang, H., Luo, Z.M., Liu, Y.L., et al.: Noble-metal-free $Ni_3C$ as co-catalyst on $LaNiO_3$ with enhanced photocatalytic activity. Appl. Catal. B: Environ. **277**, 119166 (2020). https://doi.org/10.1016/j.apcatb.2020.119166

147. Zeng, Q., Lai, Y.Q., Jiang, L.X., et al.: Integrated photorechargeable energy storage system: next-generation power source driving the future. Adv. Energy Mater. **10**, 1903930 (2020). https://doi.org/10.1002/aenm.201903930

148. Ishii, Y., Kurimoto, K., Hosoe, K., et al.: Photo-rechargeable fuel cell using photo-hydrogenation reactions of quinone molecules. New J. Chem. **44**, 2275–2280 (2020). https://doi.org/10.1039/c9nj04782d

149. Zhu, Z., Shi, X.M., Fan, G.L., et al.: Photo-energy conversion and storage in an aprotic Li-O2 battery. Angew. Chem. Int. Ed. **58**, 19021–19026 (2019). https://doi.org/10.1002/anie.201911228

150. Zhu, D.D., Zhao, Q.C., Fan, G.L., et al.: Photoinduced oxygen reduction reaction boosts the output voltage of a zinc-air battery. Angew. Chem. Int. Ed. **58**, 12460–12464 (2019). https://doi.org/10.1002/anie.201905954

151. Wang, K., Mo, Z.H., Tang, S.T., et al.: Photo-enhanced Zn–air batteries with simultaneous highly efficient *in situ* $H_2O_2$ generation for wastewater treatment. J. Mater. Chem. A **7**, 14129–14135 (2019). https://doi.org/10.1039/c9ta04253a

152. Xu, X.Y., Zhao, H., Wang, R., et al.: Identification of few-layer $ReS_2$ as photo-electro integrated catalyst for hydrogen evolution.

Nano Energy **48**, 337–344 (2018). https://doi.org/10.1016/j.nanoen.2018.03.078

153. Lv, J., Abbas, S.C., Huang, Y.Y., et al.: A photo-responsive bifunctional electrocatalyst for oxygen reduction and evolution reactions. Nano Energy **43**, 130–137 (2018). https://doi.org/10.1016/j.nanoen.2017.11.020

154. Cai, C., Han, S.B., Caiyang, W.N., et al.: Tracing the origin of visible light enhanced oxygen evolution reaction. Adv. Mater. Interfaces **6**, 1801543 (2019). https://doi.org/10.1002/admi.201801543

155. Liu, Z.R., Wang, L.W., Yu, X., et al.: Piezoelectric-effect-enhanced full-spectrum photoelectrocatalysis in p-n heterojunction. Adv. Funct. Mater. **29**, 1807279 (2019). https://doi.org/10.1002/adfm.201807279

156. Chen, P., Li, G.R., Li, T.T., et al.: Solar-driven rechargeable lithium-sulfur battery. Adv. Sci. **6**, 1900620 (2019). https://doi.org/10.1002/advs.201900620

157. Liu, X.R., Yuan, Y.F., Liu, J., et al.: Utilizing solar energy to improve the oxygen evolution reaction kinetics in zinc-air battery. Nat. Commun. **10**, 1–10 (2019). https://doi.org/10.1038/s41467-019-12627-2

158. Liu, Y., Li, N., Liao, K.M., et al.: Lowering the charge voltage of $Li–O_2$ batteries via an unmediated photoelectrochemical oxidation approach. J. Mater. Chem. A **4**, 12411–12415 (2016). https://doi.org/10.1039/c6ta03583c

159. Zhang, B.Q., Wang, S.Y., Fan, W.J., et al.: Photoassisted oxygen reduction reaction in $H_2$–$O_2$ fuel cells. Angew. Chem. Int. Ed. **55**, 14748–14751 (2016). https://doi.org/10.1002/anie.201607118

160. Paolella, A., Faure, C., Bertoni, G., et al.: Light-assisted delithiation of lithium iron phosphate nanocrystals towards photorechargeable lithium ion batteries. Nat. Commun. **8**, 1–10 (2017). https://doi.org/10.1038/ncomms14643

161. Liu, Y., Li, N., Wu, S.C., et al.: Reducing the charging voltage of a $Li–O_2$ battery to 1.9 V by incorporating a photocatalyst. Energy Environ. Sci. **8**, 2664–2667 (2015). https://doi.org/10.1039/c5ee01958c

162. Wang, B., Zhang, H., Lu, X.Y., et al.: Solar photocatalytic fuel cell using $CdS$-$TiO_2$ photoanode and air-breathing cathode for wastewater treatment and simultaneous electricity production. Chem. Eng. J. **253**, 174–182 (2014). https://doi.org/10.1016/j.cej.2014.05.041

163. Shan, X., Ke, O.Y., Yan, S.: A solar responsive photocatalytic fuel cell with a heterostructured $ZnFe_2O_4/TiO_2$-NTs photoanode and an air-breathing cathode. Int. J. Hydrog. Energy **42**, 29201–29209 (2017). https://doi.org/10.1016/j.ijhydene.2017.10.059

164. Huang, J.S., Yuan, Y.B., Shao, Y.C., et al.: Understanding the physical properties of hybrid perovskites for photovoltaic applications. Nat. Rev. Mater. **2**, 17042 (2017). https://doi.org/10.1038/natrevmats.2017.42

165. Aristidou, N., Eames, C., Sanchez-Molina, I., et al.: Fast oxygen diffusion and iodide defects mediate oxygen-induced degradation of perovskite solar cells. Nat. Commun. **8**, 15218 (2017). https://doi.org/10.1038/ncomms15218

166. Li, C., Guerrero, A., Huettner, S., et al.: Unravelling the role of vacancies in lead halide perovskite through electrical switching of photoluminescence. Nat. Commun. **9**, 5113 (2018). https://doi.org/10.1038/s41467-018-07571-6

167. Eames, C., Frost, J.M., Barnes, P.R.F., et al.: Ionic transport in hybrid lead iodide perovskite solar cells. Nat. Commun. **6**, 7497 (2015). https://doi.org/10.1038/ncomms8497

168. Walsh, A., Stranks, S.D.: Taking control of ion transport in halide perovskite solar cells. ACS Energy Lett. **3**, 1983–1990 (2018). https://doi.org/10.1021/acsenergylett.8b00764

169. Wang, B.Y., Cai, Y.X., Dong, W.J., et al.: Photovoltaic properties of $Li_xCo_{3-x}O_4/TiO_2$ heterojunction solar cells with high

open-circuit voltage. Sol. Energy Mater. Sol. Cells **157**, 126–133 (2016). https://doi.org/10.1016/j.solmat.2016.05.036

170. Christoforidis, K.C., Fornasiero, P.: Photocatalytic hydrogen production: a rift into the future energy supply. ChemCatChem **9**, 1523–1544 (2017). https://doi.org/10.1002/cctc.201601659



**Bin Zhu** Chief scientist in Jiangsu Provincial Key Laboratory of Solar Energy Science and Technology/Energy Storage Joint Research Center, School of Energy and Environment, Southeast University. Since 1998 he started the research as principal investigator at KTH and 1999 became associate professor/senior researcher in KTH until 2018, then as a visiting professor position in Loughborough University, UK. In 2013, based on the great invention of single layer electrolyte-free fuel cell—a research breakthrough, he was selected by Hubei provincial 100-overseas talents program to establish and lead research team in Hubei University, then extended to China University of Geoscience (Wuhan). 2019–now, a lecturer professor in Xi'an Jiaotong University, and 2020–now, Southeast University. He has published about 400 research papers. Together with Prof. Peter Lund, Aalto University as the recipient of 2018 WSSET (World Society of Sustainable Energy Technologies) Innovation award for Power Generation. He is one of the Most Cited scholars in China (Energy sector, Elsevier) since 2014. His current research interests lie in the energy conversion, especially next generation semiconductors based LTSOFCs, PCFCs (proton ceramic fuel cells), and joint fuel cells and solar fuels or battery science and technology based on semiconductor-ionics and semiconductor electrochemistry, where electron–ion coupling enhanced ionic transport, multi-charge transfer and super proton transport processes, surficial and interfacial superionic conduction, nano-redox process and nano-redox units/devices for high ion-flux energy devices and technologies.



**Liangdong Fan** is a Research Associate Professor in the Department of New Energy Science and Technology, College of Chemistry and Environmental Engineering, Shenzhen University, China. He received his double Ph.D. degree, one in Energy Technology from the Royal Institute of Technology (KTH, Sweden) in 2014 and another in Chemical Technology from Tianjin University, in 2012. He was a postdoctoral Research Fellow at Nanyang Technological University (2014.06–2015.11). Since the end of 2015, Dr. Fan joined Shenzhen University as a Lecturer/Research Associate Professor (Principal Investigator). His current research interests are developing inorganic functional materials such as perovskite oxides for high temperature fuel cells/electrolysis cells and low temperature electrocatalysis applications.



**Naveed Mushtaq** is a Post-doctoral researcher at Jiangsu Provincial Key Laboratory of Solar Energy Science and Technology/Energy Storage Joint Research Center, School of Energy and Environment, Southeast University, Nanjing. Dr. Naveed obtained his Master degree in Physics from COMSATS University Islamabad, Lahore campus and Ph.D. from Hubei University, Wuhan, China. His main research interests include fuel cells oxygen reduction electrocatalysts and nanostructured functional materials for energy devices. Dr. Naveed has published ~ 30 journal papers in his research.



**Rizwan Raza** is a Tenured Associate Professor at COMSATS University Islamabad, Lahore Campus, Pakistan and Visiting Researcher at Linkoping University and Chalmers University of Technology, Sweden. Raza completed PhD in Energy Technology from KTH, Sweden in 2012. Dr. Raza has 15 years of experience in Energy materials research and teaching. Raza has published more than 200 journal papers. He has edited 02 books and 10 book chapters. He has been working on several multidisciplinary projects regarding "Energy conversion & Energy storage devices (Fuel cells, Solar cells, Batteries, Supercapacitor)". He received some of the remarkable awards the world over; Gold Medalist from Pakistan Academy of Sciences 2018, Winner of the Award "idea to product "I2P ® Stockholm-2011", Raza is awarded a "Youngest Scientist in Pakistan" for 2016 and 2017. Raza has also established a well-equipped fuel cell research laboratory in Pakistan. It is one of the earliest fuel cell research laboratories in Pakistan.



**Muhammad Sajid** is currently doing his Ph.D. from School of Chemistry and Materials Science, University of Science and Technology of China (USTC), China. He received his MS in Physics from COMSATS University Islamabad, Lahore Campus, Pakistan under supervision of Dr. Rizwan Raza. His research interests mainly focus on Batteries, water electrolysis, catalysis, nanomaterials and SOFCs.

**Yan Wu** is an Associate Professor at the Faculty of Material Science and Chemistry, China University of Geoscience (Wuhan). She received a Ph.D. from the Royal Institute of Technology in 2010, with Prof. K.V. Rao and Lyuba Belova. Then She joined the China University of Geoscience and was promoted to Associate Professor in Dec. 2011. Her current research interests are advanced energy and resources utilization with nanotechnology and new semiconducting photocatalysis.

**Wenfeng Lin** FRSC (Fellow of Royal Society of Chemistry, UK), is the Professor of Chemical Engineering and Departmental Research Director at Loughborough University, England. He obtained his BSc, MSc and PhD from Xiamen University, with his PhD thesis work on combined studies of quantum chemistry and spectro-electrochemistry on electrocatalysis and interfaces, under the supervision of Profs. Z. W. Tian, S. G. Sun and Z. Q. Tian. He was awarded two prestigious Humboldt-Foundation and Max-Planck-Society Postdoc Research Fellowships and worked with Nobel Laureate Prof. Ertl in the Fritz-Haber-Institute in Berlin, Germany. In the UK, he worked in Newcastle University and Queen's University Belfast before joining Loughborough University in 2015. The primary themes of his research are related to electrochemical energy and environmental technologies. He collaborates internationally and has led a significant number of externally funded projects, ranging from fundamental understanding of electro-catalysis at atomic and molecular levels to applied R&D in energy materials, fuel cells, batteries, hydrogen production, carbon dioxide utilization, ozone generation and advanced oxidation technology. He has over 170 publications and contributed to 2 high tech spin-outs in UK.

**Jung-Sik Kim** is a senior lecturer at the Department of Aero & Auto Eng. Loughborough University, UK. He is an experienced researcher and teacher specialising in the investigation of electrochemical processes for energy conversion and storage. His work in the field of solid oxide fuel cells has been supervised by Professor Alan Atkinson and Professor John Kilner at the Department of Materials, Imperial College London since 2006, and commenced his research activity at Loughborough University since 2010 as a lecturer and then senior lecturer since 2015. Dr Kim has obtained his PhD in the Department of Mechanical Engineering & at the University of Birmingham, UK in 2006. His component level SOFC research commitments have been evolved into their system level R&D based on thermo-electrochemical analysis, deploying multi-thermal sensing technology which generates an enormous amount of data, so that he continues contributing effectively in this role by suggesting hybrid interconversion energy systems utilising renewable and traditional energy materials.

**Peter D. Lund** is Professor in Engineering Physics and Advanced Energy Systems at Aalto University, Finland. His D.Sc. is from Helsinki University of Technology; he is a London Business School Alumni. He has had visiting positions in China and Germany, and he is Honorary Professor at Southeast University in Nanjing. He has chaired the Advisory Group Energy of the European Commission and the Energy Steering Panel of European Academies Science Advisory Council. He is vice-chair of the Finnish Climate Change Panel. He is member of the Finnish Academy Science and Letters and Swedish Engineering Academy in Finland. His research interest encompasses sustainable energy, nanomaterials, fuel cell, and solar cells. He has published 350 journal papers and has received several international awards.

**Sining Yun** is a Professor in School of Materials Science and Engineering, Xi'an University of Architecture and Technology, China. He obtained his PhD at Xi'an Jiaotong University in 2007 and was a postdoctoral fellow in Yonsei University (Korea). He is a visiting professor at State Key Lab. of Fine Chemicals (China), University of Reading (UK), Prof. Michael Grätzel and Prof. Anders Hagfeldt's laboratory at EPFL (Switzerland). He is currently a Research Director and Group Leader of Functional Materials Laboratory and Key Lab of Nanomaterials and Nanotechnology of Shaanxi Province (China). His research focuses on the new energy such as solar cells, fuel cells, supercapacitors, hydrogen generation and anaerobic digestion. Details can be found at: http://xy.xauat.edu.cn/gnclyjs/listyjsgk.asp?id=262&bh=2080; https://www.x-mol.com/groups/Sining_Yun.

## Authors and Affiliations

**Bin Zhu[1] · Liangdong Fan[2] · Naveed Mushtaq[1] · Rizwan Raza[3] · Muhammad Sajid[3] · Yan Wu[4] · Wenfeng Lin[5] · Jung-Sik Kim[6] · Peter D. Lund[7] · Sining Yun[8]**

[1] Jiangsu Provincial Key Laboratory of Solar Energy Science and Technology/Energy Storage Joint Research Center, School of Energy and Environment, Southeast University, Nanjing 210096, Jiangsu, China

[2] Shenzhen Key Laboratory of New Lithium-Ion Batteries and Mesoporous Materials, College of Chemistry and Environmental Engineering, Shenzhen University, Shenzhen 518060, Guangdong, China

[3] Clean Energy Research Lab (CERL), Department of Physics, COMSATS University Islamabad, Lahore Campus, Lahore 54000, Pakistan

[4] Engineering Research Center of Nano-Geo Materials of Ministry of Education, Faculty of Materials Science and Chemistry, China University of Geosciences, Wuhan 430074, Hubei, China

[5] Department of Chemical Engineering, School of Aeronautical, Chemical and Materials Engineering, Loughborough University, AutomotiveLoughborough LE11 3TU, UK

[6] Department of Aeronautical & Automotive Engineering, School of Aeronautical, Chemical and Materials Engineering, Loughborough University, Automotive LE113TU, UK

[7] Department of Engineering Physics/Advanced Energy Systems, School of Science, Aalto University, 00076 Aalto, Espoo, Finland

[8] Functional Materials Laboratory (FML), School of Materials Science and Engineering, Xi'an University of Architecture and Technology, Xi'an 710055, Shaanxi, China